NASA Contractor Report 177983

The Evaluation of Failure Detection and Isolation Algorithms for Restructurable Control

P. Motyka, W. Bonnice, S. Hall, E. Wagner

THE CHARLES STARK DRAPER LABORATORY, INC.
555 Technology Square
Cambridge, Massachusetts 02139

CONTRACT NAS1-17556
November 1985

National Aeronautics and
Space Administration

Langley Research Center
Hampton, Virginia 23665

NASA Contractor Report 177983

The Evaluation of Failure Detection and Isolation Algorithms for Restructurable Control

P. Motyka, W. Bonnice, S. Hall, E. Wagner

THE CHARLES STARK DRAPER LABORATORY, INC.
555 Technology Square
Cambridge, Massachusetts 02139

CONTRACT NAS1-17556
November 1985

National Aeronautics and
Space Administration

Langley Research Center
Hampton, Virginia 23665

TABLE OF CONTENTS

TABLE OF CONTENTS (Cont.)

TABLE OF CONTENTS (Cont.)

LIST OF ACRONYMS

CSDL	The Charles Stark Draper Laboratory
CPU	Control Processing Unit
FDI	Failure Detection and Isolation
GLR	Generalized Likelihood Ratio
LLR	Log Likelihood Ratio
LR	Likelihood Ratio
NASA	National Aeronautics and Space Administration
OSGLR	Orthogonal Series Generalized Likelihood Ratio
STOL	Short Take Off or Landing

LIST OF SYMBOLS

a_i	unknown coefficients of series expansion of failure mode shape for OSGLR algorithm
$\underline{a}$	column vector which augments A-λI matrix; vector of a_i's
A	linear system state matrix, dimension n×n
A_a	state transition matrix of the unknown coefficient vector a in the continuous time OSGLR algorithm
A_ϕ	state matrix that defines the OSGLR basis functions ϕ_i in continuous time
$\underline{b}_i$	ith column of B matrix
$\underline{b}(k)$	known vector denoting type of failure and its effect on the system through B
B	linear system state input matrix of dimension n×m
$\underline{c}$	$P^\dagger \underline{r}$; projection of residuals onto the normalized C ($\underline{b}_i$ - K$\underline{d}_i$) vectors and $\tilde{\underline{d}}_{1_N}$ and $\tilde{\underline{d}}_{2_N}$; also column vector which augments C
$\underline{c}_f$	components of $\underline{c}$ which correspond to $\underline{d}_i$ and have been filtered with the same eigenvalue as the detection filter
c_i	ith component of the C vector
C	linear system output matrix, dimension p×n
d	distance between hypotheses
$\underline{d}_i$	ith column of the D matrix
$\underline{d}(k)$	known vector denoting type of failure and its effect on the system through D
$\tilde{d}_{1N}, \tilde{d}_{2N}$	linearly independent normalized columns of D
D	linear system control input matrix for the output equation, dimension p×m
DF_i	detection decision function for control surface i, i = 1, 2, ..., 6

DF_{ij}	isolation decision function between control surfaces i and j, i,j = 1, 2, ..., 6
$DF(k_f)$	GLR decision function at final iteration k_f
$DF(t_f)$	OSGLR decision function at time t_f
$\underline{e}_1, \underline{e}_2, \underline{e}_3$	unit vectors
$\underline{e}_i$	column vector with zeroes in every row except for a one in ith row
$\underline{e}(k)$	estimation error
$\underline{e}_{qi}$	q-dimensional vector with unity in the ith coordinate direction
$E(\ )$	mean or expected value
$\underline{f}$	vector of nonlinear functions of the states and controls
$f(\cdot)$	function evaluated using all available data
$f(t)$	mode shape of failure
$\underline{f}(k, \theta)$	influence of failure mode on the state estimation error at increment k, failure occuring at time θ
$\underline{g}$	vector of nonlinear functions of the states and controls
$\underline{g}(k)$	known bias vector of dimension n
$g(k, \theta)$	signature of failure at increment k, failure occuring at time θ
$G(t)$	influence of vector of coefficients $\underline{a}$ on the residuals
$\underline{h}(k)$	known bias vector of dimensional p
H_0	no failure hypothesis
H_1	failure hypothesis
I	identity matrix
k	kth discrete time step
$\underline{k}_i$	ith column of the K matrix
K	detection filter or Kalman filter gain matrix
$\ell(k_f, \theta, \nu)$	log likelihood ratio at final iteration k_f for failure of magnitude ν occurring at time θ

$\ell(t_f)$	log likelihood ratio of time t_f
$L_2^m[t_o,t_f]$	set of square-integrable, m-dimensional vector functions on the interval $[t_o, t_f]$
$\underline{m}_i$	mean in the residual $\gamma(t)$ under hypothesis H_i
M(k)	covariance of Kalman filter residual at time step k
n(t),n(k)	unexpected control input
n(k,θ)	failure mode shape
N(a,b)	normal distribution with mean a and variance b
O( )	higher order terms
p	number of basis functions of OSGLR algorithm
p(x/y)	conditional probability of x given that y has occurred
P	the columns of $\underline{P}$ are the normalized $C(\underline{b}_i - K\underline{d}_i)$, $\tilde{\underline{d}}_{1N}$ and $\tilde{\underline{d}}_{1N}$ vectors
P(k),P(t)	covariance of Kalman filter estimation error
$\underline{q}$	$\underline{x} - \underline{x}'$, difference between the system state vector and the detection filter state vector
$\underline{q}'$	state vector of the secondary filter used in the modified detection filter
Q(k)	state driving noise covariance
$\underline{r}$	$\underline{y} - \underline{y}'$, residual vector
r_f	components of $\underline{r}$ which correspond to $\underline{d}_i$ and have been filtered with the same eigenvalue as the detection filter
R	matrix operator which, when applied to $\underline{c}$, nulls out the components corresponding to the projections of the residual onto the $\tilde{\underline{d}}_{1N}$ and $\tilde{\underline{d}}_{2N}$ vectors
R(k)	measurement noise covariance

s	Laplace transform variable
S	variance or matrix operator which, when applied to c, forms a two-dimensional vector containing the components corresponding to the projections of the residual onto the $\tilde{d}_{1N}$ and $\tilde{d}_{2N}$ vectors.
$S(k_f, \theta)$	discrete-time information matrix at increment k_f, failure occurring at time θ
$S(t_f)$	continuous-time information matrix
t	time
t_k	time at the kth sampling interval
T	threshold
$\underline{u}$	nonlinear or linear system control input vector, dimension m
$\underline{u}'$	detection filter control input vector
$\underline{u}_a$	control vector with actuator failure present
$\underline{u}_c$	control system commands to the actuators
$\underline{u}_{nominal}$	nominal control surface deflections
$\underline{v}(t), \underline{v}(k)$	zero mean Gaussian white noise vector with spectral density R(t), R(k) respectively
$\underline{v}_i$	vector whose elements are zero except for the ith which is 1, i = 1,2, ..., n
V_j	subspace of L_2^m
$\underline{w}(t), \underline{w}(k)$	zero mean Gaussian white noise vector with spectral intensity Q(t), Q(k) respectively
$\underline{x}$	nonlinear or linear system state vector, dimension n
$\underline{x}'$	detection filter state vector, dimension n
x_{jp}	perturbation in jth state from the nominal
$\underline{y}$	nonlinear or linear system output vector, dimension p

$\underline{y}'$	detection filter output vector, dimension p
$\underline{y}_{nominal}$	nominal output vector, dimension p
z	z-transform variable or exponential decay term
$\alpha_{ij}(f_i(\ ), t_f)$	angular distinguishability measure between control surfaces i and j at the time t_f based upon a failure of control surface i using all available data
$\underline{\gamma}_i$	ith column of the Γ matrix
$\underline{\gamma}(k), \underline{\gamma}(t)$	Kalman filter residual at increment k, time t
Γ	gamma function or discrete state input matrix
$\Gamma(t)$	invertible linear transformation at time t
$\delta_{a_r}, \delta_{a_l}$	right and left ailerons, respectively
δ_E	elevator
δ_{ij}	Kronecker delta, $= 0 \quad i \neq j$ $= 1 \quad i = j$
$\delta(t_1-t_2)$	Dirac delta
Δ	increment
Δt	time increment
$\underline{\Delta u}'$	linear input vector to the detection filter, dimension m
$\underline{\Delta x}'$	linear detection filter state vector, dimension n
$\underline{\Delta y}'$	linear detection filter output vector, dimension p
$\Delta_{ij}(f_i(\cdot), t_f)$	distance distinguishability measure between control surfaces i and j at time t_f based upon a failure of control surface i
$\underline{\eta}_i$	column vector with unity in the ith row and zero in the other rows
θ	time of failure
λ	detection filter eigenvalue or false alarm rate for OSGLR
$\Lambda(k_f, \theta, \nu)$	likelihood ratio at final iteration k_f for failure of magnitude ν occuring at time θ
ν	magnitude of failure

σ_ω	standard deviation of turbulence, ft/s
τ	relative time from end of observation interval
$\phi_i(k)$, $\phi_i(t)$	basis function of OSGLR algorithm at increment k, time t
$\Phi(k)$	linear system discrete time state transition matrix, dimension n×n
Φ_a	state transition matrix of the unknown coefficient vector a for the discrete-time OSGLR algorithm
Φ_ϕ	state transition matrix matrix that defines the OSGLR basis functions ϕ_i in discrete time
$\underline{\chi}(t)$	information vector at time t
$\psi_i(k)$	OSGLR basis functions
$\|\|x\|\|$	norm of x
$<x,y>$	inner product between x and y

Superscript

-1	inverse
†	pseudo inverse
-	quantity prior to filter update
+	quantity after filter update

Subscript

a	refers to OSGLR basis function coefficients
AR	right aileron
AL	left aileron
d	discrete
E	elevator
f	final
FR	right flap
FL	left flap
N	vector has been normalized
w	window
^	estimate
0	initial or nominal
1	intermediate representation
*	minimum
ϕ	refers to OSGLR basis functions

SECTION 1

INTRODUCTION

Recently, there has been much interest in the problem of restructuring the control law of aircraft following the failure of control surfaces or actuators (References 1,2,3). This interest is motivated in part by two incidents involving commercial aircraft. In the case of Delta flight 1080 on April 12, 1977, the left elevator became stuck in the 19° up position at takeoff (Reference 4). The pilot was able to compensate for the failure, in part by manipulating thrust to control the pitch axis. However, the pilot of the DC10 that crashed in Chicago (Reference 5) was unable to recover from the left engine breaking loose and the resulting retraction of the left wing's outboard leading edge slats. Simulations indicate that the aircraft could have been flown if impending stall conditions had been recognized and the proper corrective action taken. Restructuring the control system on-line to counteract the effect of these failures may be one solution to such problem situations. Although the need for restructurable control has been demonstrated for state-of-the-art aircraft systems, it can be expected to be most applicable to future aircraft where redundant control surfaces will very likely be extensively employed.

A feasible and practical restructurable control system requires the correct and timely detection and isolation of the control system failure so that the proper corrective action can be taken. The evaluation of various failure detection and isolation (FDI) algorithms for application in aircraft restructurable flight control systems is the focus of this

interim report. The work described was conducted by the Charles Stark Draper Laboratory, Inc. (CSDL) for the NASA Langley Research Center under contract NAS1-17556 entitled, "Evaluation of Failure Detection and Identification Techniques for Application in Aircraft Restructurable Control Systems." The specific goals of this effort are twofold:

- o To analyze and compare various failure detection and identification techniques to determine their usefulness in detecting and identifying failures in an aircraft flight control system, excluding sensor and flight control computer failures. Issues such as the types of failures which can be detected, the degree of failure that can be detected, the time delay between failure and detection, etc. are to be addressed. This evaluation should also consider the maturity, reliability, false alarm performance, robustness and computational burden of each technique.
- o To develop a system monitoring strategy to implement the failure detection and identification techniques. This strategy should identify the mix of sensors and analytic redundancy; that is, the mix of direct measurement of failures versus the computation of failures.

Three specific FDI algorithms were evaluated under this study: the detection filter, the Generalized Likelihood Ratio test and the Orthogonal Series Generalized Likelihood Ratio test. The detection filter (References 6,7,8) has the form of an observer, much like that of a Kalman filter. The feedback gain matrix is chosen so that each type of failure produces a uniquely defined residual. The FDI system is therefore insensitive to the mode of the failure, be it bias, ramp, etc. A shortcoming of the detection filter is that its application to time-varying systems is limited.

Basic detection filter theory assumes a system with no direct input-output coupling. This assumption is violated in the aircraft application considered in this study due to the use of acceleration

measurements for detecting and isolating failures. With this coupling, residuals produced by control surface failures may only be constrained to a known plane rather than to a single direction as in the case of the basic detection filter. A detection filter design with such planar failure signatures is considered and the design issues associated with it addressed. In addition, a modification to the basic detection filter, to constrain the residual to a single known direction even with direct input-output coupling, is also presented. The approach employed is to use secondary filtering of the detection filter residuals to produce unidirectional failure signals.

The Generalized Likelihood Ratio (GLR) test (Reference 9) is derived based upon the assumption of a step failure. The magnitude of the failure and its time of occurrence are estimated using maximum Likelihood Estimation. These estimates are used to form a likelihood ratio which is the test statistic.

The third algorithm investigated is the Orthogonal Series Generalized Likelihood Ratio (OSGLR) test (Reference 10). This algorithm assumes a failure in the form of a truncated series of orthonormal basis functions. The coefficients of the series expansion are estimated using maximum likelihood estimation and a generalized likelihood ratio is formed using these estimates. The rationale for adopting this approach is that most failures should be represented fairly well using a truncated orthogonal series expansion and this algorithm should be more robust to failure mode uncertainty than the conventional GLR test.

The three algorithms just described were evaluated by testing their ability to detect and isolate control surface failures in a nonlinear simulation of a C-130 transport aircraft. Elevator, rudder, aileron and flap failures were investigated.

This report is organized as follows. Section 2 describes the C-130 aircraft and simulation used to evaluate the FDI algorithms under consideration. Basic detection filter theory and its application to restruc-

turable control is addressed in Section 3, while the modified version of the detection filter is discussed in Section 4. Both GLR tests are evaluated and compared in Section 5. It was found during the course of this study that failures of some aircraft controls are difficult to distinguish because they have a similar effect on the dynamics of the vehicle. Quantitative measures for evaluating the distinguishability of failures are considered in Section 6. Section 7 is devoted to a comparison of the FDI algorithms considered based upon their ability to detect and isolate failures in aircraft systems in general and the C-130 in particular. Considerations in the development of a system monitoring strategy in a transport aircraft are discussed in Section 8. The material described in the report is summarized and the major conclusions presented in Section 9. Appendix A includes a description of the methodology employed to develop the linear model of the C-130 aircraft required for each of the FDI algorithms. The discrete time version of the detection filter is briefly described in Appendix B.

SECTION 2

C-130 SIMULATION DESCRIPTION

2.1 Introduction

The FDI algorithms under consideration will be evaluated by testing their ability to detect and isolate control surface and flap failures that have occurred in a simulation of a Lockheed C-130 aircraft. The C-130 aircraft is a military, medium- to long-range transport propelled by four turboprop engines located on a high wing. The particular version of the C-130 aircraft used for this program has short takeoff and landing (STOL) capability provided by trailing-edge double-slotted flaps.

2.2 Simulation Description

The simulation of the C-130 aircraft uses the standard six degree-of-freedom aircraft nonlinear equations of motion. The aerodynamic forces and moments are described by one-, two-, or three-dimensional look-up tables. These look-up tables are functions of angle of attack, sideslip angle, thrust, flap deflection, or the control surface deflections. Each of the four engines are assumed to provide the same thrust. Actuator dynamics have been included; however, sensor dynamics were not included.

The surfaces available for control of the aircraft are the ailerons, flaps, rudder and elevator. The simulation allows for independent motion of the left and right ailerons and the left and right flaps so that failures of these individual surfaces could be simulated

and used along with rudder and elevator surface failures to evaluate the performance of the FDI algorithms. Since aileron and flap failures are similar in their effect on the dynamics of the vehicle, detecting and isolating aileron and flap failures should provide an adequate test for the various algorithms to be evaluated.

The eleven measurements available for detecting and isolating failures are those typically available onboard aircraft. These measurements are listed in Table 2.1, along with the six control inputs described above and the ten states that describe the aircraft dynamics. The measurements are generated in the simulation by superimposing zero-mean Gaussian distributed noise on the output variables. The noise statistics used for this study are shown in Table 2.2.

Wind turbulence is also incorporated in the simulation. The turbulence velocity along each body axis is modeled by passing white noise through shaping filters to produce signals with desired one-dimensional power spectral densities. The Dryden form of the spectra, defined in Reference 11, is modeled. This reference suggests an intensity of 1.98 m/s (6.5 ft/s) for clear air turbulence at the altitude of 304.8 m (1000 ft) used in this evaluation. However, this level characterizes severe turbulence and a less severe level was selected for initial evaluation. Therefore, an intensity of 0.3 m/s (1 ft/s) was used to obtain the results presented in this report unless otherwise noted. The turbulence scale lengths were the clear air values defined in Section 3.7.3.2 of Reference 11.

Each of the FDI algorithms evaluated requires a linear model of the system. Appendix A includes a discription of the methodology employed to develop the linear model of the C-130 aircraft for this purpose.

Table 2.1. Inputs, Outputs, and States of the C-130 Aircraft

Inputs
Elevator
Right aileron
Left aileron
Right flap
Left flap
Rudder
Outputs
Airspeed
Acceleration at the cg along the y body axis
Acceleration at the cg along the z body axis
Angular velocity about the x body axis[1]
Angular velocity about the y body axis[2]
Angular velocity about the z body axis[3]
Roll
Pitch
Yaw
Altitude rate
Altitude
States
Airspeed
Sideslip angle
Angle of attack
Angular velocity about the x body axis[1]
Angular velocity about the y body axis[2]
Angular velocity about the z body axis[3]
Roll
Pitch
Yaw
Altitude

[1] Will be referred to as body axis roll rate.
[2] Will be referred to as body axis pitch rate.
[3] Will be referred to as body axis yaw rate.

Table 2.2. Standard Deviation of Sensor Noise

SENSOR	STANDARD DEVIATION	
Airspeed	3.35 m/s	11 ft/s
Accelerometers	.3 m/s^2	.98 ft/s^2
Roll Rate Gyro	.0024 rad/s	.1375 deg/s
Pitch and Yaw Rate Gyros	.0007 rad/s	.04 deg/s
Attitude Gyros	.01 radians	.573 degrees
Altitude Rate	.08 m/s	.25 ft/s
Altitude	3.05 m	10 ft

SECTION 3

THE DETECTION FILTER

3.1 Detection Filter Review[1]

The evaluation of the basic detection filter is considered in this section. A block diagram of a nonlinear system and its detection filter is shown in Figure 3.1. For this study the actuator dynamics were assumed to be modeled perfectly. Therefore, the control surface deflections of the nonlinear system, $\underline{u}(t)$, and the control surface deflections input to the detection filter, $\underline{u}'(t)$, are equal unless an actuator failure has occurred. A linear model of the system in its nominal operating condition is incorporated in the detection filter. Note that there is no direct coupling between the inputs and the outputs. (Direct input-to-output coupling will be considered in Section 3.2.) Any discrepancy between the system sensor outputs and the simulation of those outputs generated by the filter model is fed back to the filter input through the gain matrix K. One of the requirements on the design of the detection filter is that K be chosen to make the filter stable. Thus, as long as the system remains in its nominal operating condition, any initial condition errors of the filter will die away and the filter will track the behavior of the system. The output error, $\underline{r}(t)$, is in that case zero except for disturbances, noises, or other real system effects not modeled in the filter.

[1] Much of this detection filter description is taken from Reference 12.

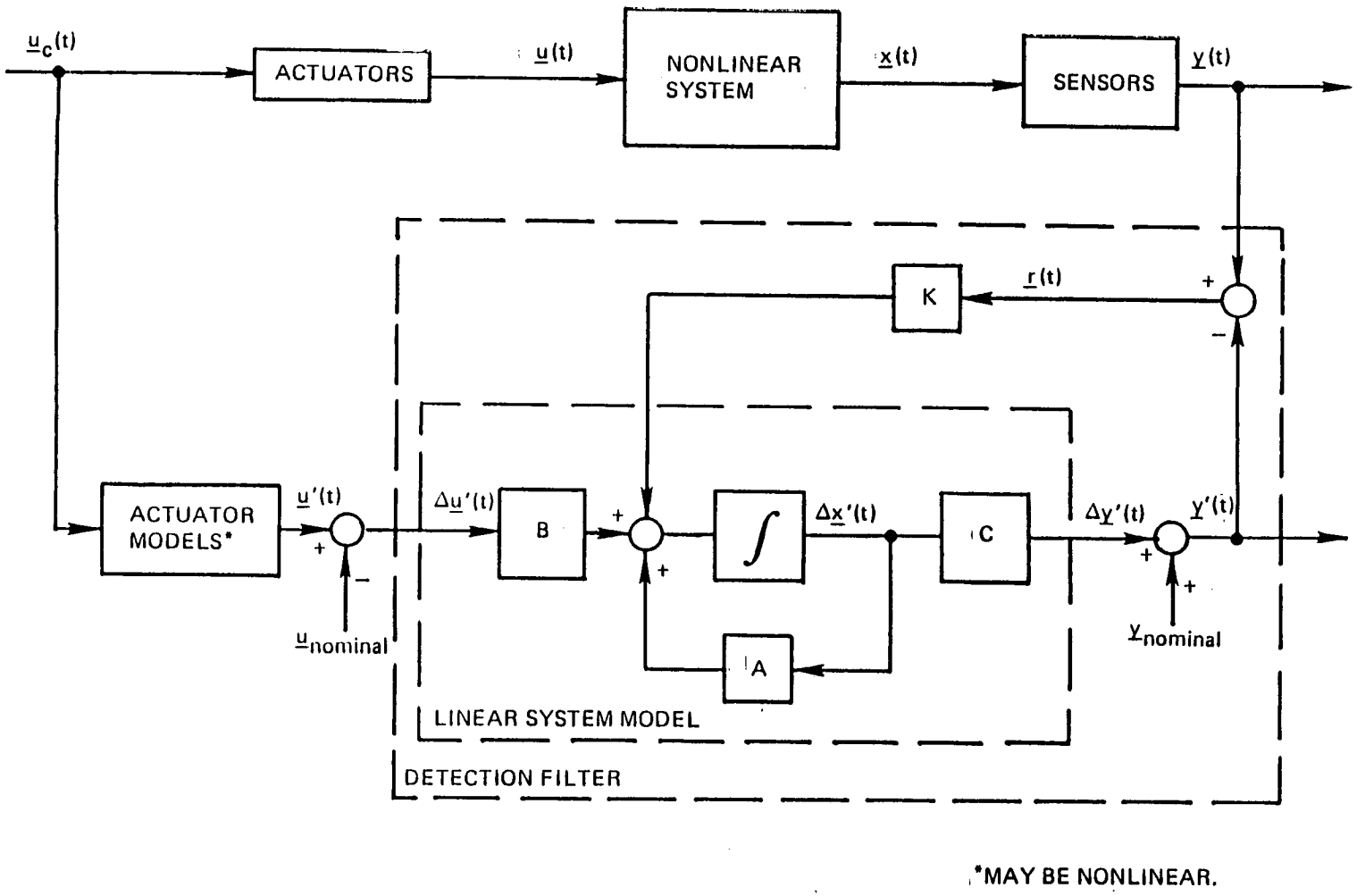

Figure 3.1. Detection filter block diagram

If one of the system components fails, the actuator models or the filter no longer model the actuators, the system, or the sensors accurately. It is clear, then, that the output error will be significantly different from zero following the failure of a system component. This would be true of any filter which models the nominal system; it would be true, for example, of a Kalman filter which estimates the state of this system. But the failure detection filter is designed under a different set of constraints than other filters; it is designed to hold the output error corresponding to any one component failure in one direction only. Thus a component failure is detected by observing a significant magnitude in the output error; the failed component is identified by observing the direction of that significant error in the space of $\underline{r}(t)$.

Perhaps the most important advantage of this approach to FDI is that the behavior described above does not depend in any way upon the mode of the component failure. Many other forms of FDI are tuned to hypotheses about the mode of component failures. But in most cases one cannot realistically expect to enumerate a comprehensive list of possible failure modes and characterize somehow the behavior of the component following each of those modes of failure. Although the specification of this kind of information is, in principle, useful and may be expected to permit more sensitive failure detection, the uncertainties involved in specifying failure mode information may more than offset such a potential advantage. No assumption with regard to the mode of failure will be made in this section.

The theory of the failure detection filter, in its present state, applies to a linear, time-invariant system. In its application to aircraft the inherently nonlinear behavior of the vehicle will be linearized and any discrepancy between the actual system and the model of it in the filter will produce an output residual which contributes to the background against which the output due to failures must be detected. The continuous-time development is presented in this section. As the

detection filter will actually be implemented in a digital computer, the extension to discrete-time is stated in Appendix B.

3.1.1 System and Filter Models

The linear, continuous-time analytic model of the perturbations about the operating point of the nonlinear system may be written in the form

$$\dot{\underline{x}} = A\underline{x} + B\underline{u} \tag{3.1}$$

$$\underline{y} = C\underline{x} \tag{3.2}$$

Here $\underline{x}$ is the state vector characterizing the system, $\underline{u}$ is the input or control vector and $\underline{y}$ is the vector of measurements available from the system sensors. This development will not consider the effect of noises disturbing the system nor corrupting the measurements. Those effects will be evaluated in a simulation of the system with its detection filter. Note that the delta (Δ) notation for the linear state, input, and measurement vectors used in Figure 3.1 has been dropped for convenience. This notation change produces an ambiguity in that the same symbols are used for both the nonlinear and linear state, input, and measurement vectors. However, as detection filter theory is limited to linear systems, the symbols should be understood as referring to the linear state, input, and measurement vectors.

As seen in Figure 3.1, the detection filter state and residual satisfy

$$\dot{\underline{x}}' = A\underline{x}' + B\underline{u}' + K\underline{r} \tag{3.3}$$

$$\underline{r} = \underline{y} - \underline{y}' \tag{3.4}$$

where

$$\underline{y}' = C\underline{x}' \tag{3.5}$$

This $\underline{r}$ is the accessible output error. Define in addition the full state error

$$\underline{q} = \underline{x} - \underline{x}' \tag{3.6}$$

In the absence of failures, and supposing that the filter has an accurate model of the system, this error satisfies the differential equation

$$\begin{aligned} \dot{\underline{q}} &= \dot{\underline{x}} - \dot{\underline{x}}' \\ &= (A - KC)\underline{q} \end{aligned} \tag{3.7}$$

One of the requirements on the design of the detection filter is that K must be chosen to make (A - KC) stable. Thus even though the filter may not be initialized to match the system initial conditions, the error will die out and then $\underline{x}'(t)$ will track $\underline{x}(t)$. So a detection filter is a state estimating filter, but that is not its primary purpose.

3.1.2 Model of a Failure

First consider an actuator failure. In Eq. (3.1) each element of $\underline{u}$ relates to one actuator. Thus the corresponding column of B expresses how that actuator drives the system state. Call the column of B corresponding to the ith actuator $\underline{b}_i$. If that actuator fails, $u_i(t)$ will not behave as expected. This can be modeled by changing Eq. (3.1) to

$$\dot{\underline{x}} = A\underline{x} + B\underline{u}' + \underline{b}_i n(t) \tag{3.8}$$

where n(t) is an arbitrary scalar function of time expressing the difference between what the failed actuator is doing and what the nominal model says it should be doing. If, for example, an actuator fails by sticking in the zero position, then $n(t) = - u_i'(t)$ where $u_i'(t)$ is the expected actuator position time history. The fact that n(t) is treated as an arbitrary function is the mathematical expression of the fact, cited

previously, that we will not depend on any information about the mode of component failures.

With the system behavior given by Eq. (3.8) and the detection filter characterized by Eq. (3.3), the error in the presence of an actuator failure obeys the differential equation

$$\dot{\underline{q}} = (A - KC)\underline{q} + \underline{b}_i n(t) \tag{3.9}$$

The output error is then

$$\begin{aligned} \underline{r} &= \underline{y} - \underline{y}' \\ &= C\underline{q} \end{aligned} \tag{3.10}$$

In addition to making the filter stable with favorable transient characteristics, K is designed to restrict the response of Eq. (3.9) to a subspace of the full space of $\underline{q}$, which has a projection through C to the output space having one dimension only. This property is independent of n(t) and depends only on the vector $\underline{b}_i$, which gives the direction in state space in which the failed actuator drives the state error. The component whose failure is to be detected is therefore characterized, for the purpose of detection filter design, by $\underline{b}_i$. It is called the <u>event vector</u> for this particular failure. Any scalar multiple of $\underline{b}_i$ can be used as its magnitude is of no consequence; it is the direction of $\underline{b}_i$ that is important.

If it is possible to design a detection filter that restricts the output error (residual) due to the failure event $\underline{b}_i$ to one dimension, the direction of the residual will be $C\underline{b}_i$. Only if the $C\underline{b}_i$ corresponding to all the $\underline{b}_i$ assigned to one detection filter are linearly independent can their output errors be restricted to single, orthogonal directions in the output space or in any transformation of the output space. If the $C\underline{b}_i$ are not linearly independent, one may wish to remove one or more $\underline{b}_i$

from the group to achieve independence. This limits the number of failures which can be identified by one filter to the number of independent measurements which are available.

However, there is one exception to the above. If any $\underline{b}_i$ as first defined has the property

$$C\underline{b}_i = 0 \tag{3.11}$$

then that event vector should be replaced by $\underline{b}_i'$, which is the first vector in the sequence

$$\underline{b}_i^{(k)} = A^k \underline{b}_i \qquad k = 1,2,\ldots \tag{3.12}$$

for which

$$C\underline{b}_i^{(k)} \neq 0 \tag{3.13}$$

In the above discussion it was assumed that this redefinition of $\underline{b}_i$ has been made whenever necessary, and the resulting event vector was still referred to as $\underline{b}_i$ for convenience.

In the case of a sensor failure, for a sensor whose output is not fed back through a controller to the system input, the modeling is very similar but the effect is more complex. In the output expression, Eq. (3.2), each element of $\underline{y}$ is one sensor output. The corresponding row of C determines the linear combination of states which characterize that measurement. If the ith sensor fails, the result is modeled as

$$\underline{y} = C\underline{x} + \underline{v}_i n(t) \tag{3.14}$$

where again n(t) is an arbitrary scalar function and $\underline{v}_i$ is a vector whose

elements are zero except for the ith which is 1. This represents an arbitrary discrepancy between the sensor output after failure and the nominal output. The filter error in this case obeys the relations

$$\dot{\underline{q}} = (A - KC)\underline{q} - \underline{k}_i n(t) \tag{3.15}$$

$$\underline{r} = C\underline{q} + \underline{v}_i n(t) \tag{3.16}$$

The arbitrary function n(t) appears both at the input to the error differential equation and in the output relation. The input direction, $\underline{k}_i$, is in this case the ith column of the detection filter gain matrix, K.

As in the case of actuator failures, it may be possible to restrict the residual produced by the $\underline{k}_i n(t)$ term to a single direction. For the sensor failure case, the direction would be $C\underline{k}_i$. However, in general, this direction will not be the same as the direction $\underline{v}_i$ which appear directly in the residual expression, Eq. (3.16). Thus the residual, in the case of failures of sensors which do not feed back into the system through a controller, can be restricted to a plane but not a line. This plane is defined by the vectors $C\underline{k}_i$ and $\underline{v}_i$.

Failures of sensors whose output is fed back through a controller to the system input may be modeled in the same manner as actuator failures (Eq. (3.8)). This is true also for significant changes in system dynamics corresponding to changes in the elements of A or B. For these cases, $\underline{b}_i$ is no longer necessarily a column of B but a general event vector which appropriately models the failure. As in the case of actuator failures, the residual produced by these failures may be restricted to a line defined by $C\underline{b}_i$.

3.2 The Effect of Explicit Coupling of Inputs to Outputs

The development of the detection filter to date, as discussed in Section 3.1, has assumed that there is no direct coupling between the inputs and the outputs. However, there is direct input-output coupling

due to the lateral and normal acceleration measurements available on-board the C-130 aircraft chosen for use in this study. This coupling results in a nonzero D matrix in the linearized system model:

$$\dot{\underline{x}} = A\underline{x} + B\underline{u} \tag{3.17}$$

$$\underline{y} = C\underline{x} + D\underline{u} \tag{3.18}$$

The effect of this coupling on actuator failure signatures will be presented here. Only actuator failures are considered since this is the type of failure of interest in the Restructurable Controls Program.

Consider a failure in the ith actuator. The actual control surface deflections, $\underline{u}(t)$, can be expressed as the sum of the expected control surface deflections input to the detection filter, $\underline{u}'(t)$, and the difference in the actual and expected ith control surface deflection $n(t)$.

$$\underline{u}(t) = \underline{u}'(t) + \underline{e}_i n(t) \tag{3.19}$$

$\underline{e}_i$ is a column vector with zeros in every row except for a one in the ith row. As before, no assumption has been made with regard to the actual form of $n(t)$. A model of the effect of the failure on the system is developed by substituting Eq. (3.19) into Eqs. (3.17) and (3.18).

$$\dot{\underline{x}} = A\underline{x} + B\underline{u}' + \underline{b}_i n(t) \tag{3.20}$$

$$\underline{y} = C\underline{x} + D\underline{u}' + \underline{d}_i n(t) \tag{3.21}$$

Here, $\underline{d}_i$ is the ith column of the D matrix. The differences between the actuator failure model with input-output coupling and the model without coupling are the two D matrix terms in the measurement equation.

The detection filter is still of the form given in Eqs. (3.3) and (3.4). These equations are repeated here for reference.

$$\dot{\underline{x}}' = A\underline{x}' + B\underline{u}' + K\underline{r} \tag{3.3}$$

$$\underline{r} = \underline{y} - \underline{y}' \tag{3.4}$$

However, the expression for $\underline{y}'$ now contains a nonzero D matrix term

$$\underline{y}' = C\underline{x}' + D\underline{u}' \tag{3.22}$$

Given the system behavior in response to an actuator failure (Eqs. (3.20) and (3.21)) and the detection filter equations (Eqs. (3.3), (3.4) and (3.22)), the error dynamics of the filter are found to be

$$\dot{\underline{q}}(t) = (A - KC)\underline{q}(t) + (\underline{b}_i - K\underline{d}_i)n(t) \tag{3.23}$$

$$\underline{r}(t) = C\underline{q}(t) + \underline{d}_i n(t) \tag{3.24}$$

These error dynamics are similar to the error dynamics produced by a detection filter <u>without</u> input-output coupling in response to a failure of a sensor whose output does not feedback into the system through a controller. The unexpected control surface deflection appears both at the input to the error differential equation and in the residual equation. It may be possible to restrict the residual produced by $(\underline{b}_i - K\underline{d}_i)n(t)$ term to a single direction $C(b_i - Kd_i)$. But as this direction differs, in general, from the $\underline{d}_i$ direction, which also appears in the residual equation, the failure signature will be planar. This plane is spanned by the vectors $C(\underline{b}_i - K\underline{d}_i)$ and $\underline{d}_i$. Notice that the gain matrix K has an effect on the direction $C(\underline{b}_i - K\underline{d}_i)$ and therefore on the resultant plane. A unidirectional residual would result if the direction of $C(\underline{b}_i - K\underline{d}_i)$ could be aligned with $\underline{d}_i$. However, aligning

$C(\underline{b}_i - K\underline{d}_i)$ with $\underline{d}_i$ would not allow the failure to be distinguishable in this application as there are only two distinct directions of the columns of D (there are only two measurements which produce nonzero entries in the D matrix). Therefore, without basic modification of the detection filter, the effect of input-output coupling is to cause actuator failure signatures to be planar instead of unidirectional.

This result prompted a re-examination of the use of the acceleration measurements. However, it was decided not to substitute angle of attack and sideslip angle measurements for the acceleration measurements as the acceleration measurements are of higher quality. This decision limited the remaining options to two: testing a detection filter with the planar signature property or modifying the detection filter to regain the property of unidirectional actuator failure signatures. Both of these options were developed and tested. The results of the planar signature detection filter are shown in Section 3.5. The modification of the detection filter and the results obtained using this filter will be presented in Section 4.

3.3 Detection Filter Design

A detection filter is designed by calculating the gain matrix so that actuator failures produce unidirectional residuals in the case of no direct input-output coupling or planar signatures when there is direct input-output coupling. This desired residual behavior may be produced for a fully measured system (i.e., rank [C] equals the number of states) by choosing K such that, for some λ,

$$A - KC = \lambda I \tag{3.25}$$

As the measurement set chosen for this evaluation is such that the system is fully measured, this design approach will be used. The filter eigenvalues can be seen to be the eigenvalues of (A - KC) by rewriting Eq. (3.3).

$$\dot{\underline{x}}' = (A - KC)\underline{x}' + B\underline{u}' + K(\underline{y} - D\underline{u}') \qquad (3.26)$$

Thus the eigenvalue λ should be chosen to give a stable filter that has acceptable transient response characteristics.

3.3.1 Design Procedure

Using the previous approach, the following procedure can be used to design a detection filter:

(1) Choose the measurement scaling.

(2) Select the filter eigenvalue λ.

(3) Calculate the gain matrix.

(4) Set thresholds.

Each of these steps will now be discussed in more detail.

Measurement scaling was used to reduce the effect of noisy measurements and enhance the contribution of higher quality measurements. Scaling the measurements effectively changes the numerical values of the standard deviation of the noise.

The next step is to choose the filter eigenvalue. One obvious requirement is that the eigenvalue be chosen so the filter is stable. In addition, it is desirable to make the filter fast, so as to reduce the effect of modeling errors and to have short failure detection times. However, a fast eigenvalue also reduces the magnitude of the residual produced by a failure, making detection more difficult in a noisy environment. If noise is a problem, though, it might be better to low-pass filter the residual instead of making the filter slower. This supplemental noise filtering can be employed in such a way that the quick detection of a large failure is not sacrificed for the detection of smaller failures. This is achieved by passing the residual through a bank of parallel low-pass filters with different time constants. One such filter would have a small time constant to allow for quick detection of large failures while other filters would have larger time constants to allow

for detection of moderate and small failures. The filter eigenvalue chosen for this evaluation was approximately twice as fast as the fastest eigenvalue of the system.

The final two steps are to calculate the gain matrix and to set detection and isolation thresholds. The gain matrix calculation will be discussed below. While selecting thresholds is an important aspect of detection filter design, thresholds will not be selected in this study as the algorithms will be evaluated qualitatively.

3.3.2 Gain Matrix Calculation

Given choices for scaling and the filter eigenvalue, actual calculation of the gain matrix to satisfy the equality shown in Eq. (3.25) is still uncertain in this application because there are eleven measurements and only ten states. K is underdetermined as there are ten more unknowns than equations in satisfying Eq. (3.25). Recall that in order to be guaranteed that Eq. (3.25) can be satisfied, the rank of C must be equal to the number of states.[2] Therefore, one measurement could be eliminated such that the rank of C remains ten. In this case, the gain matrix K would becompletely determined by constraining A - KC to be the diagonal matrix λI. However, eliminating a measurement just to simplify the gain matrix calculation seemed undesirable since information is thereby lost, and this approach was not taken. In addition, the ten degrees of freedom remaining in the gain matrix after Eq. (3.25) has been satisfied might be useful in separating the failure signature directions $C(\underline{b}_i - K\underline{d}_i)$ if their effect on these directions were known.

Two techniques for choosing K were explored: (1) the augmentation of A - λI and C each with one column prior to solution by matrix inversion, and (2) the minimum norm column solution of K. The first technique was used in a rather ad hoc manner since there is at present no systematic approach to constraining the degrees of freedom. The purpose of

[2] Note that the rank of C cannot be greater than the number of states.

augmenting C with a column, $\underline{c}$, is to make the matrix invertible. This places the restriction on the column $\underline{c}$ that it be independent of the columns of the matrix C. The matrix A - λI must be augmented with a column $\underline{a}$ in order to have the multiplication by the inverted augmented C matrix dimensionally correct. The solution for the gain matrix is then

$$K = [A - \lambda I \vdots \underline{a}] [C \vdots \underline{c}]^{-1} \tag{3.27}$$

A detection filter designed using this approach is evaluated in the following sections.

A second technique for obtaining the filter gain matrix is to use the pseudo inverse or generalized inverse (Reference 13) of C, $C^{\dagger}$, to calculate the gain matrix K whose columns are the minimum norm solutions of the equality Eq. (3.25). Here, K can be calculated

$$K = (A - \lambda I)C^{\dagger} \tag{3.28}$$

Note that this technique avoids explicit assignment of the twenty parameters in the augmentation approach. But imposing this minimum norm constraint on the ten fundamental degrees of freedom ultimately also lacks theoretical justification. A detection filter design using this approach will also be examined in the following section.

3.4 Test for Planar Failures

As described in Section 3.2, the plane in which the signature for a failure of the ith control surface lies for the detection filter is determined by the vectors $C(\underline{b}_i - K\underline{d}_i)$ and $\underline{d}_i$. A possible failure detection and isolation test is to calculate the orthogonal projection onto a particular failure plane. Then, the control surface associated with that failure plane would be identified as failed if the magnitude of the projection is greater than some threshold. If, however, one is willing

to make a slightly restrictive assumption about the form of the surface failure, it is possible to restrict the failure signature for a given control surface to two segments of the plane. The assumption is that the unexpected control input, n(t), be either always positive or always negative. The advantage of restricting the failure signatures to two plane segments is the failures should be more distinguishable; the disadvantage is that failures where n(t) is changing sign frequently may be difficult to detect. The initial evaluation of the detection filter only considered constant bias failures. For this subset of failures, n(t) was either positive or negative. Therefore, the planar test discussed below assumes that the failure signature for a given control surface is restricted to either of two plane segments.

Before discussing this test, however, the two plane segments must be defined. These failure signature plane segments can be determined by examining Eqs. (3.23) and (3.24). These equations for the state estimation error and the observation residual are repeated here for convenience.

$$\dot{\underline{q}}(t) = (A - KC)\underline{q}(t) + (\underline{b}_i - K\underline{d}_i)n(t) \qquad (3.23)$$

$$\underline{r}(t) = C\underline{q}(t) + \underline{d}_i n(t) \qquad (3.24)$$

Consider first the case where n(t) is positive. As described in Section 3.2, the $(\underline{b}_i - K\underline{d}_i)n(t)$ term in Eq. (3.23) would produce a unidirectional residual along $C(\underline{b}_i - K\underline{d}_i)$, except for the presence of the additive $\underline{d}_i n(t)$ term in the residual equation. Therefore, the failure signatures for n(t) positive will lie in the segment of the plane defined by the vectors $C(\underline{b}_i - K\underline{d}_i)$ and $\underline{d}_i$ (See Figure 3.2). For n(t) negative, the residual directions produced by the failure will be the negative of the vectors $C(\underline{b}_i - K\underline{d}_i)$ and $\underline{d}_i$. Therefore, the failure signatures for n(t) negative will lie in the segment of the plane defined by the negative of the vectors $C(\underline{b}_i - K\underline{d}_i)$ and $\underline{d}_i$.

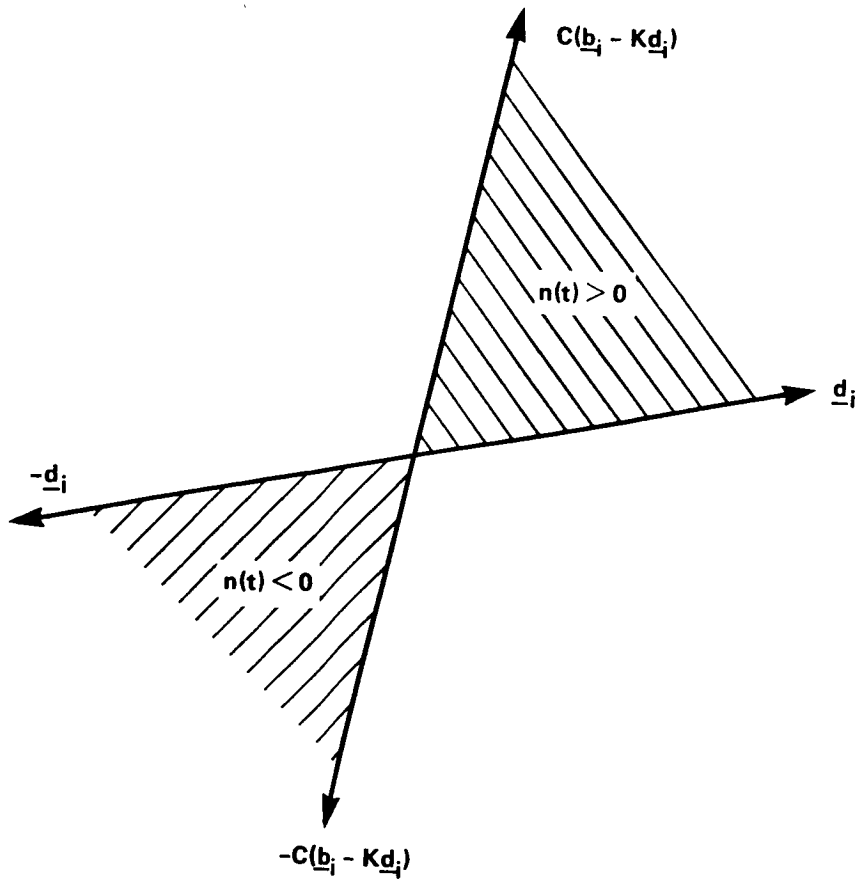

Figure 3.2. Signature regions corresponding to the failure of the ith control surface

The test to detect and isolate planar failures in this evaluation is the projection of the residual onto the two plane segments defined in Figure 3.3. This test is similar to the test described for sensor failures in Section 4.3.2 of Reference 8. The residual projection, in the case when the orthogonal projection of the residual onto a particular failure signature plane lies in either of the two plane segments, is simply the orthogonal projection onto the plane or the negative of the orthogonal projection. If the orthogonal projection lies outside these two plane segments, the residual projection is the projection of the residual or the negative of the projection onto the closest of the normalized $C(\underline{b}_i - K\underline{d}_i)$, $\underline{d}_i$, $-C(\underline{b}_i - K\underline{d}_i)$, or $-\underline{d}_i$.

3.5 Detection Filter Results

To design and test the detection filter, a single cruise flight condition at an altitude of 304.8 m (1000 ft) and an airspeed of 77.2 m/s (150 knots) was chosen. First, the specific choices made in designing the detection filter will be discussed, and then the simulation results produced by this filter will be presented.

As described previously in Section 3.3, the design of a detection filter was broken into three steps:

(1) measurement scaling selection

(2) eigenvalue selection

(3) gain matrix calculation

The measurements were scaled to have the units shown in Table 3.1, reducing the reliance of the detection filter on the airspeed and normal acceleration measurements in detecting and isolating failures and accentuating the contribution of the angular velocity and attitude measurements. The normal acceleration measurement was seriously affected by the turbulence while the angular velocity and attitude measurements were of better quality than the other measurements. In addition, the airspeed measurement was very noisy.

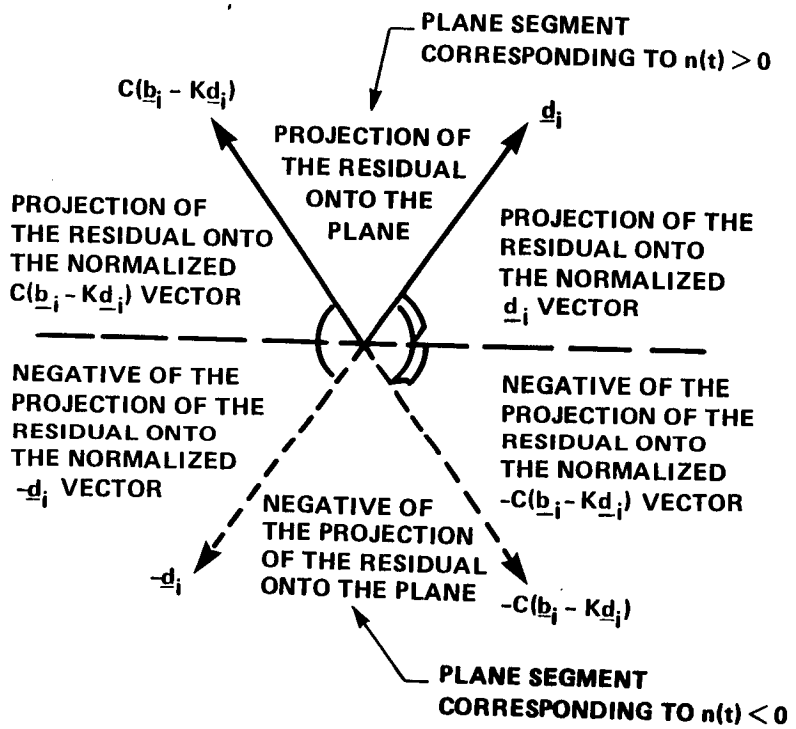

Figure 3.3. Detection filter planar test

Table 3.1. Measurement Units for Unmodified Detection Filter Evaluation

MEASUREMENT	UNITS	
Airspeed	7.6 m/s	25 ft/sec
Lateral Acceleration	0.3 m/s^2	ft/sec^2
Normal Acceleration	1.5 m/s	5 ft/sec^2
Angular Velocity	.0175 rad/sec	deg/sec
Attitude	.0175 rad	degrees
Altitude Rate	0.3 m/s	ft/sec
Altitude	0.3 m	ft

The detection filter eigenvalue was chosen to be approximately twice as fast as the fastest eigenvalue of the system. Specifically, the discrete-time eigenvalue chosen was 0.95. For the sample time of 20 ms used in the simulation, .95 corresponds approximately to an eigenvalue of -2.6 (a time constant of .4 s) in continuous-time domain.

Finally, the gain matrix may be calculated by either the augmentation of the C matrix or by using the pseudo-inverse of C. The detection filter for which simulation results are presented was designed using the augmentation approach. The ten degrees of freedom associated with the underdetermination of the gain matrix were removed by eliminating the effect of one measurement on the filter. In order to determine which measurement to eliminate, detection filters were designed with each eliminating the effect of a different measurement. The normal acceleration measurement was chosen for suppression because this maximized the signature plane separation. The normal acceleration measurement was still used in the calculation of the residual and therefore in detecting and isolating failures. However, the effect of the measurement on the filter was eliminated by forcing the corresponding column of the gain matrix to be zero.

This design produced elevator and rudder failure signature planes that were orthogonal to each other and to all of the other failure planes. However, the separation between the failure planes corresponding to the ailerons and the flaps were much smaller. For the purpose of defining a measure of separation between these planes, the eleven-dimensional residual space may be reduced to a three-dimensional space, since all but three components of the vectors which define these planes are approximately zero. These three components are the normal acceleration, body axis roll rate, and altitude rate components, and thus these measurements will be most sensitive to these control surface failures. In a three-dimensional space, the angle between signature planes is a possible measure of separation and is the measure used here. The

separation between the failure planes for the two ailerons was about 0.349 rad (20°); the separation between failure planes corresponding to the aileron and the flap on the same wing was about 0.5235 rad (30°). Given these results, it might be anticipated that this detection filter should be able to detect and isolate elevator and rudder failures and be able to detect but not isolate wing surface failures.

The pseudo-inverse approach to calculating the detection filter gain matrix was also investigated. While the pseudo-inverse approach produced directions of the columns of C(B - KD) and D that were more separated than the augmentation approach, the failure signature planes were less distinct. Using the scaling presented in Table 3.1, the pseudo-inverse design resulted in identical failure planes for the two ailerons and about 0.349 rad (20°) separation between the failure planes corresponding to the aileron and the flap on the same wing. The failure plane segments for the two ailerons, while not overlapping as with other scalings tried with the pseudo-inverse approach, are adjacent to each other as shown in Figure 3.4, making isolation difficult.

As the detection filter designed using the augmentation approach produced slightly better plane separation, this filter was chosen for testing. The test cases for which results are presented in this section are described in Table 3.2. The results presented are in terms of the residual projected onto the two plane segments for each surface which was defined earlier in this section. These results are shown in Figures 3.5 through 3.13. In addition, the residual projection values were averaged from the time of failure until the end of the 40 s simulation run to approximately determine the size of the bias in the residual projection caused by the failure. These results are shown in Table 3.3. The residuals were low-pass filtered with a time constant of 1.0 s to reduce the effects of noise and turbulence.

Conclusions were made regarding the ability of the detection filter to detect and isolate failures using results from the nine test cases presented. FDI performance was assessed by comparing the magnitude

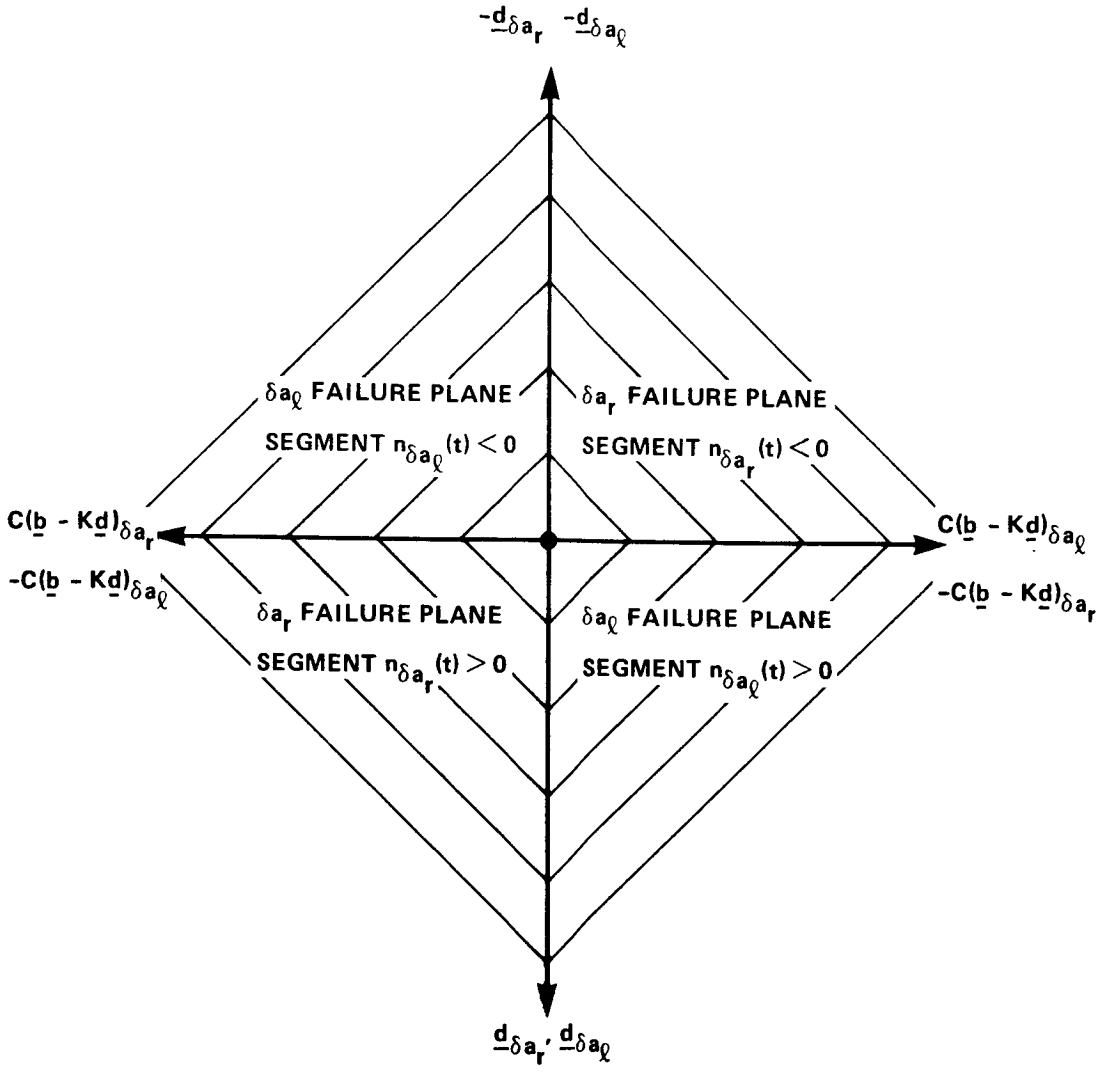

Figure 3.4. Failure plane segments for the left and right aileron

Table 3.2
Test Cases for the Evaluation of the Unmodified Detection Filter

ALTITUDE m (ft)	AIRSPEED m/s (knots)	SURFACE FAILED	FAILURE TYPE	MAGNITUDE	TIME OF OCCURRENCE (s)	TURBULENCE LEVEL m/s (ft/sec)	RESULTS IN FIGURE
304.8(1000)	77.2(150)	None				0.3(1.0)	3.5
304.8(1000)	77.2(150)	None				1.98(6.5)	3.6
304.8(1000)	77.2(150)	Elevator	bias	-0.0349 rad(-2°)	5	0.3(1.0)	3.7
304.8(1000)	77.2(150)	Elevator	bias	-0.0349 rad(-2°)	5	1.98(6.5)	3.8
304.8(1000)	77.2(150)	Rudder	bias	-0.0349 rad(-2°)	5	0.3(1.0)	3.9
304.8(1000)	77.2(150)	Right Aileron	bias	-0.0349 rad(-2°)	5	0.3(1.0)	3.10
304.8(1000)	77.2(150)	Right Flap	bias	10%	5	0.3(1.0)	3.11
457.2(5000)	102.8(200)	None				0.3(1.0)	3.12
457.2(5000)	102.8(200)	Right Aileron	bias	-0.0349 rad(-2°)	5	0.3(1.0)	3.13

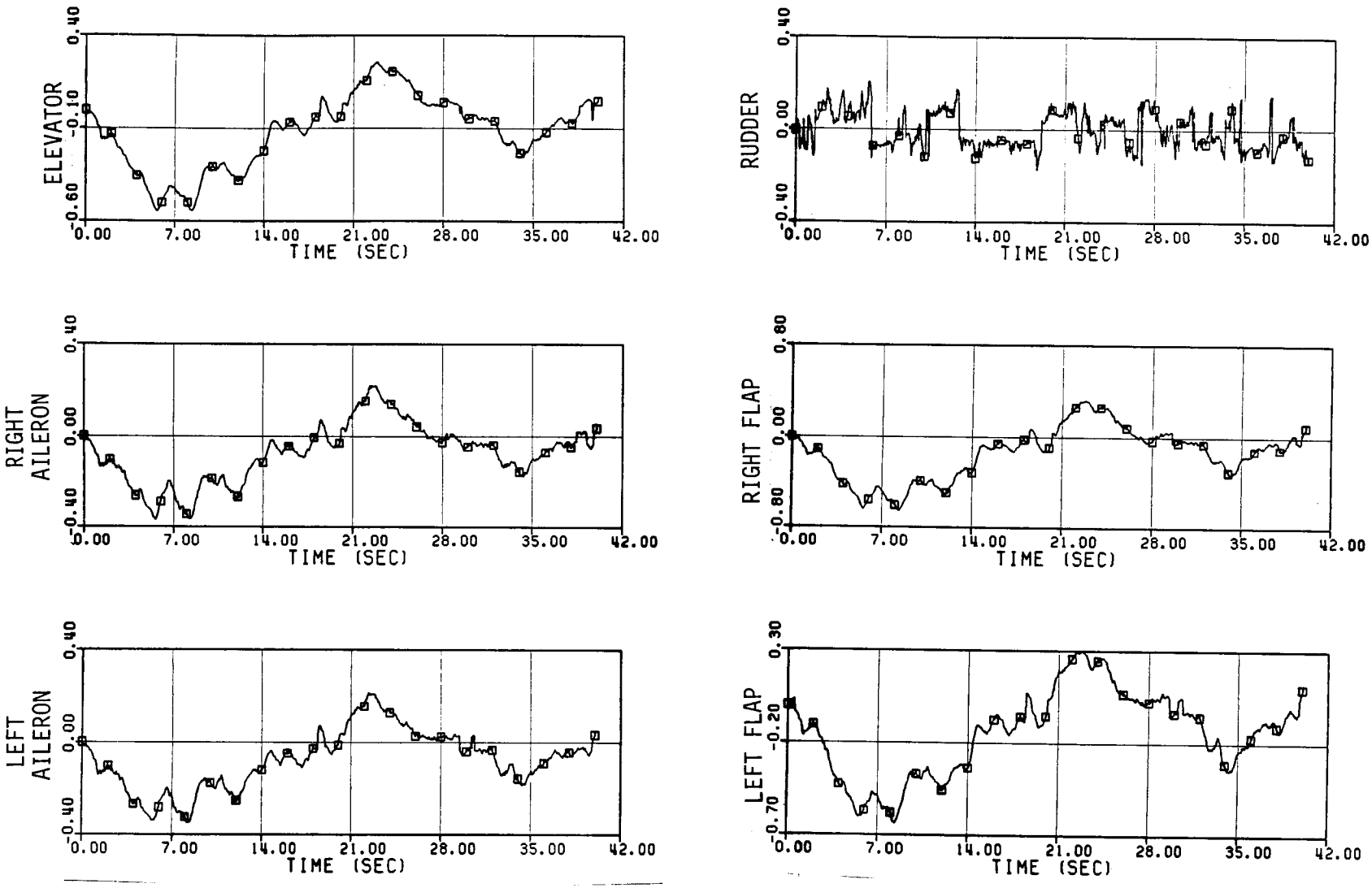

Figure 3.5. Projection of the residual onto the failure signature plane segments, no failure case, minor turbulence

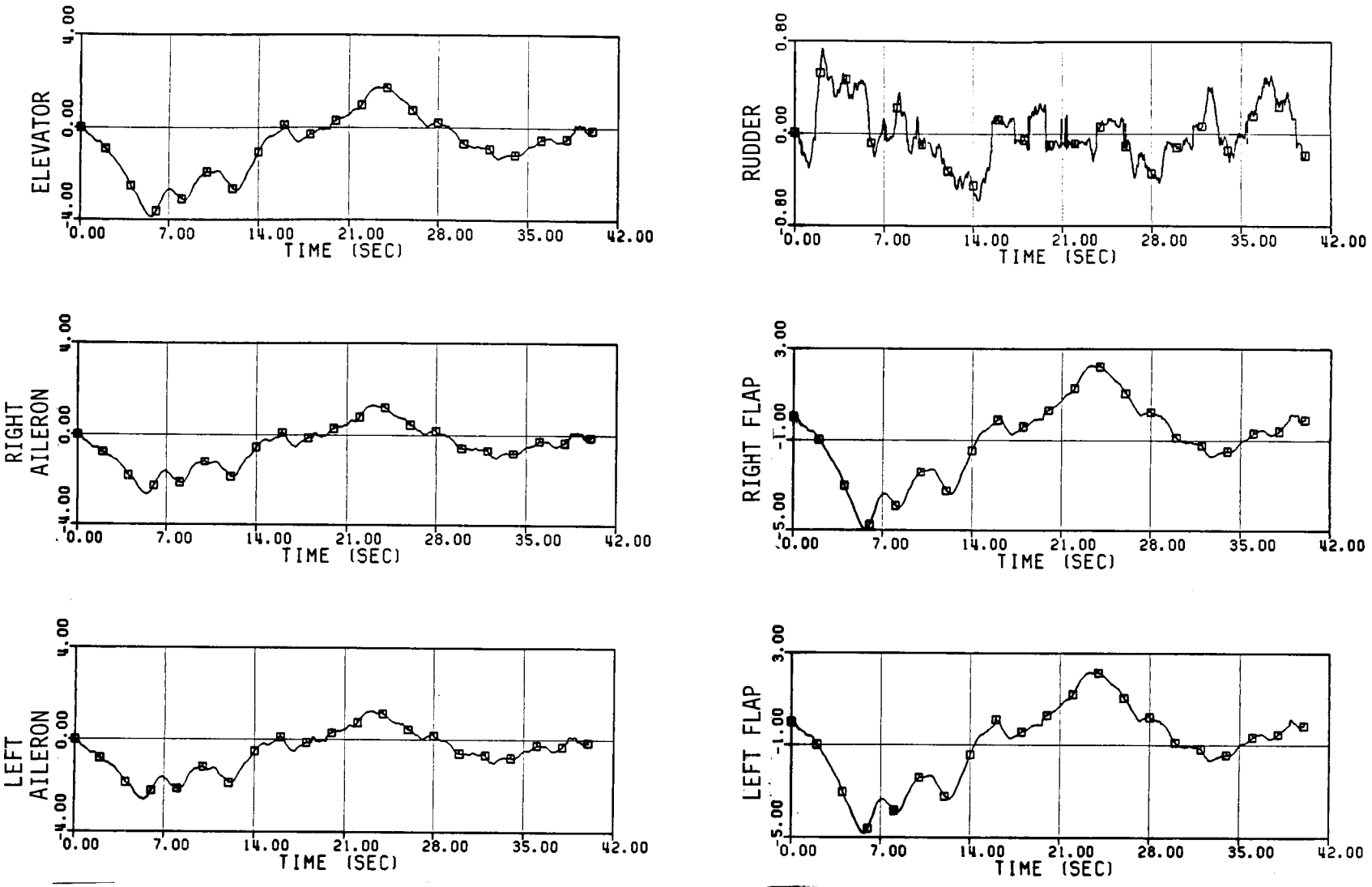

Figure 3.6. Projection of the residual onto the failure signature plane segments, no failure case, severe turbulence

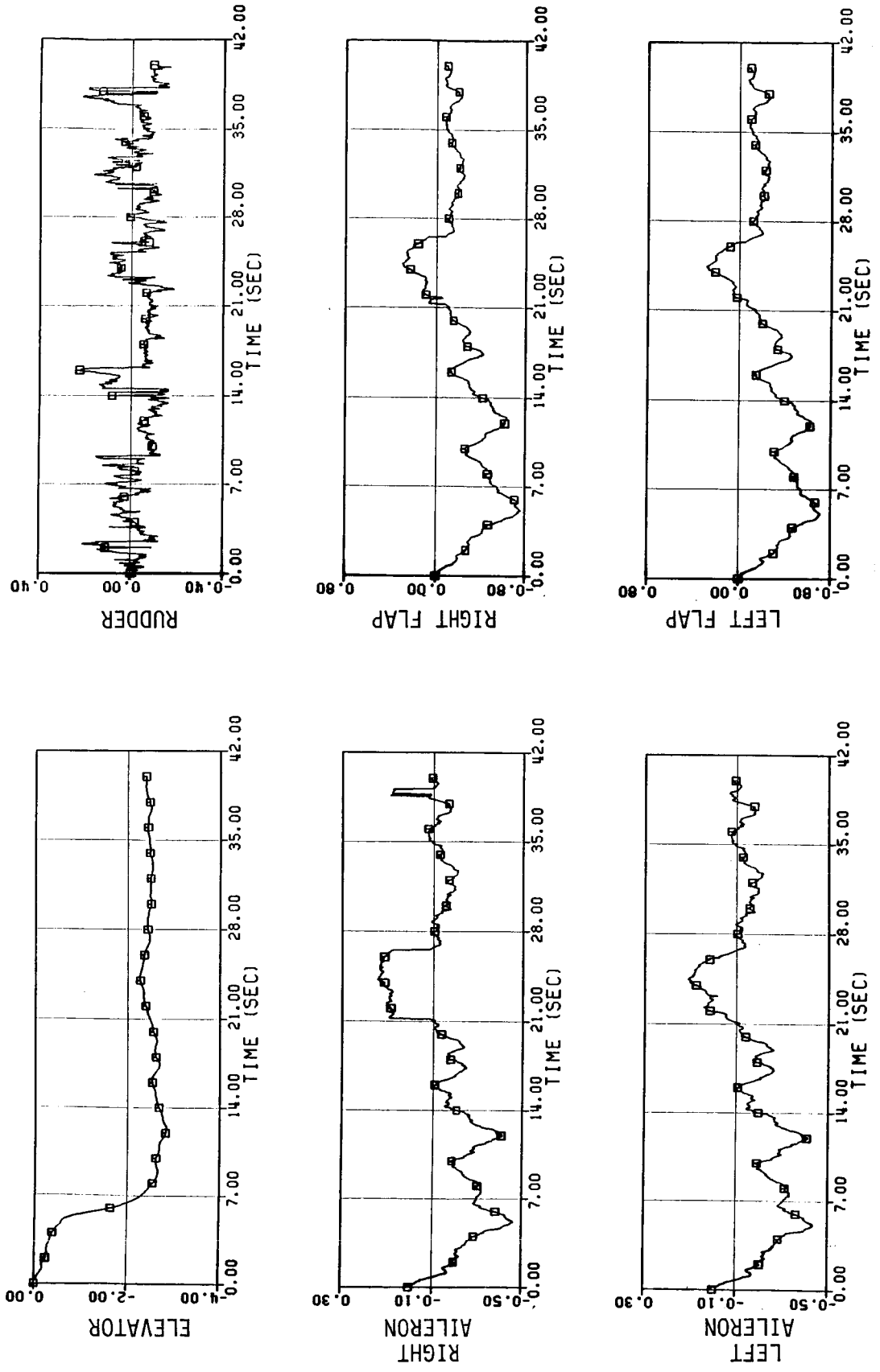

Figure 3.7. Projection of the residual onto the failure signature plane segments, elevator failure, -0.0349 rad (-2°) bias

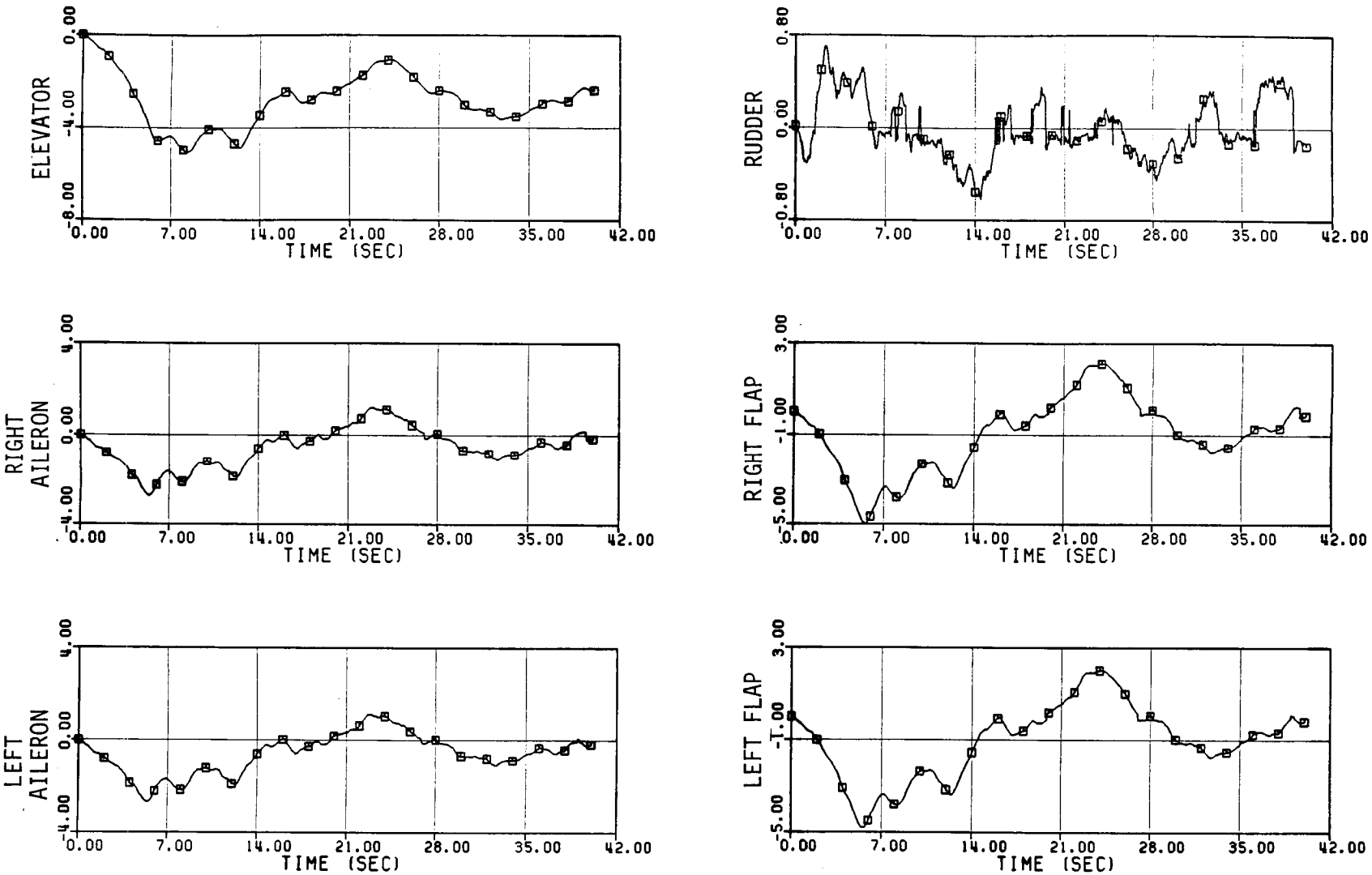

Figure 3.8. Projection of the residual onto the failure signature plane segments, elevator failure, -0.0349 rad (-2°) bias, severe turbulence

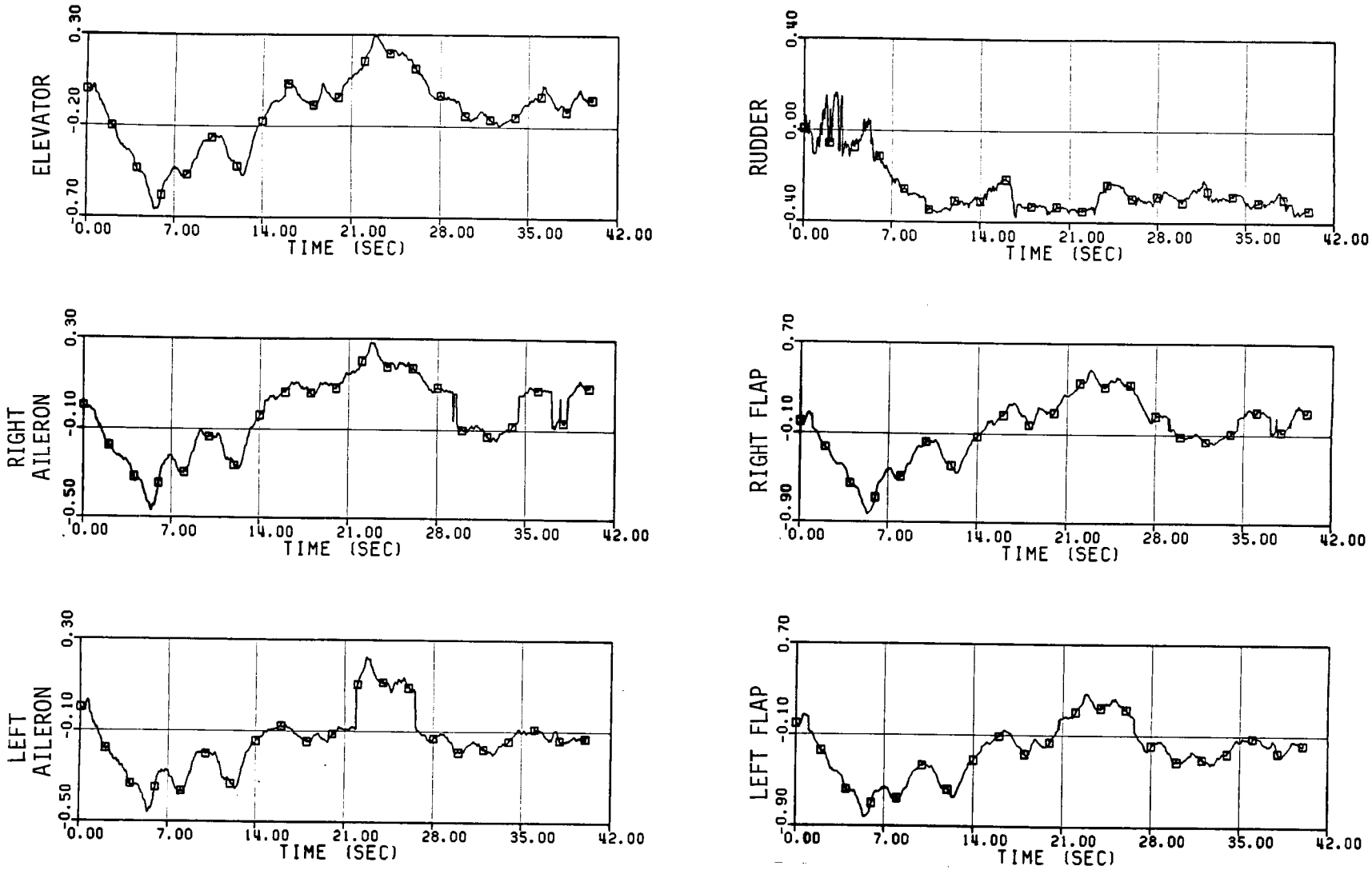

Figure 3.9. Projection of the residual onto the failure signature plane segments, rudder failure, -0.0349 rad (-2°) bias

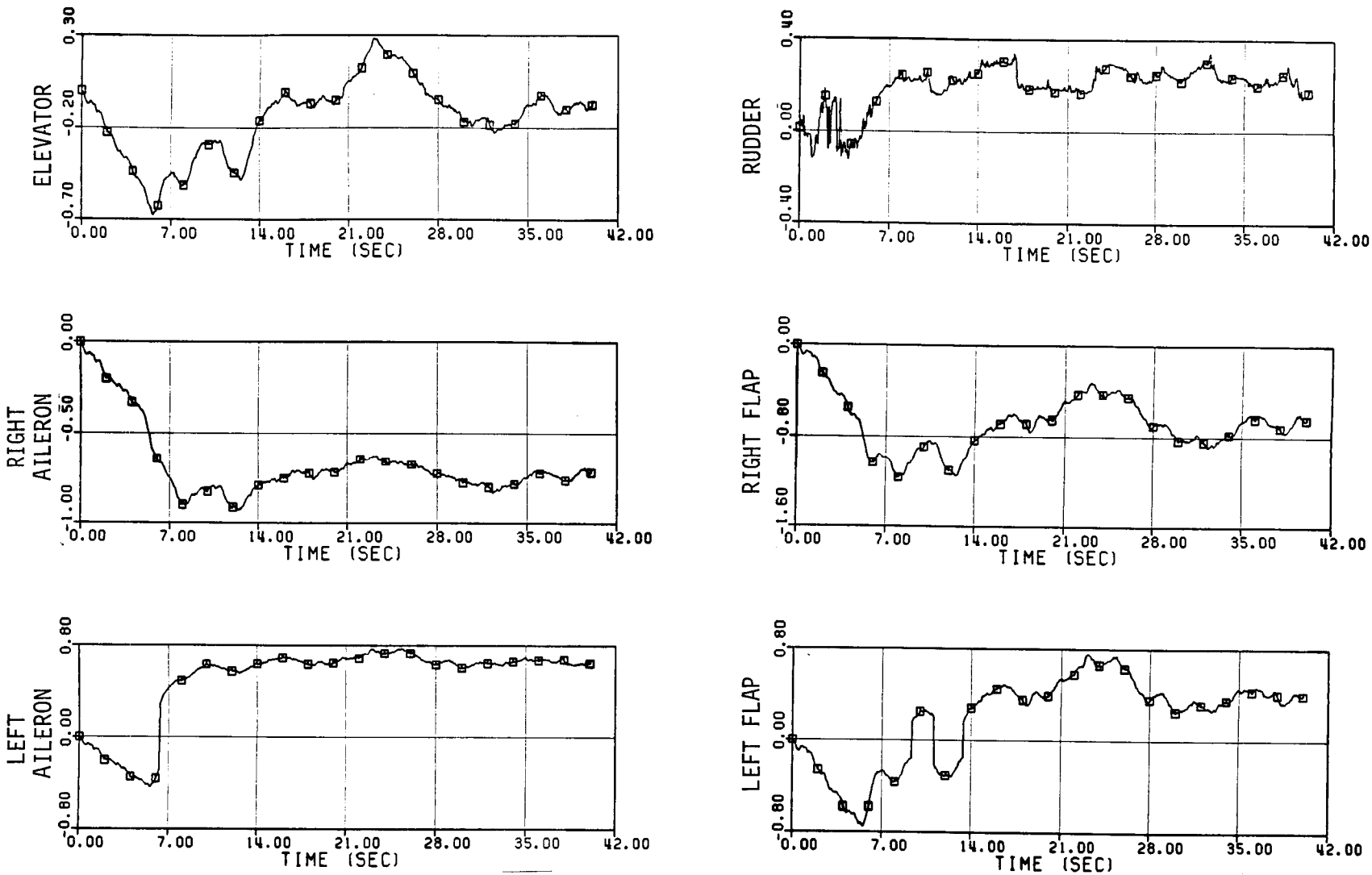

Figure 3.10. Projection of the residual onto the failure signature plane segments, right aileron failure, -0.0349 rad (-2°) bias

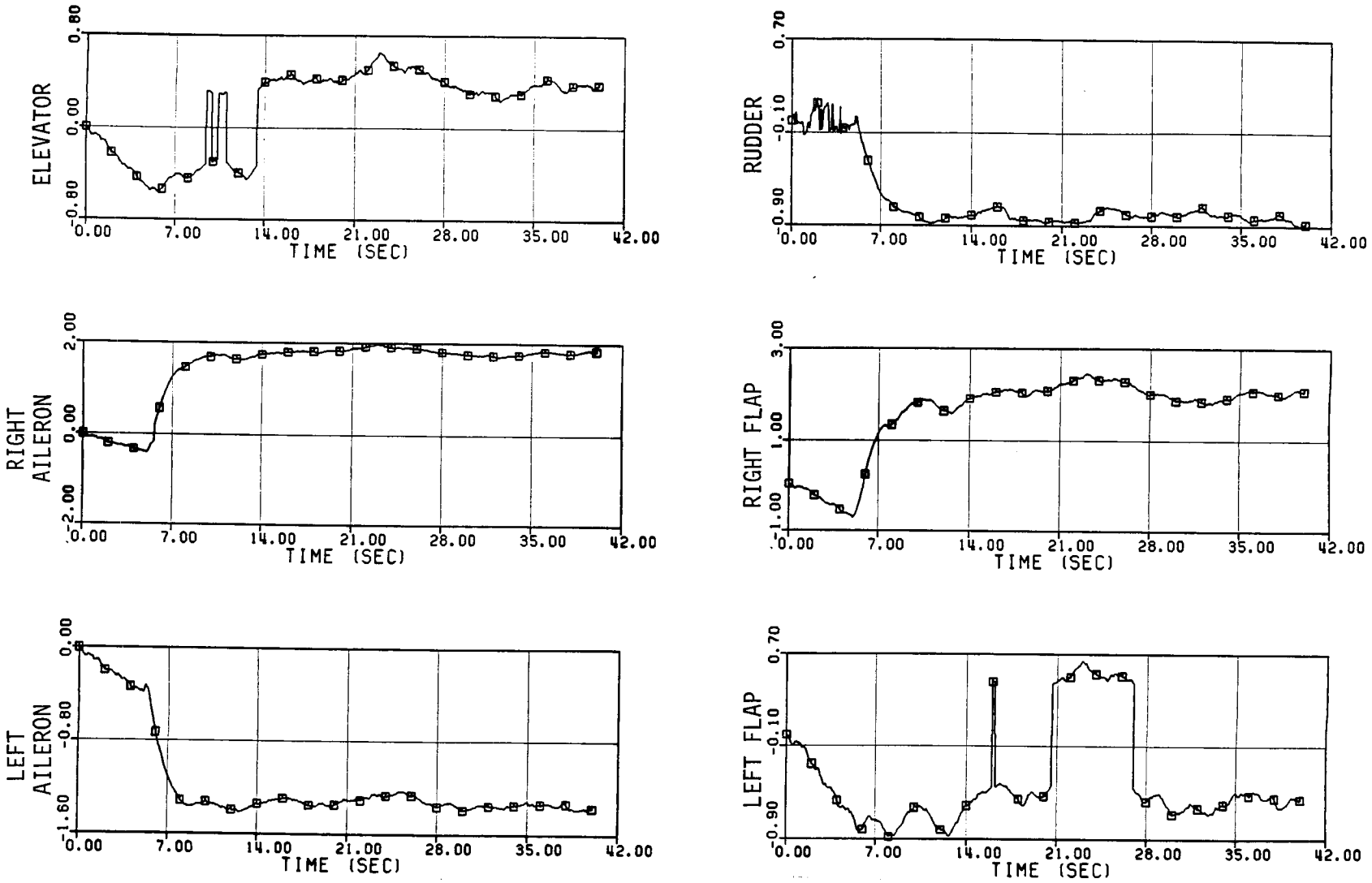

Figure 3.11. Projection of the residual onto the failure signature plane segments, right flap failure, 10% bias

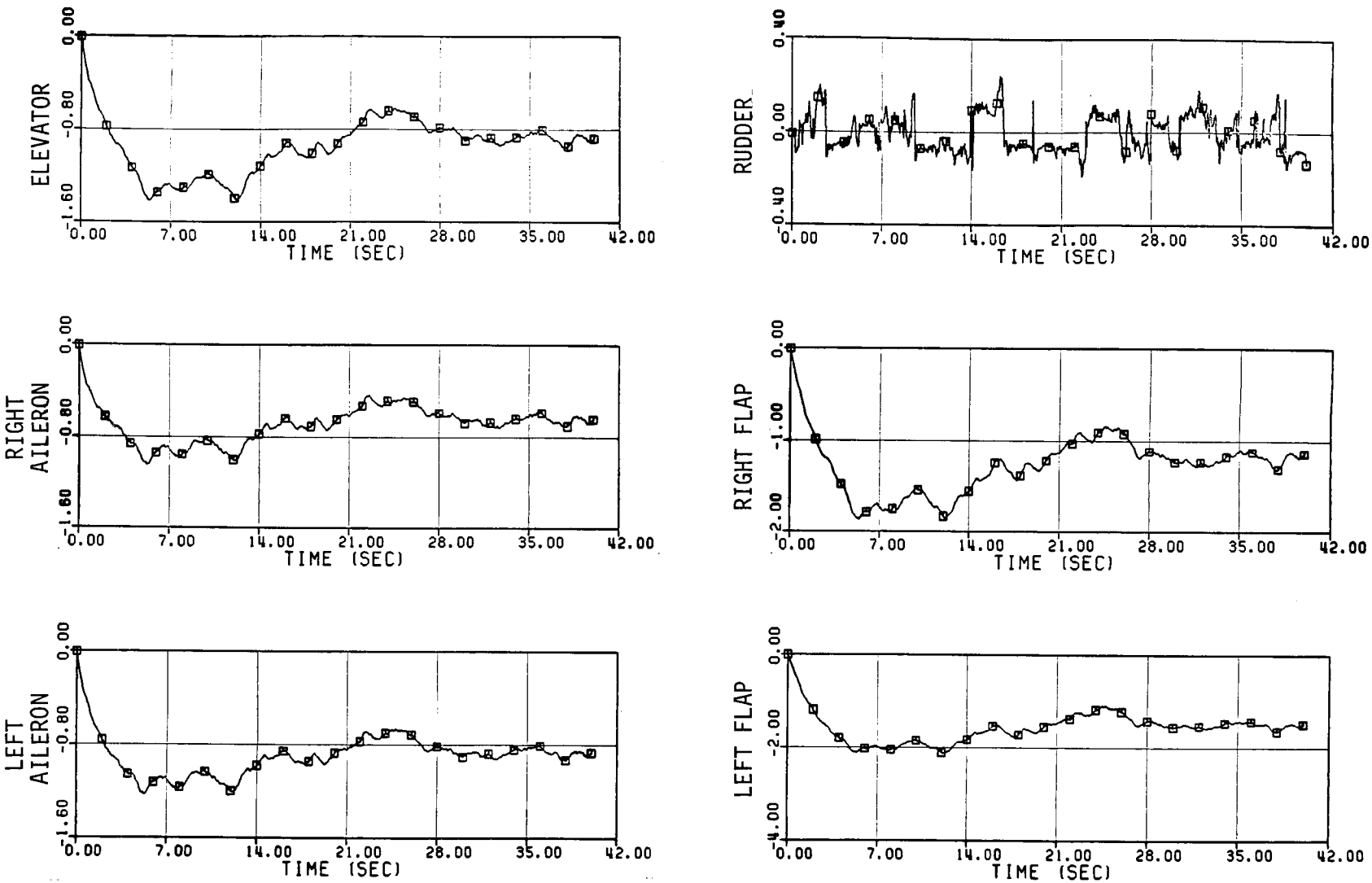

Figure 3.12. Projection of the residual onto the failure signature plane segments, no failure case, off-nominal cruise flight condition

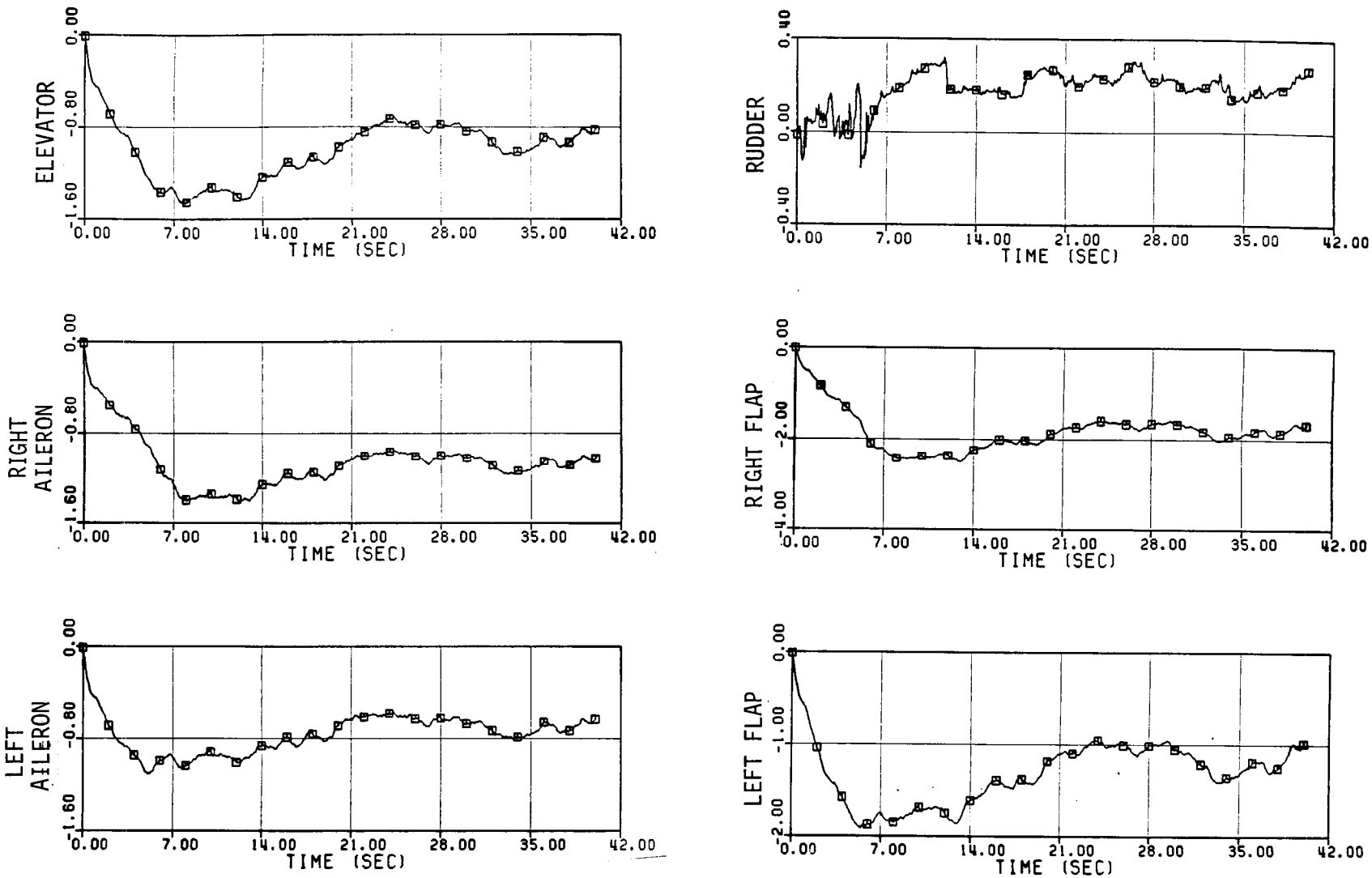

Figure 3.13. Projection of the residual onto the failure signature plane segments, right aileron failure, -0.0349 rad (-2°) bias, off-nominal cruise flight condition

Table 3.3
Mean Residual Projection Magnitudes for the
Unmodified Detection Filter

PROJECTION ONTO THE FAILURE SIGNATURE PLANE SEGMENTS FOR	FAILURE CASES								
	NOMINAL CRUISE CONDITION							OFF-NOMINAL CRUISE CONDITION	
	MINOR TURBULENCE					SEVERE TURBULENCE		MINOR TURBULENCE	
	NONE	ELEVATOR	RIGHT AILERON	RUDDER	RIGHT FLAP	NONE	ELEVATOR	NONE	RIGHT AILERON
Elevator	-0.10	-2.50	-0.14	-0.11	0.23*	-0.70	-3.01	-0.96	-1.04
Right Aileron	-0.07	-0.15	-0.75	-0.01	1.70	-0.46	-0.52	-0.70	-1.14
Left Aileron	-0.07	-0.16	0.60	-0.13	-1.29	-0.45	-0.53	-0.91	-0.77
Rudder	-0.01	-0.03	0.23	-0.29	-0.79	-0.03	-0.05	-0.01	0.20
Right Flap	-0.14	-0.22	-0.73	-0.04	1.89	-0.91	-0.96	-1.31	-1.95
Left Flap	-0.13	-0.24	0.28	-0.23	-0.40*	-0.89	-0.96	-1.61	-1.35

*Value not representative as the projection changes sign several times.

of the residual projections onto the planar segments as a result of the failures relative to the projections where a failure was not present. The following major conclusions were drawn.

(1) The detection filter was able to detect and isolate at least moderate elevator and rudder failures in the presence of noise and minor turbulence (0.3 m/s or 1 ft/s). A 0.0349 rad (2°) elevator bias failure test case is shown in Figure 3.7, while the 0.0349 rad (2°) rudder bias failure case is shown in Figure 3.9.

(2) The filter was able to detect but not isolate moderate wing surface (aileron and flap) failures in the presence of dis turbances. In the case of the right aileron failure shown in Figure 3.10, the detection filter correctly indicated that this surface had failed. However, the filter also indicated incorrectly that the failure might have occurred in the right flap or left aileron. A failure of the rudder has been eliminated as a possibility since it causes only a slight change in the aileron and flap residual projections (Figure 3.9). In the case of the right flap failure shown in Figure 3.11, the filter correctly detected a right flap failure but it also suggested that a right aileron failure was possible.

This difficulty in isolating wing surface failures is more a property of the system and the measurements chosen than the detection filter itself. The effect of the flaps and the ailerons were largely evident in the body axis roll rate and less evident in the normal acceleration, body axis yaw rate, and altitude rate measurements. However, the effects of the flaps and ailerons on the latter three measurements were not significant enough to be able to distinguish one aileron from the other or an aileron and a flap on the same wing.

(3) Based on the time of response for the decision function to reach a new steady state condition after a failure, the time to detect elevator and wing surface failures would be

approximately two seconds. The time required to detect a moderate rudder failure would be approximately five seconds. Detection times, in general, depend on the magnitude of the failure, the thresholds selected, the eigenvalue of the detection filter, and the time constant of the low-pass filter used to suppress noise in the residual.

(4) Turbulence significantly degrades the performance of the detection filter. By comparing the no-failure cases shown in Figures 3.5 and 3.6, severe turbulence (1.98 m/s or 6.5 ft/s) can be seen to increase the likelihood of false alarms. In addition, severe turbulence significantly degrades the ability of the detection filter to even detect a moderate elevator failure. This can be seen by comparing Figures 3.7 and 3.8.

(5) Modeling errors also degrade detection filter performance. In order to test this detection filter - which was designed for a cruise flight condition at an altitude of 304.8 m (1,000 ft) and an airspeed of 77.2 m/s (150 knots) - with regard to modeling errors, test cases were generated for the aircraft in a cruise flight condition at an altitude of 1524.0 m (5,000 ft) and an airspeed of 102.9 m/s (200 knots). The no-failure case shown in Figure 3.12 reveals a bias in most of the decision functions. The major reason for this bias is a nonzero body axis roll rate residual caused by modeling errors. This bias is likely to increase the false alarm rate and to degrade the filter's ability to detect wing surface failures. The right aileron bias failure test case at the off-nominal cruise condition is shown in Figure 3.13. One method of reducing the sensitivity of the detection filter to modeling errors might be to estimate the bias caused by mismodeling and appropriately compensate the residual.

3.6 Conclusions

The following general conclusions have been drawn from this phase of the study.

(1) The detection filter can be used to detect control surface failures.

(2) The detection filter can isolate failures of surfaces that produce independent effects on the aircraft but may not be able to isolate failures among surfaces that produce similar effects on the aircraft. The detection filter was unable to isolate wing surface (aileron and flap) failures. The main reason for this result is that these surfaces have similar effects on the aircraft dynamics. Isolation of failures will be difficult whenever there are functionally redundant control surfaces. If isolation of control surface failures is required for restructuring of the control system, additional software or hardware will be required.

(3) The magnitude of the failures that can be detected depends on the sensor noise, disturbances, and modeling errors. The detection filter was especially sensitive to turbulence and modeling errors. Moderate (-0.0349 rad (-2°) elevator, aileron, rudder and 10% flap) failures could be detected in minor turbulence. However, detecting moderate failures in severe turbulence was much more difficult. While hardover failures were not tested, they should be easily detected even in severe turbulence. Modeling errors also degraded the ability of the detection filter to detect moderate failures. Detection of hard failure, though, should still be possible.

(5) The failure detection and isolation times for the detection filter depend on the magnitude of the failure, the thresholds selected, the eigenvalue chosen for the detection filter, and the time constant of the low-pass filter, if any,

required to suppress noise in the residual. Approximately two seconds would be required to detect a moderate failure with the residual being low-pass filtered with a time constant of one second. Approximately five seconds would be required for a moderate rudder failure. Larger magnitude failures could be detected faster as much less, if any, filtering would be necessary. On the other hand, the detection and isolation of small magnitude failures would require heavy low-pass filtering for noise suppression which would impact the failure detection time because of the relatively long time required to reach steady state.

(6) Detection filter theory is mature for restructurable controls application to linear, time-invariant systems with no input-to-output coupling. This is not the case for systems with input-to-output coupling for which actuator or control surface failure signatures become planar instead of uni-directional. Another effect of coupling is that scaling now impacts detection filter performance and there is no systematic method available to use it to improve performance. In addition, no systematic method is available to use the degrees of freedom which exist by having more measurements than states. Finally, there is no theory for applying the detection filter to time-varying systems.

(7) There is limited experience in applying the detection filter to systems. References 8 and 12 describe two of these applications.

SECTION 4

A MODIFICATION TO THE DETECTION FILTER FOR SYSTEMS WITH DIRECT INPUT-TO-OUTPUT COUPLING

4.1 Introduction

This section presents and evaluates a modification to the basic detection filter. The basis and need for the consideration of the modified detection filter arises from a limitation of the basic detection filter when it is applied to the aircraft restructurable control systems problem. Basic detection filter theory has been developed for systems for which no direct input-output (control surface deflection to measurement) coupling exists. In this case, the detection filter is designed so that an actuator or a control surface failure produces a unidirectional filter residual. This residual direction depends only on the component (actuator or control surface) that has failed and is independent of the mode of the failure (e.g., bias, ramp, etc.). Therefore, failures are detected and isolated simply by observing the magnitude and the direction of the residual.

However, direct input-output coupling arises with regard to the restructurable controls problem because of acceleration measurements present on aircraft. As acceleration measurements are common onboard measurements and are, in general, of higher quality than angle of attack and sideslip angle measurements, detection filter design with direct input-to-output coupling was investigated instead of eliminating these measurements. The previous section on the detection filter showed that, with direct input-to-output coupling, the residual produced by an

actuator or control surface failure could be, at best, constrained to a plane using current detection filter design theory. Detection and isolation of failures with planer signatures is possible but more difficult.

This section presents and evaluates a modification to the detection filter to restore the unidirectional residual property produced by actuator or control surface failures when there is direct input-to-output coupling. The approach employed is to use secondary filtering of the detection filter residuals to produce unidirectional failure signatures. As before, the evaluation was conducted using the C-130 aircraft simulation. Failures were introduced into the simulation to assess the failure detection and identification capability of this modification.

The modification is presented in Section 4.2. The results are presented in Section 4.3, and Section 4.4 contains the conclusions of this evaluation of the modification of the detection filter.

4.2 Modification of the Detection Filter

The effect of direct input-output coupling on actuator failure signatures for the detection filter, discussed in Section 3.2, forms the basis for the material in this section. Recall that without basic modification of the detection filter, the effect of input-output coupling is to cause actuator failure signature to be planar instead of unidirectional. In the course of applying the detection filter to the restructurable control problem, it was discovered that secondary filtering of the detection filter residual could lead to unidirectional failure signatures even when there is direct coupling between inputs and measurements. Consider the discrete-time transfer function between the unexpected input from the ith actuator and the residual obtained by taking the z-transform of Eqs. (3.23) and (3.24).

$$\underline{r}(z) = [C(zI - A + KC)^{-1}(\underline{b}_i - K\underline{d}_i) + \underline{d}_i]n(z) \qquad (4.1)$$

Assuming that the detection filter gain matrix, K, is calculated to satisfy the relationship

$$A - KC = \lambda I \tag{4.2}$$

where λ is the selected detection filter eigenvalue, it follows that

$$\underline{r}(z) = \left[\frac{C(\underline{b}_i - K\underline{d}_i)}{z - \lambda} + \underline{d}_i \right] n(z) \tag{4.3}$$

If the contribution $\underline{d}_i n(z)$ could be filtered with the same time constant as in the detection filter, the failure signature would be unidirectional, lying along $C(\underline{b}_i - K\underline{d}_i) + \underline{d}_i$.

The secondary filtering scheme, then, has several elements. First, the components of the residual along the event vectors $\underline{d}_i$ are separated from the residual. Then they are filtered using the detection filter time constant. Finally, these filtered components are then added to the other components, forming a new residual. It is this new residual that is used for failure detection and isolation.

In order for the initial separation of the components along $\underline{d}_i$ to be possible, all event vectors $\underline{d}_i$ must be mutually independent, and each must be independent of the hyperplane formed by the $C(\underline{b}_i - K\underline{d}_i)$ vectors. To obtain the components of the residual in the directions $\underline{d}_i$, first write the residual

$$\underline{r}(k) = \left[C(\underline{b}_1 - K\underline{d}_1)_N \;\middle|\; \cdots \middle| C(\underline{b}_6 - K\underline{d}_6)_N \middle| \tilde{\underline{d}}_{1N} \middle| \tilde{\underline{d}}_{2N} \middle| \right] \begin{bmatrix} c_1(k) \\ c_2(k) \\ \vdots \\ c_8(k) \end{bmatrix} \tag{4.4}$$

$$= P\underline{c}(k) \tag{4.5}$$

Here, $C(\underline{b}_i - K\underline{d}_i)$ has been normalized for each of the six actuators of

the present application, giving $C(\underline{b}_i - K\underline{d}_i)_N$, and $\tilde{\underline{d}}_{1N}$ and $\tilde{\underline{d}}_{2N}$ are the distinct directions among the columns of the D matrix (two in this application). The vector $\underline{c}(k)$ is obtained using

$$\underline{c}(k) = P^{\dagger}\underline{r}(k) \tag{4.6}$$

where $P^{\dagger}$ is the pseudoinverse (generalized inverse) [Reference 13] of P.

The magnitudes $c_7(k)$ and $c_8(k)$ of the components of r(k) along $\tilde{\underline{d}}_{1N}$ and $\tilde{\underline{d}}_{2N}$ are passed through a secondary two-state filter:

$$\underline{q}'(k) = \lambda I\underline{q}'(k-1) + \begin{bmatrix} c_7(k-1) \\ c_8(k-1) \end{bmatrix} \tag{4.7}$$

Substituting these filtered components for the unfiltered ones in $\underline{c}(k)$ leads to

$$\underline{c}_f(k) = \begin{bmatrix} c_1(k) \\ \vdots \\ c_6(k) \\ q_1'(k) \\ q_2'(k) \end{bmatrix} \tag{4.8}$$

Transforming this vector of components back into the original residual space results in

$$\underline{r}_f(k) = P\underline{c}_f(k) \tag{4.9}$$

Actuator failures may be detected and (simultaneously) isolated through projection of $\underline{r}_f(k)$ onto each of the six signature vectors $C(\underline{b}_i - K\underline{d}_i) + \underline{d}_i$.

In using the transformation P it has been assumed that $\underline{r}(k)$ lies in the eight-dimensional space spanned by columns of P. Applying transformations $P^\dagger$ and P leads to suppression of noise in the residual that is in directions orthogonal to the range of P. Because noise in these directions only interferes with failure detection and isolation, this suppression could be very beneficial.

The modified detection filter is shown in Figure 4.1. The operators S and R, where

$$S = \begin{bmatrix} 0 & 0 & 0 & 0 & 0 & 0 & 1 & 0 \\ 0 & 0 & 0 & 0 & 0 & 0 & 0 & 1 \end{bmatrix} \tag{4.10}$$

and

$$R = I_{8\times 8} - \underline{e}_7\underline{e}_7^T - \underline{e}_8\underline{e}_8^T \tag{4.11}$$

denote, respectively, the operations of forming the two-vector $[c_7 \; c_8]^T$ and of nulling out c_7 and c_8 in $\underline{c}$.

4.3 Modified Detection Filter Design

A number of modified detection filter designs were tested via simulation to evaluate the concept. As with the unmodified detection filter, all the designs assumed a nominal cruise condition of 77.2 m/sec (150 knots) at an altitude of 304.8 m (1000 ft). The modified detection filters were designed using the same approach as for the unmodified detection filter because the modification consists simply of augmenting the detection filter with secondary filtering of the residual. As the secondary filtering is determined entirely by the linear model of the

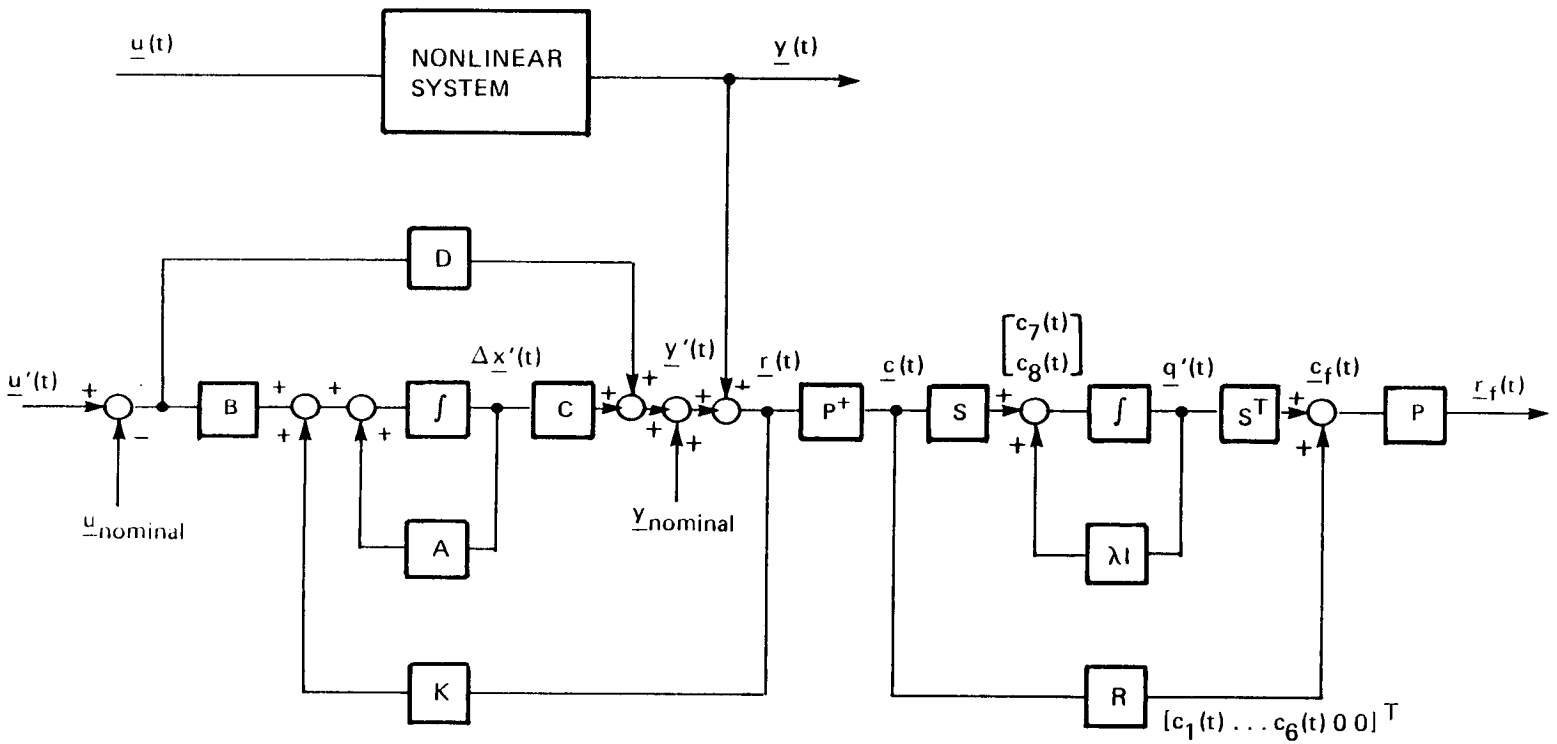

Figure 4.1. Block diagram of the modified detection filter

system, the gain matrix, and the detection filter eigenvalue, no design of the secondary filtering is required. Detection filter design, as presented in Section 3.3, consists of three steps:

(1) measurement scaling selection

(2) eigenvalue selection

(3) gain matrix calculation.

The selections which produced the best design are now described.

The measurements were scaled to have the units shown in Table 4.1. Note that these units differ from those selected for the unmodified detection filter in Table 3.1. The measurement units chosen reduce the dominance of the acceleration measurements, which are highly affected by turbulence, in detecting and isolating failures while increasing the contribution of the higher quality angular velocity and attitude measurements. Also, the airspeed residual was scaled to reduce the effect of the noisy airspeed sensor on the filter.

Scaling the lateral acceleration measurement also reduced some numerical errors produced by the secondary filtering. The idea of secondary filtering is to filter the portion of the residual produced by direct input-to-output coupling with the same time constant as the detection filter. Separating this portion of the residual from the total residual is not numerically exact. Therefore, a portion of the residual not associated with direct input-to-output coupling will be also filtered, producing small yet significant errors. (In addition, errors occur when some of the direct input-to-output contribution to the residual is not passed through the secondary filter. However, these errors are too small to have a significant effect.)

The eigenvalue chosen was the same one chosen for the unmodified detection filter. In discrete-time the eigenvalue chosen was 0.95. For the sample time of 20 ms used in the simulation, the equivalent continuous-time eigenvalue is -2.6.

Table 4.1
Measurement Units for Modified Detection Filter Evaluation

MEASUREMENT	UNITS	
Airspeed	7.6 m/s	25 ft/s
Lateral Acceleration	0.6 m/s^2	2 ft/s^2
Normal Acceleration	1.5 m/s	5 ft/s^2
Angular Velocity	.0056 rad/s	.318 deg/s
Attitude	.0175 rad	deg
Altitude Rate	0.3 m/s	ft/s
Altitude	0.3 m	ft

The gain matrix was also calculated using the same method used in producing the best design for the unmodified detection filter: the augmentation of the C matrix approach. As before, the effect of the normal acceleration measurement on the filter was suppressed by forcing the corresponding column of the gain matrix to be zero. The normal acceleration measurement was still used in the calculation of the residual and therefore in detecting and isolating failures.

4.4 Modified Detection Filter Results

The test cases used to evaluate the modified detection filter are described in Table 4.2. These cases included the no-failure simulation (Figure 4.2) and simulations of failures of elevator, right aileron, left aileron, right flap, and rudder (Figures 4.3 through 4.7) in the presence of low-level turbulence. To determine the effects of higher turbulence intensity, data for the no-failure case and the -0.0349 rad (2°) elevator bias failure case with a turbulence level of 0.3 m/s (6.5 ft/s) rather than the nominal 0.3 m/s (1 ft/s) were also processed. These results are shown in Figures 4.8 and 4.9, respectively. The cases described above assumed the aircraft to be at the nominal cruise condition of 77.2 m/s (150 knots) at an altitude of 304.8 m (1000 ft). The effect of modeling errors was determined by processing data for the no-failure and right aileron failure cases (Figures 4.10 and 4.11, respectively) at an off-nominal cruise condition using the filter designed for the nominal cruise flight condition. All failure onsets occurred at five seconds, and sensor noise was also simulated. The residuals were not low-pass filtered as they were for the unmodified detection filter, however.

Figure 4.2 shows the projection of the residual vector $\underline{r}_f$ onto each of the unitized failure signature directions for the no-failure case. Only the system noise and the unmodeled dynamics influence the residual after the filter transients die away. Turbulence affects the modified detection filter residual projections more than those of the

Table 4.2
Test Cases for the Evaluation of the Modified Detection Filter

ALTITUDE m (ft)	AIRSPEED (knots) m/s	SURFACE FAILED	FAILURE TYPE	MAGNITUDE	TIME OF OCCURRENCE (s)	TURBULENCE m/sec (ft/s)	RESULTS IN FIGURE
304.8(1000)	77.2(150)	None				0.3 (1.0)	4.2
304.8(1000)	77.2(150)	Elevator	bias	-0.0349 rad(-2°)	5	0.3 (1.0)	4.3
304.8(1000)	77.2(150)	Right Aileron	bias	-0.0349 rad(-2°)	5	0.3 (1.0)	4.4
304.8(1000)	77.2(150)	Left Aileron	bias	-0.0349 rad(-2°)	5	0.3 (1.0)	4.5
304.8(1000)	77.2(150)	Right Flap	bias	10%	5	0.3 (1.0)	4.6
304.8(1000)	77.2(150)	Rudder	bias	-0.0349 rad(-2°)	5	0.3 (1.0)	4.7
304.8(1000)	77.2(150)	None				1.98 (6.5)	4.8
304.8(1000)	77.2(150)	Elevator	bias	-0.0349 rad(-2°)	5	1.98 (6.5)	4.9
457.2(5000)	102.8(200)	None				0.3 (1.0)	4.10
457.2(5000)	102.8(200)	Right Aileron	bias	-0.0349 rad(-2°)	5	0.3 (1.0)	4.11

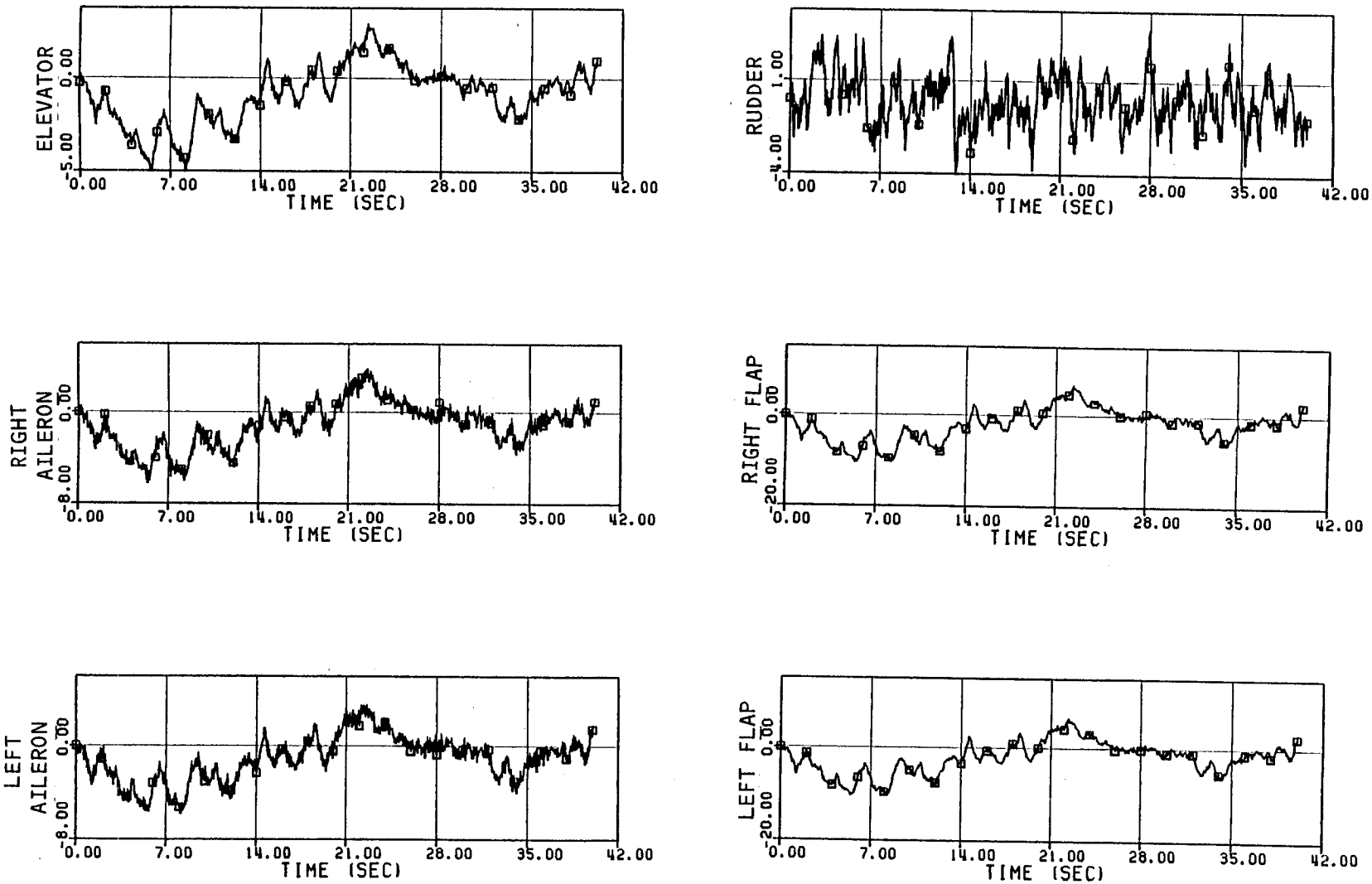

Figure 4.2. Projection of the residual onto the normalized expected failure signature directions - no failure case

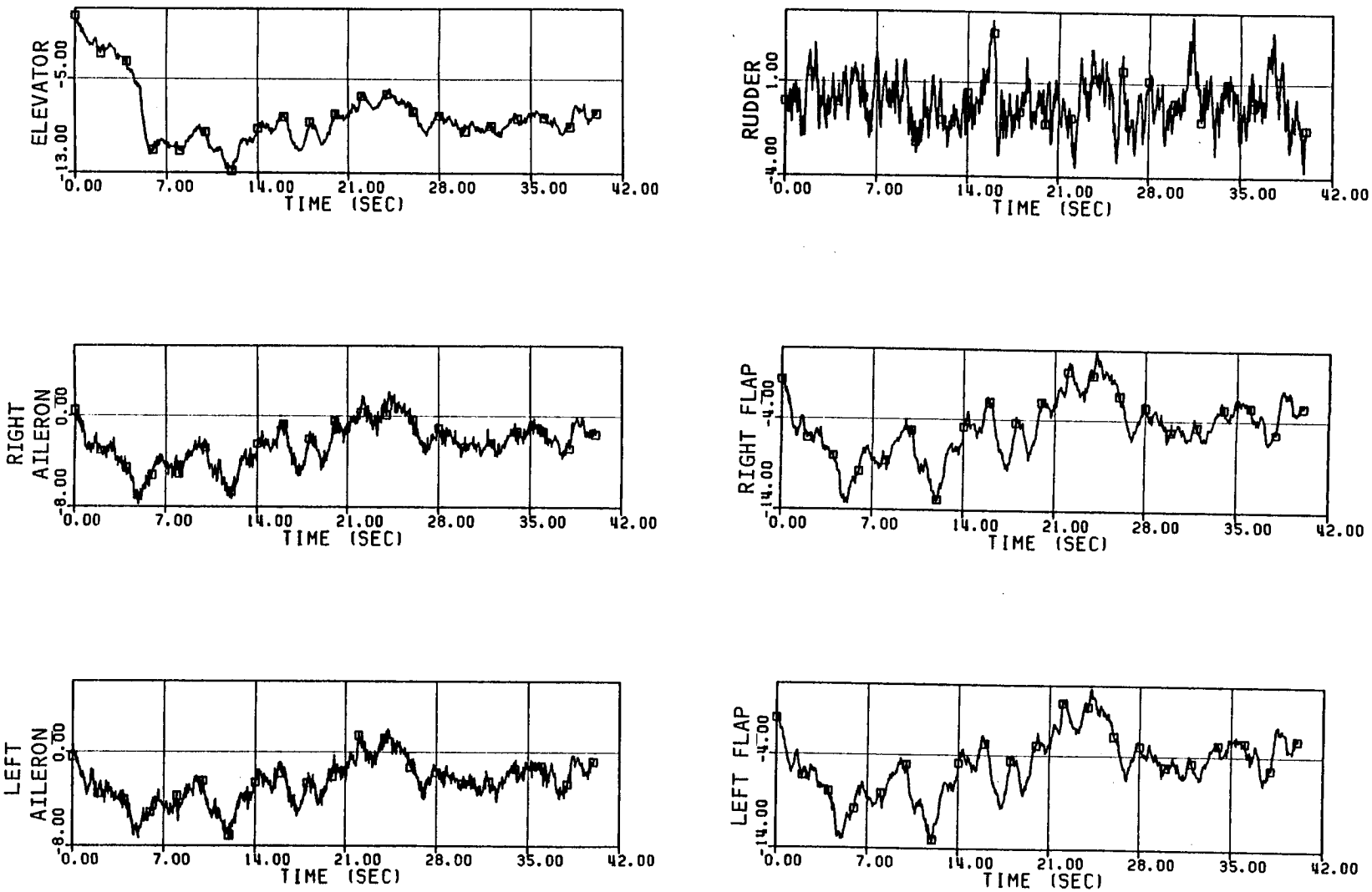

Figure 4.3. Projection of the residual onto the normalized expected failure signature directions - elevator failure (2° bias)

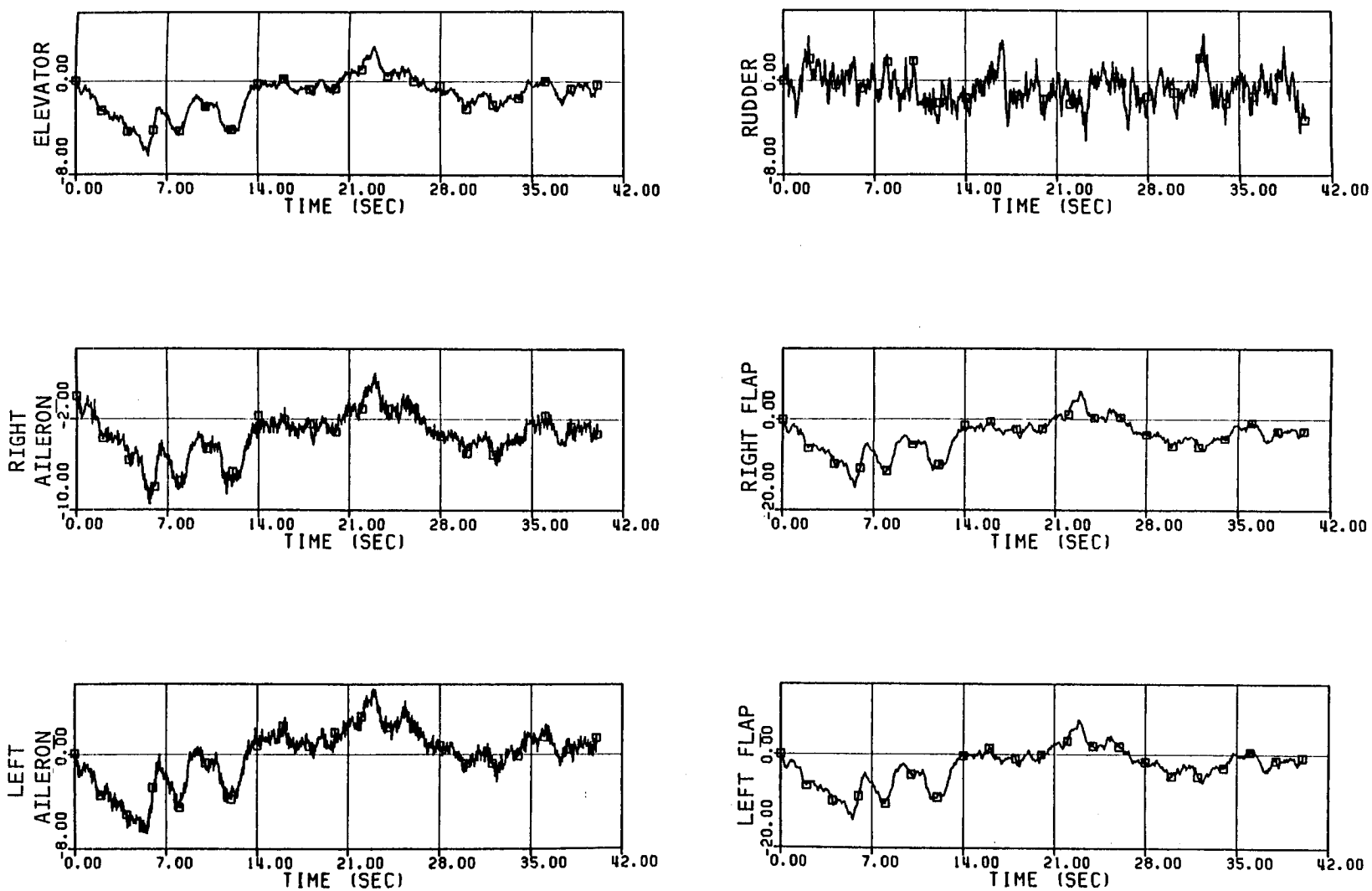

Figure 4.4. Projection of the residual onto the normalized expected failure signature directions, right aileron failure, -0.0349 rad (-2°) bias

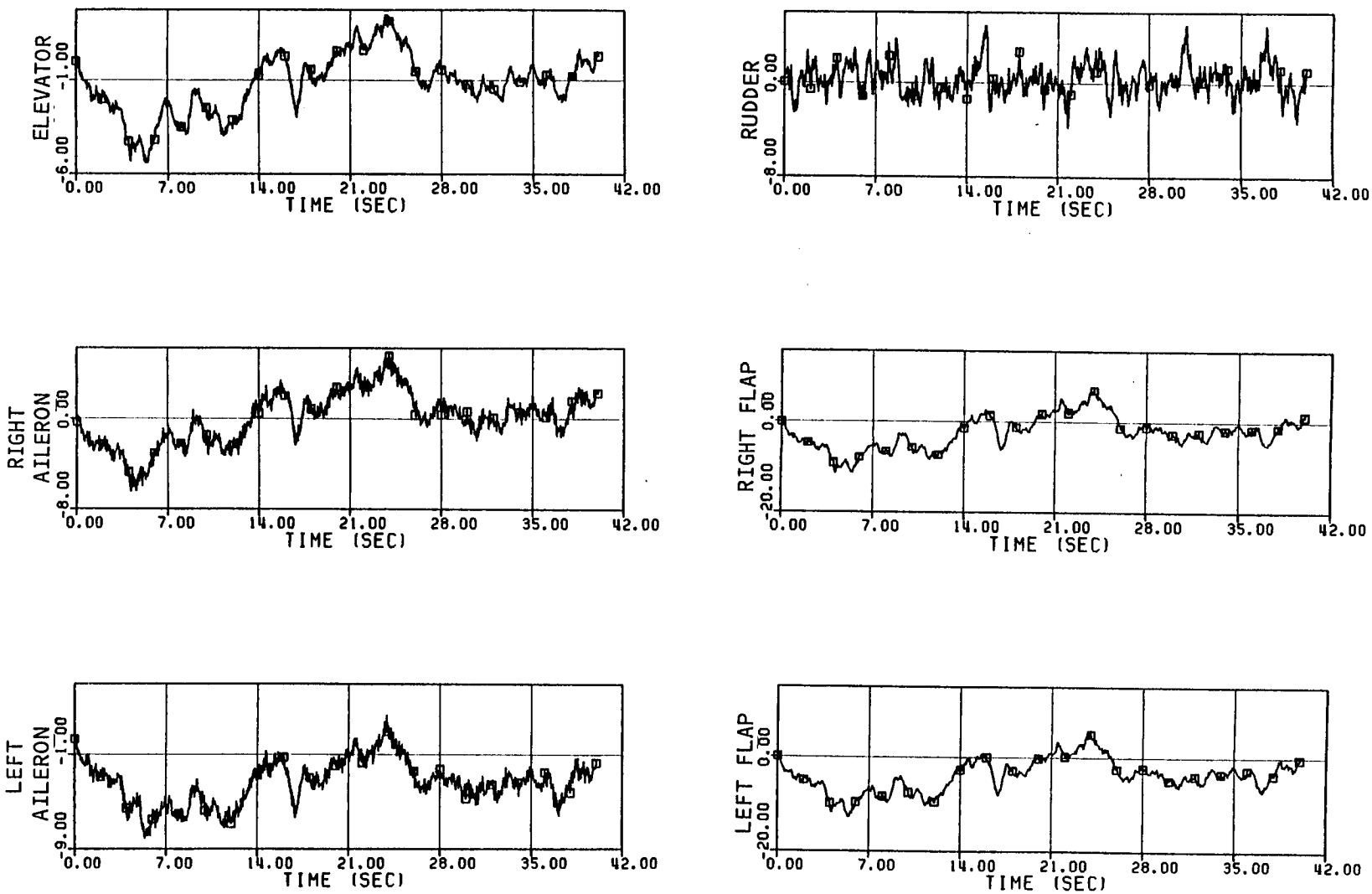

Figure 4.5. Projection of the residual onto the normalized expected failure signature directions, left aileron failure, -0.0349 rad (-2°) bias

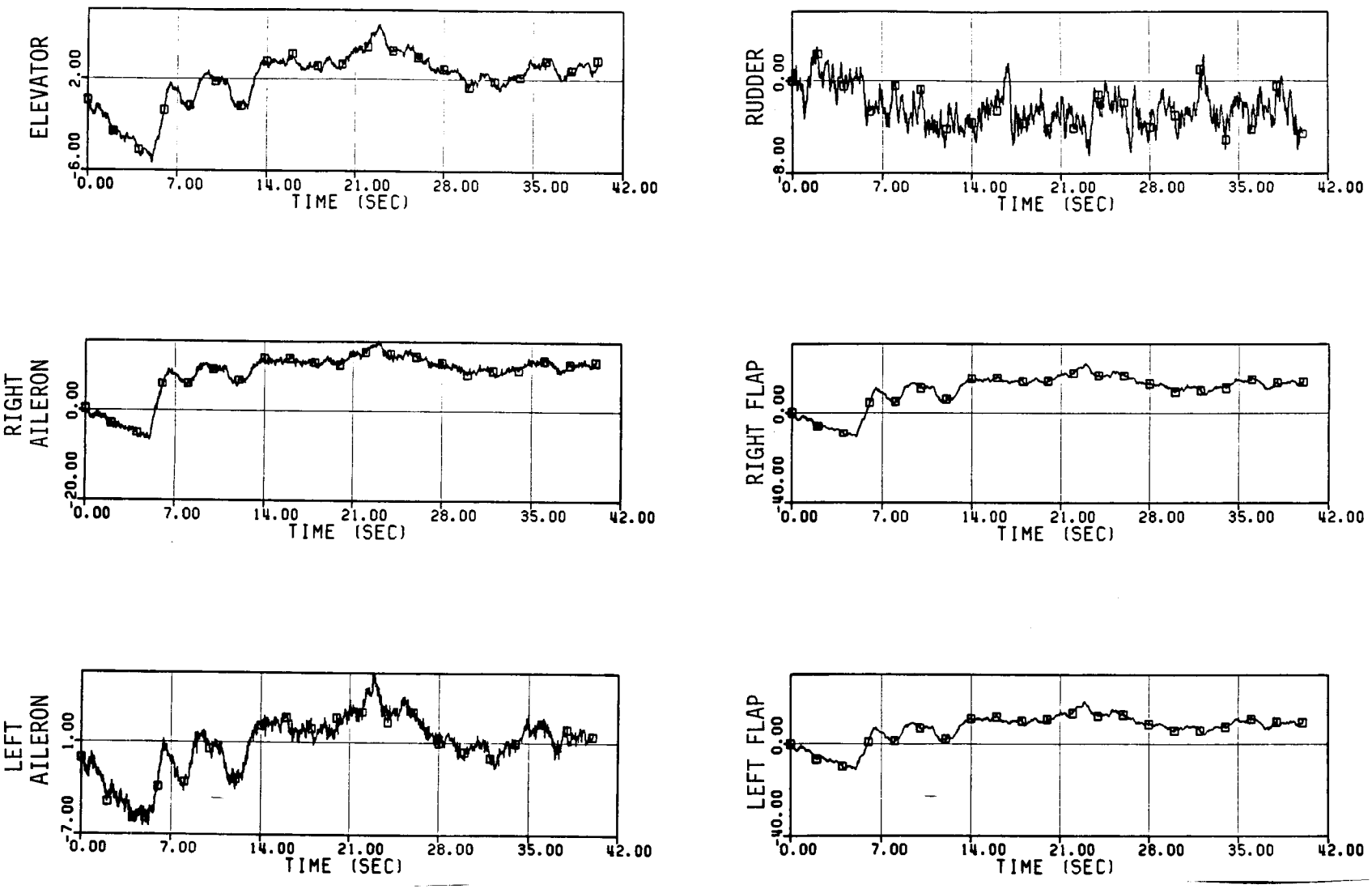

Figure 4.6. Projection of the residual onto the normalized expected failure signature directions, right flap failures, 10% bias

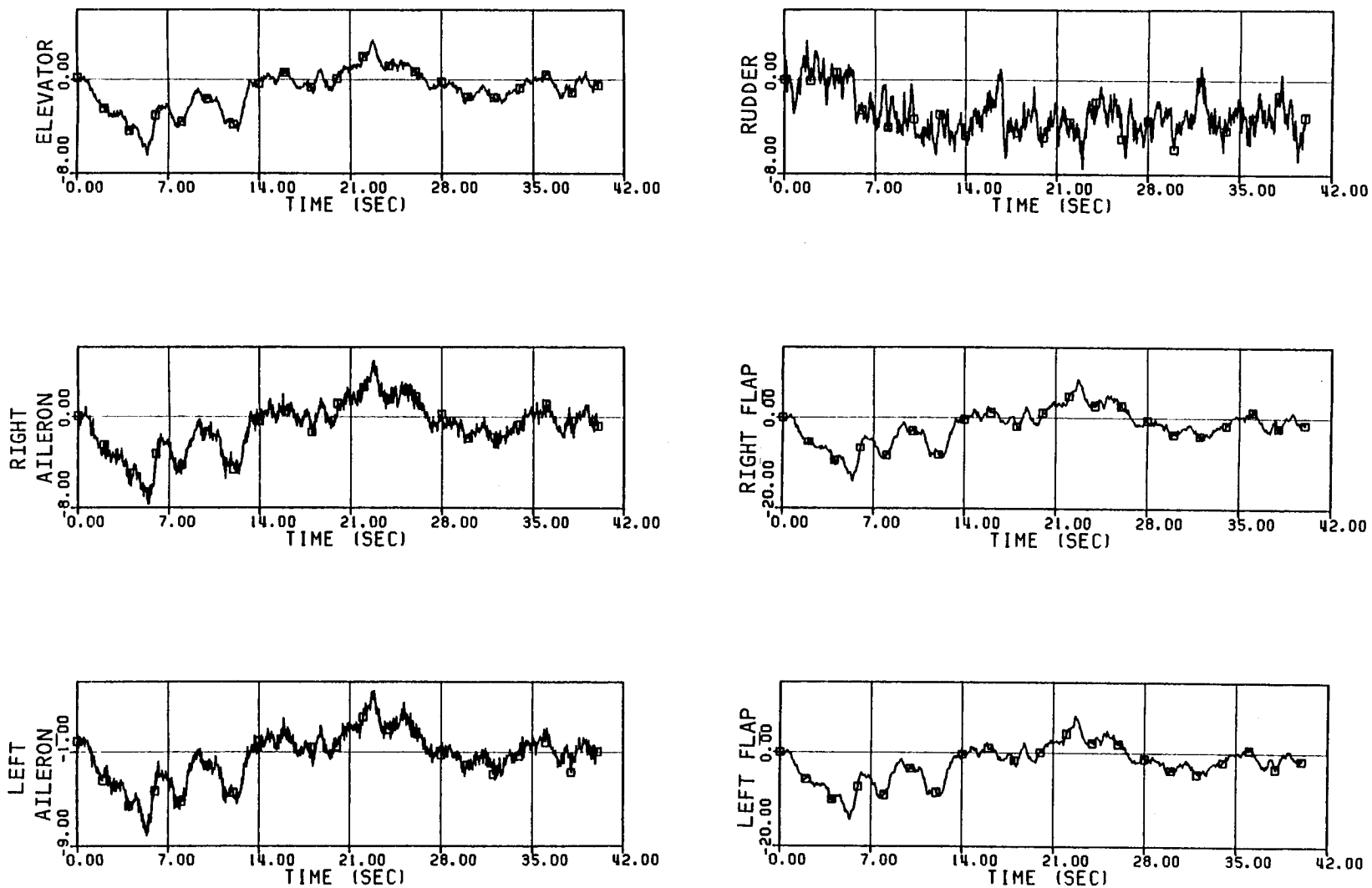

Figure 4.7. Projection of the residual onto the normalized expected failure signature directions, rudder failure, -0.9349 rad (-2^{o}) bias

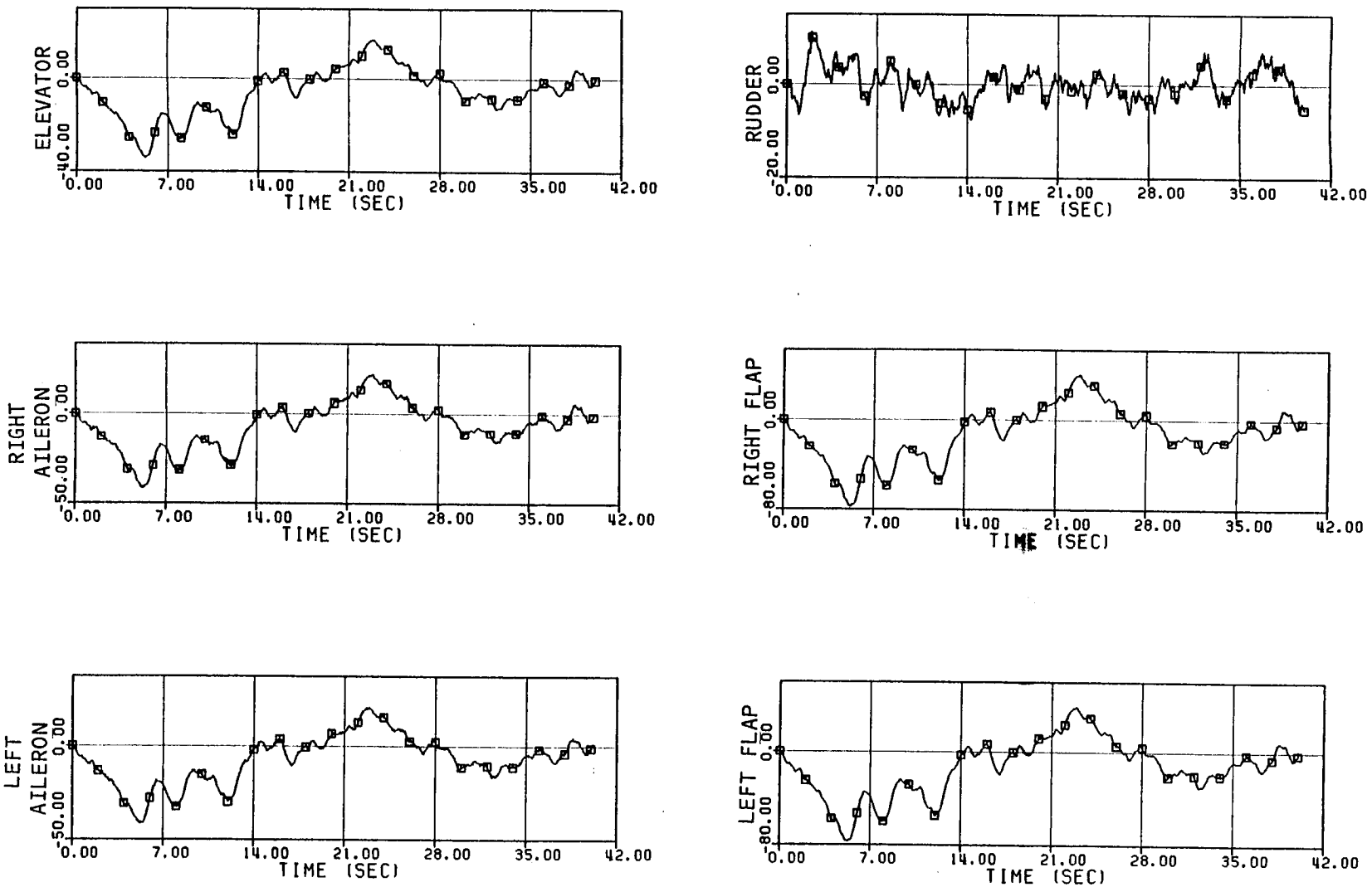

Figure 4.8. Projection of the residual onto the normalized expected failure signature directions, no failure case, severe turbulence

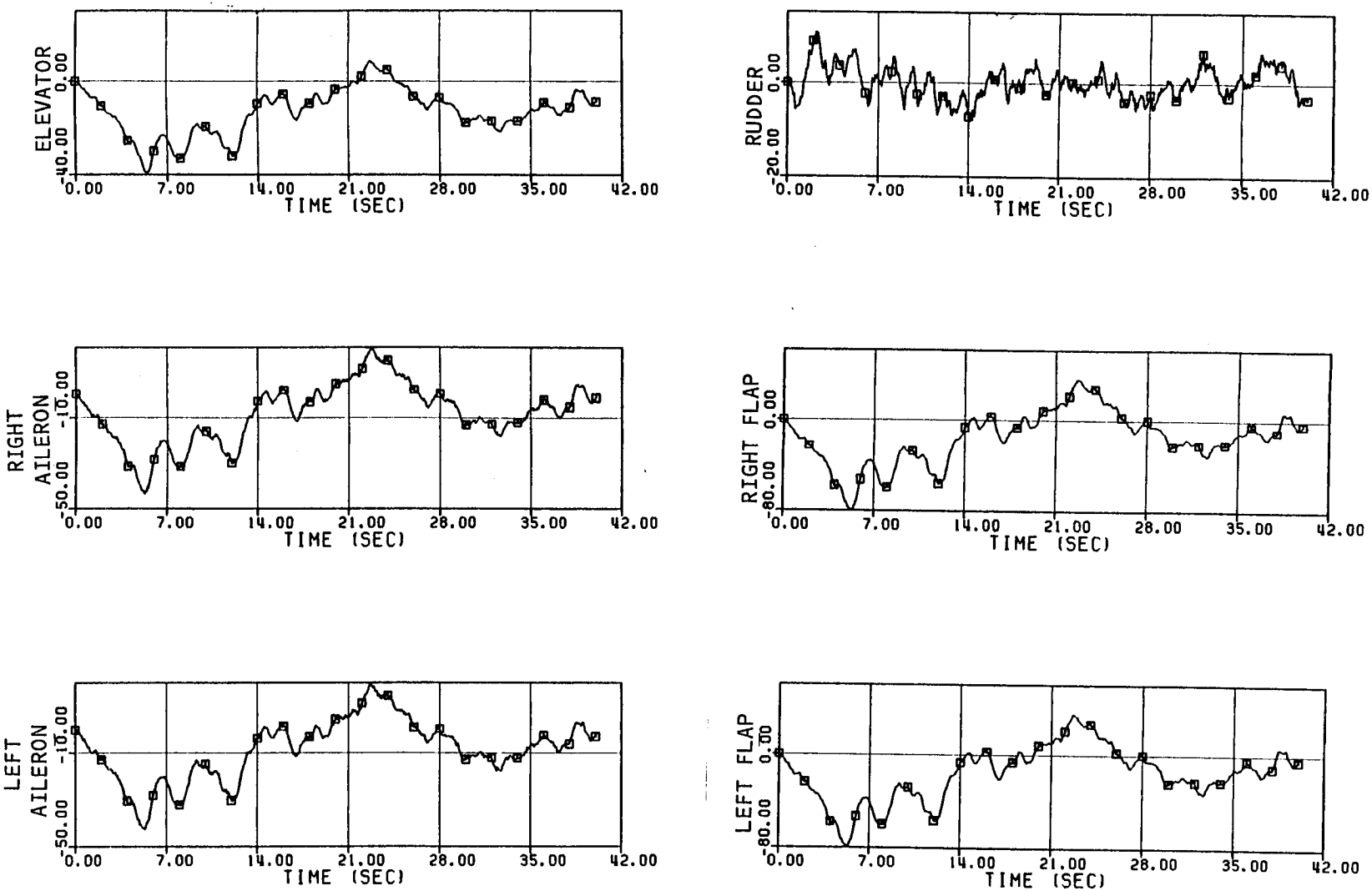

Figure 4.9. Projection of the residual onto the normalized expected failure signature directions, elevator failure, -0.0349 rad (-2°) bias, severe turbulence

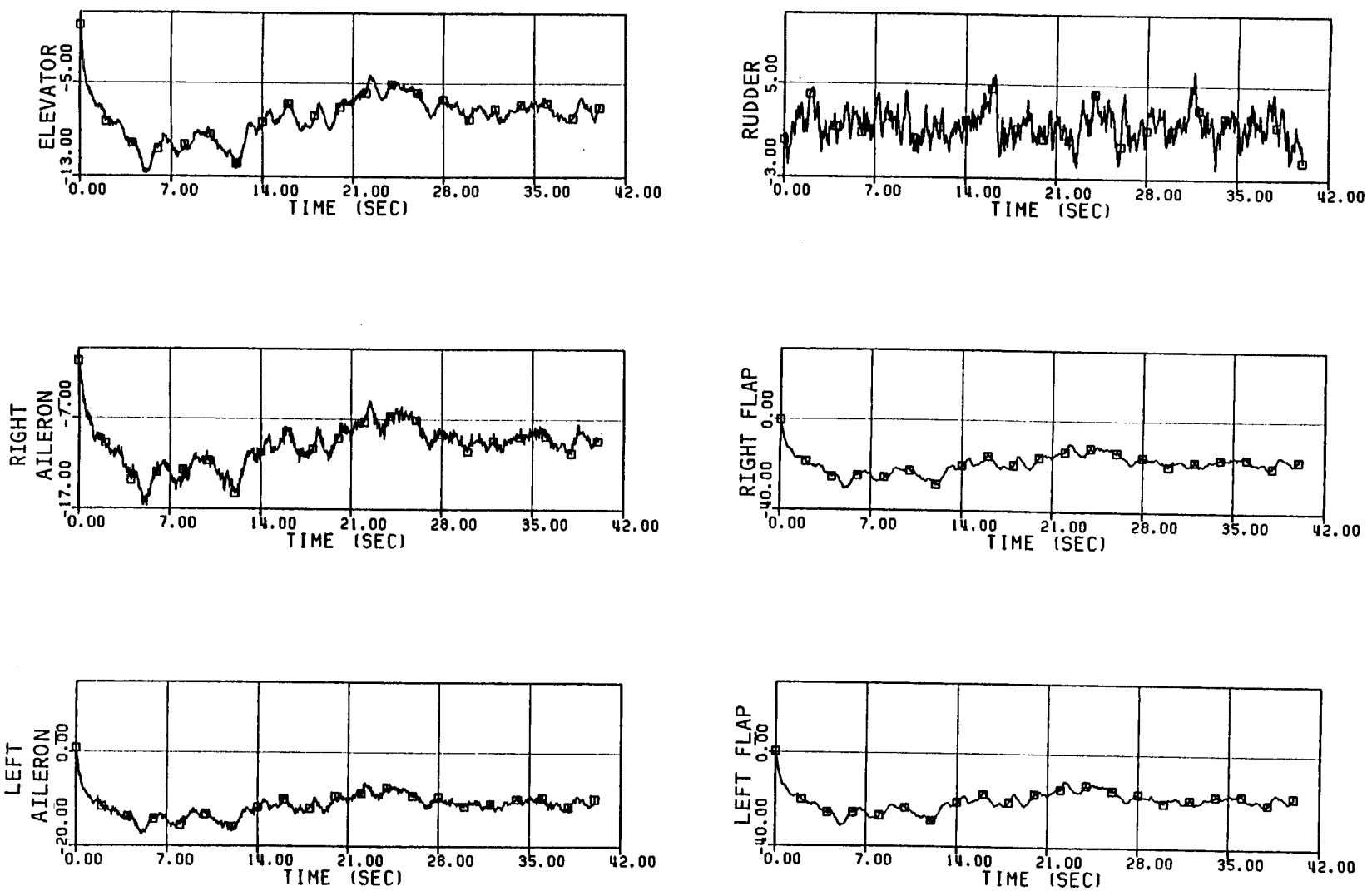

Figure 4.10. Projection of the residual onto the normalized expected failure signature directions, no failure case, off-nominal flight condition

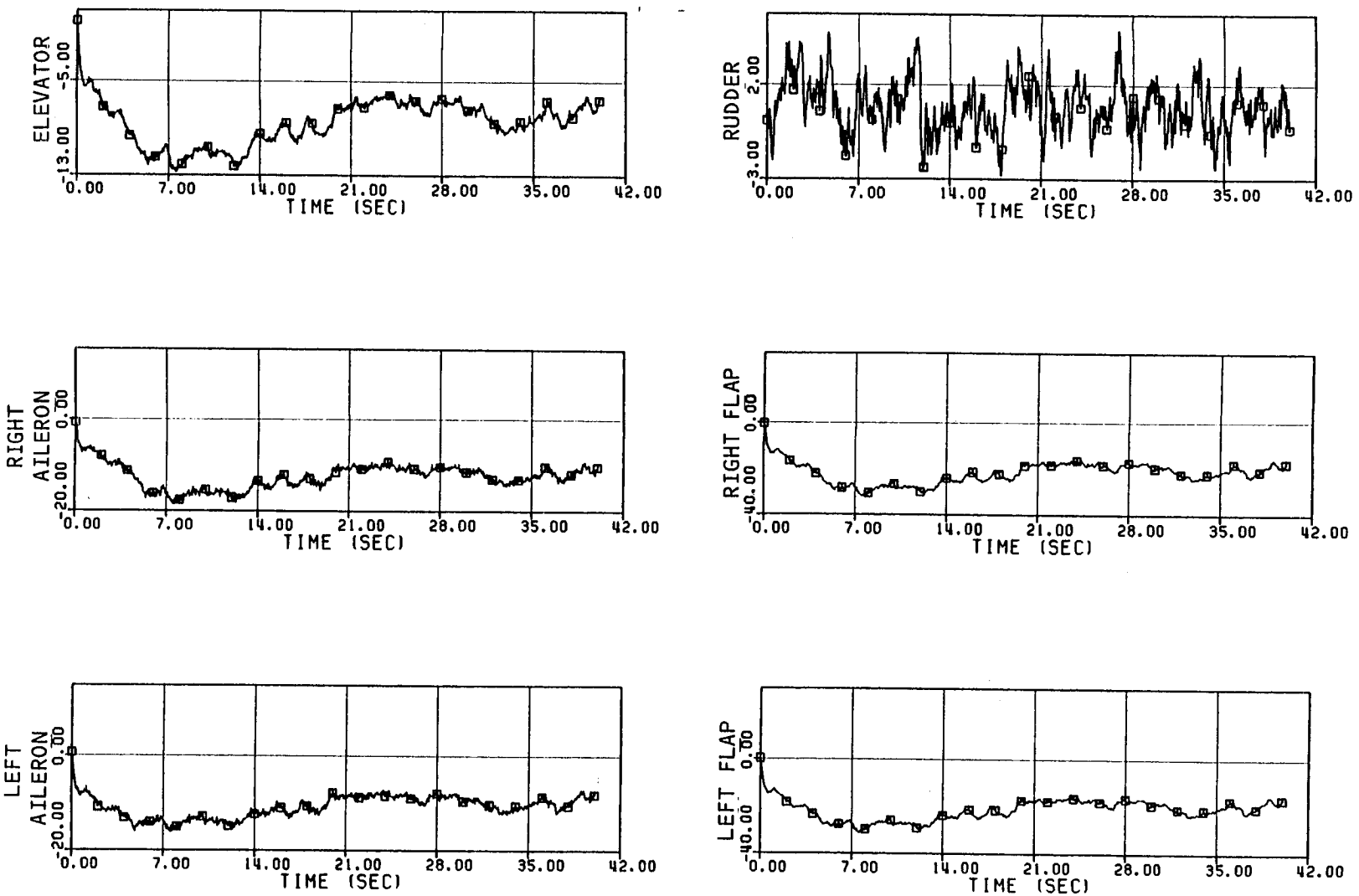

Figure 4.11. Projection of the residual onto the normalized expected failure signature directions, right aileron failure, -0.0349 rad (-2°) bias, off-nominal flight condition

unmodified filter because the modified filter relies more on the normal acceleration measurement to detect elevator, aileron, and flap failures. This is true despite the attempt to diminish the use of the normal acceleration measurement and rely more on the roll rate measurement through scaling of the measurements.

The residual projections become biased relative to the no-failure residual projections about a second after the failure. The bias appears to be approximately constant, which is a reflection of the unidirectionality of the failure signatures. In order to determine the size of the bias, the residual projection values were averaged from the time of failure until the end of 40 s simulation run. The results for the test cases are shown in Table 4.3. With suitable thresholds for decision, it is reasonable to expect that, for the case where the filter has a good model, residual projection magnitude could be used to detect any of these control surface failures at low turbulence levels. By comparing the mean residual projections onto the expected failure directions, elevator and rudder failures are clearly identified. Not unexpectedly, however, isolating specific wing surface failures was more difficult. For both aileron failure cases, the modified detection filter was able to isolate the failure to the aileron or flap on the correct wing. This conclusion was based on the mean residual projections for the aileron and flap on the correct wing being larger than the other mean residual projections. Based on the one flap failure case, isolating the failure to one of the flaps might be possible. While unable to clearly isolate wing surface failures, the modified detection filter was better able to distinguish between the wing surfaces than the unmodified detection filter.

High-level turbulence significantly affects the filter residual and therefore the residual projections. If thresholds were set to detect failures with low-level turbulence, the high-level turbulence would probably cause a failure to be indicated even in the no-failure case. Yet, when compared to the high-turbulence no-failure case, the elevator failure in high turbulence still has a detectable signature, although a flap failure is also falsely indicational.

Table 4.3
Mean Residual Projection Magnitudes
for the Modified Detection Filter

PROJECTION ONTO NORMALIZED EXPECTED FAILURE SIGNATURE FOR	FAILURE CASES									
	NOMINAL CRUISE CONDITION								OFF-NOMINAL CRUISE CONDITION	
	MINOR TURBULENCE						SEVERE TURBULENCE		MINOR TURBULENCE	
	NONE	ELEVATOR	RIGHT AILERON	LEFT AILERON	RUDDER	RIGHT FLAP	NONE	ELEVATOR	NONE	RIGHT AILERON
Elevator	-0.7	-9.0	-1.1	-1.0	-0.7	2.6	-4.8	-12.9	-7.9	-8.7
Right Aileron	-0.9	-2.5	-3.4	0.4	-0.6	9.8	-5.9	-7.3	-10.0	-13.2
Left Aileron	-0.9	-2.6	0.4	-3.4	-1.1	1.4	-5.9	-7.4	-11.3	-10.8
Rudder	-0.1	-0.1	-0.8	0.4	-3.3	-2.7	-0.2	-0.2	1.5	0.7
Right Flap	-1.6	-4.8	-3.6	-2.0	-1.4	12.1	-11.0	-13.8	-19.5	-22.8
Left Flap	-1.6	-4.8	-2.1	-3.6	-1.7	8.5	-11.0	-13.8	-20.0	-21.7

When the filter model was less representative of the actual dynamics, the effect of the mismodeling was to introduce a large bias in the filter residual. This led to large residual projections, an indication of failure - even in the no-failure case. But the residual was noticeably larger in the aileron failure case (the only failure tested at the off-nominal cruise condition), and the projections were offset from those of the no-failure case by approximately the same amounts as for the corresponding cases tested at the nominal cruise condition.

In order to reduce the sensitivity of the modified detection filter to both turbulence and modeling errors, dynamic thresholds or a method of estimating the residual biases caused by disturbances and modeling errors would be of benefit. If estimating these biases were possible, the residual could be appropriately compensated and failures could still be detected and isolated.

4.5 Conclusions

The modified detection filter has been presented and it has been evaluated with regard to its ability to detect and isolate aircraft control surface failures. The following conclusions and advantages and disadvantages of the modification to the detection filter are based on the results described in the last section. Comparisons with the unmodified detection filter are also presented where appropriate.

(1) The modified detection filter can be used to give unidirectional failure signatures in applications where there is direct coupling of inputs to measurements. The modifications required are minor. Unlike the unmodified detection filter for this application, there are straightforward detection and isolation tests based directly on mean residual projection magnitude and direction.

(2) Noise orthogonal to the $C(\underline{b}_i - K\underline{d}_i)$ and $\underline{d}_i$ directions is suppressed as a by-product of the secondary filtering.

(3) Small but significant residual errors can be caused by the secondary filtering because separating the portion of the residual produced by direct input-output coupling is not numerically exact.

(4) The modified detection filter can be used to detect control surface failures in low level turbulence with no modeling errors.

(5) The modified detection filter will have difficulty in isolating failures that produce similar effects on the aircraft. Both the unmodified and modified detection filters were not able to isolate wing surface (aileron and flap) failures to a specific wing surface. However, the modified detection filter shows more promise of being able to distinguish between these surfaces which produce similar effects.

(6) The modified detection filter is sensitive to disturbances such as turbulence and to modeling errors. Dynamic thresholds or some method of estimating the no-failure residual magnitudes could be of benefit in achieving adequate levels of FDI performance. If this is possible, detecting failures with turbulence and modeling errors would still be achieved.

(7) Based upon the time for the projection of the residual onto the failure signature directions to significantly show the effects of a failure, the failure detection and isolation times for the modified detection filter in low turbulence were on the order of a second, approximately the same as those obtained for the unmodified filter.

(8) As the modification is a new concept, it is not mature in either theory or application.

(9) Given our experience with both the unmodified and the modified detection filter, it is our judgment that the modified detection filter holds more promise for applications with direct input-to-output coupling and therefore deserves continued investigation.

SECTION 5

LIKELIHOOD RATIO TESTS

5.1 Introduction

Likelihood Ratio Tests are evaluated in this section with regard to their ability to detect and isolate control system failures. Two tests are evaluated: the Generalized Likelihood Ratio Test and the Orthogonal Series Generalized Likelihood Ratio Test. An analytical development of each algorithm is presented. Simulation results, which directly compare the FDI capability of both algorithms, are shown and discussed. Most of the material contained in this section is taken from Reference 10.

5.2 The GLR Test for Dynamic Systems

The details of the GLR test may be found in Reference 9. A discrete-time system is assumed for the present discussion. In the normal mode of operation (H_0), the state dynamics and measurement equation are given by

$$\underline{x}(k+1) = \Phi(k)\underline{x}(k) + B(k)\underline{u}(k) + \underline{w}(k) + \underline{g}(k) \qquad (5.1)$$

$$\underline{y}(k) = C(k)\underline{x}(k) + D(k)\underline{u}(k) + \underline{v}(k) + \underline{h}(k) \qquad (5.2)$$

$\underline{g}(k)$ and $\underline{h}(k)$ are bias vectors. $\underline{w}(k)$ and $\underline{v}(k)$ are independent, zero-mean, white Gaussian sequences with covariances given by

$$E[\underline{w}(k)\underline{w}^T(j)] = Q(k)\delta_{kj} \tag{5.3}$$

$$E[\underline{v}(k)\underline{v}^T(j)] = R(k)\delta_{kj} \tag{5.4}$$

The GLR failure hypothesis is that

$$\underline{x}(k+1) = \Phi(k)\underline{x}(k) + B(k)\underline{u}(k) + \underline{w}(k) + \underline{g}(k) + \underline{b}(k)n(k,\theta)\nu \tag{5.5}$$

$$\underline{y}(k) = C(k)\underline{x}(k) + D(k)\underline{u}(k) + \underline{v}(k) + \underline{h}(k) + \underline{d}(k)n(k,\theta)\nu \tag{5.6}$$

where $\underline{b}(k)$ and $\underline{d}(k)$ are known vectors that depend on the *type* of the failure. For example, if an actuator failure is modeled, $\underline{b}(k)$ will be the column of the matrix $B(k)$ corresponding to that actuator, and $\underline{d}(k)$ will be the corresponding column of $D(k)$. If a sensor failure is modeled, $\underline{b}(k)$ will be the zero vector, and $\underline{d}(k)$ will be given by

$$d_i(k) = \delta_{ij}, \quad i = 1, 2, \ldots, m \tag{5.7}$$

where j is the index corresponding to the failed sensor. $n(k,\theta)$ is the *mode shape*, or simply *mode*, of the failure, which occurs at time θ. Generally, we have that

$$n(k,\theta) = 0, \quad k < \theta \tag{5.8}$$

For example, if a bias failure is assumed, then

$$n(k,\theta) = \begin{cases} 0 & k < \theta \\ 1 & k \geq \theta \end{cases} \tag{5.9}$$

Finally, ν is the *magnitude* of the failure.

For the analysis that follows, the deterministic input and bias terms in the state and measurement equations that are common to both hypotheses may be eliminated, due to the linearity of the equations. Therefore, the no-failure hypothesis (H_0) and the failure hypothesis (H_1) are represented by

$$H_0: \quad \underline{x}(k+1) = \Phi(k)\underline{x}(k) + \underline{w}(k) \tag{5.10}$$

$$\underline{y}(k) = C(k)\underline{x}(k) + \underline{v}(k) \tag{5.11}$$

$$H_1: \quad \underline{x}(k+1) = \Phi(k)\underline{x}(k) + \underline{w}(k) + \underline{b}(k)n(k,\theta)\nu \tag{5.12}$$

$$\underline{y}(k) = C(k)\underline{x}(k) + \underline{v}(k) + \underline{d}(k)n(k,\theta)\nu \tag{5.13}$$

Suppose the data $\underline{y}(k)$ are observed over the observation interval

$$k_0 \leq k \leq k_f \tag{5.14}$$

For a given time of failure, θ, and magnitude of failure, ν, the Likelihood Ratio (LR) is given by

$$\Lambda(k_f,\theta,\nu) = \frac{p(\underline{y}(k_0), \underline{y}(k_0+1), \ldots, \underline{y}(k_f) \mid H_1, \theta, \nu)}{p(\underline{y}(k_0), \underline{y}(k_0+1), \ldots, \underline{y}(k_f) \mid H_0)} \tag{5.15}$$

Because the $\underline{y}(k)$ are not independent from time step to time step, the evaluation of the conditional probabilities is difficult. To evaluate the LR, a Kalman filter is implemented, based on the normal mode (H_0) system. The filter equations are

$$\hat{\underline{x}}^-(k+1) = \Phi(k)\hat{\underline{x}}^+(k) \tag{5.16}$$

$$\underline{\hat{x}}^{+}(k) = \underline{\hat{x}}^{-}(k) + K(k)\underline{\gamma}(k) \tag{5.17}$$

where K(k) is the Kalman gain matrix, and $\underline{\gamma}(k)$ is the residual, given by

$$\underline{\gamma}(k) = \underline{y}(k) - C(k)\underline{\hat{x}}^{-}(k) \tag{5.18}$$

The Kalman gain matrix is given by

$$K(k) = P^{-}(k)C^{T}(k)M^{-1}(k) \tag{5.19}$$

where $P^{-}(k)$ is the covariance of the estimation error

$$\underline{e}^{-}(k) = \underline{x}(k) - \underline{\hat{x}}^{-}(k) \tag{5.20}$$

and M(k) is the covariance of $\underline{\gamma}(k)$, given by

$$M(k) = C(k)P^{-}(k)C^{T}(k) + R(k) \tag{5.21}$$

The covariance is propagated by

$$P^{-}(k+1) = \Phi(k)P^{+}(k)\Phi^{T}(k) + Q(k) \tag{5.22}$$

$$P^{+}(k) = [I - K(k)C(k)]P^{-}(k) \tag{5.23}$$

The LR may then be written in terms of the residual sequence $\underline{\gamma}(k)$ rather than the measurement sequence. Because the residual sequence is (conditionally) a white Gaussian sequence, the LR is easier to determine in terms of $\underline{\gamma}(k)$ than in terms of $\underline{y}(k)$.

Due to the linearity of the state equation and the filter equations, the residual may be expressed under each hypothesis as

$$H_0: \quad \underline{\gamma}(k) = \underline{\gamma}_0(k) \tag{5.24}$$

$$H_1: \quad \underline{\gamma}(k) = \underline{\gamma}_0(k) + \underline{g}(k,\theta)\nu \tag{5.25}$$

where $\underline{\gamma}_0(k)$ is a zero-mean, white Gaussian sequence with covariance $M(k)$. $\underline{g}(k,\theta)$ is the failure signature of a failure occurring at time θ. $\underline{g}(k,\theta)$ is given by

$$\underline{g}(k,\theta) = C(k)\underline{f}(k,\theta) + \underline{d}(k)n(k,\theta) \tag{5.26}$$

where $\underline{f}(k,\theta)$ is the influence of the failure mode $n(k,\theta)$ on the state estimation error. $\underline{f}(k,\theta)$ may be generated recursively by

$$\underline{f}(k+1,\theta) = \Phi(k)[I - K(k)C(k)]\underline{f}(k,\theta) + [\underline{b}(k) - \Phi(k)K(k)\underline{d}(k)]n(k,\theta) \tag{5.27}$$

with the initial condition

$$\underline{f}(k_0,\theta) = \underline{0} \tag{5.28}$$

It can be seen therefore that

$$\underline{f}(k,\theta) = \underline{0}, \quad k \leq \theta \tag{5.29}$$

The LR is given by

$$\Lambda(k_f,\theta,\nu) = \frac{p(\underline{\gamma}(k_0), \underline{\gamma}(k_0+1), \ldots, \underline{\gamma}(k_f) \mid H_1,\theta,\nu)}{p(\underline{\gamma}(k_0), \underline{\gamma}(k_0+1), \ldots, \underline{\gamma}(k_f) \mid H_0)} \tag{5.30}$$

Because the residual sequence is (conditionally) Gaussian and white, the Log Likelihood Ratio (LLR) ratio has a particularly simple form:

$$\ell(k_f, \theta, \nu) = \nu\, \chi(k_f, \theta) - \frac{1}{2}\, \nu^2 S(k_f, \theta) \tag{5.31}$$

where

$$\chi(k_f, \theta) = \sum_{k=\theta}^{k_f} \underline{g}^T(k, \theta) M^{-1}(k) \underline{\gamma}(k) \tag{5.32}$$

$$S(k_f, \theta) = \sum_{k=\theta}^{k_f} \underline{g}^T(k, \theta) M^{-1}(k) \underline{g}(k) \tag{5.33}$$

Now, the generalized likelihood ratio is given by

$$\ell(k_f) = \max_{\hat{\theta}, \hat{\nu}} \ell(k_f, \hat{\theta}, \hat{\nu}) \tag{5.34}$$

Performing the maximization over $\hat{\nu}$ first, we have that

$$\hat{\nu}(k_f, \theta) = \frac{\chi(k_f, \theta)}{S(k_f, \theta)} \tag{5.35}$$

Hence, the GLR test statistic is given by

$$\ell(k_f) = \max_{\hat{\theta}} \frac{1}{2}\, \frac{\chi^2(k_f, \hat{\theta})}{S(k_f, \hat{\theta})} \tag{5.36}$$

As a matter of convenience, the GLR decision function is defined by

$$DF(k_f) = 2\, \ell(k_f) = \max_{\hat{\theta}}\, \frac{\chi^2(k_f, \hat{\theta})}{S(k_f, \hat{\theta})} \tag{5.37}$$

A failure is detected when the decision function exceeds the detection threshold.

A closed-form solution to the above maximization does not exist in general. Therefore, in order to implement the GLR, the statistic $\ell(k_f, \theta)$ must be computed for all possible times of failure, θ. As a result, a bank of matched filters that grows linearly with time is required. To avoid this unlimited growth in the amount of computation, the assumed time of failure may be restricted, say, to be in the range $k_f - N < \theta \leq k_f$. Even so, the amount of computation required to implement the GLR can be quite large, especially if N is large.

5.3 The Orthogonal Series GLR Test

The Generalized Likelihood Ratio methods of FDI tend to be computationally burdensome. This complexity arises from the need to estimate the random onset time of the failure, which generally requires a nonlinear estimation structure. In addition, these methods may not be robust to failure mode uncertainty.

An FDI algorithm that is robust to failure mode uncertainty is the detection filter. Unfortunately, the applicability of the detection filter is limited by a number of factors. One restriction is that the theory is limited to linear time-invariant systems. Also, the detection filter design process breaks down for systems where two or more failure types are not "output separable," even though it should be possible to detect and isolate failures for some such systems. Finally, little guidance exists on how to choose the free parameters in the design process, such as the filter eigenvalues.

In this section, an algorithm that addresses these problems, the Orthogonal Series Generalized Likelihood Ratio (OSGLR) Test, is proposed. As suggested by its name, the OSGLR test is indeed a GLR test. The hypothesis upon which the test is based is that the failure modes can be represented as truncated orthogonal series of time functions. Because such a series can represent a broad class of failure modes, the test should be robust to failure mode uncertainty. The test

is not as computationally complex as other GLR methods, because the time of failure does not enter the failure hypothesis explicitly. The only unknowns in the failure hypothesis are the coefficients of the terms in the orthogonal series. Because they enter the state and measurement equations linearly, these unknowns can be estimated by relatively simple linear schemes. In practice, the discrete-time case is likely to be more useful, because it is more amenable to computer implementation. However, continuous-time systems will be dealt with here because the mathematics are less cumbersome.

5.3.1 OSGLR Hypotheses

We are interested in detecting failures in linear dynamic systems, which under normal conditions are modeled by

$$\frac{d\underline{x}(t)}{dt} = A(t)\underline{x}(t) + B(t)\underline{u}(t) + \underline{w}(t) \tag{5.38}$$

$$\underline{y}(t) = C(t)\underline{x}(t) + D(t)\underline{u}(t) + \underline{v}(t) \tag{5.39}$$

$\underline{w}(t)$ and $\underline{v}(t)$ are independent, zero-mean, Gaussian processes with autocorrelation functions given by

$$E[\underline{w}(t_1)\underline{w}^T(t_2)] = Q(t_1)\delta(t_1-t_2) \tag{5.40}$$

$$E[\underline{v}(t_1)\underline{v}^T(t_2)] = R(t_1)\delta(t_1-t_2) \tag{5.41}$$

When a failure occurs, either the state dynamics change or the measurement equation changes. For example, if the ith actuator fails, the actual input vector, $\underline{u}_a(t)$, differs from the commanded input, $\underline{u}(t)$, as follows:

$$\underline{u}_a(t) = \underline{u}(t) + \underline{e}_{qi}f(t) \tag{5.42}$$

where $\underline{e}_{qi}$ is a q-dimensional unit vector in the ith coordinate direction, i.e., the elements of $\underline{e}_{qi}$ are given by

$$(\underline{e}_{qi})_j = \delta_{ij}, \quad j = 1, 2, \ldots, q \tag{5.43}$$

where δ_{ij} is the Kronecker delta. f(t) is the mode shape of the failure. For example, if the failure is a bias shift, then f(t) is a step function of some magnitude at the time of the failure. Thus, the state dynamics and measurement equations become

$$\frac{d\underline{x}(t)}{dt} = A(t)\underline{x}(t) + B(t)\underline{u}(t) + \underline{b}_i(t)f(t) + \underline{w}(t) \tag{5.44}$$

$$\underline{y}(t) = C(t)\underline{x}(t) + D(t)\underline{u}(t) + \underline{d}_i(t)f(t) + \underline{v}(t) \tag{5.45}$$

where $\underline{b}_i(t)$ and $\underline{d}_i(t)$ are the ith columns of B(t) and D(t), respectively.

Similarly, a failure in the ith sensor can generally be represented in the measurement equation as

$$\underline{y}(t) = C(t)\underline{x}(t) + D(t)\underline{u}(t) + \underline{e}_{mi}(t)f(t) + \underline{v}(t) \tag{5.46}$$

As in the case of an actuator failure, f(t) depends on the mode of the failure. For example, if the output of the ith sensor is fixed at zero (except for the additive noise), then

$$f(t) = -\underline{c}_i^T(t)\underline{x}(t) - \underline{d}_i^T(t)\underline{u}(t) \tag{5.47}$$

where $c_i^T(t)$ is the ith row of C(t). The situation is more complicated for changes in the plant dynamics. Reference 10 should be consulted in this regard.

For most types of failures (actuator failures, sensor failures, and some types of dynamics changes), the effect of the failure can be captured in the state and measurement equations as

$$\frac{d\underline{x}(t)}{dt} = A(t)\underline{x}(t) + B(t)\underline{u}(t) + \underline{b}(t)f(t) + \underline{w}(t) \tag{5.48}$$

$$\underline{y}(t) = C(t)\underline{x}(t) + D(t)\underline{u}(t) + \underline{d}(t)f(t) + \underline{v}(t) \tag{5.49}$$

The vectors $\underline{b}(t)$ and $\underline{d}(t)$ are known ahead of time for each type of failure, whereas the mode of the failure, $f(t)$, is generally unknown *a priori*. In the analysis that follows, the terms due to the input $\underline{u}(t)$ in the state and measurement equations can be neglected, due to the linearity of the equations and the fact that $B(t)$, $D(t)$, and $\underline{u}(t)$ are known. It is important to remember, however, that these terms must be included in any implementation of the OSGLR algorithm. Specifically, these terms must be included in the Kalman filter that estimates $\underline{x}(t)$. The discussion will be confined to the binary hypothesis testing case. That is, we will assume that we are only trying to detect a single failure type, rather than detect and isolate from a set of failure types. Later, the results will be extended to include the isolation problem.

The OSGLR test will be derived in the following manner. The fixed-length data test for data observed over the interval

$$t_0 \leq t \leq t_f$$

will be found. This fixed data test will then be suitably modified to form a sequential test. The no-failure (H_0) and failure (H_1) hypotheses are given by

$$H_0: \quad \frac{d\underline{x}(t)}{dt} = A(t)\underline{x}(t) + \underline{w}(t) \tag{5.50}$$

$$\underline{y}(t) = C(t)\underline{x}(t) + \underline{v}(t) \tag{5.51}$$

$$H_1: \quad \frac{d\underline{x}(t)}{dt} = A(t)\underline{x}(t) + \underline{w}(t) + \underline{b}(t)f(t) \tag{5.52}$$

$$\underline{y}(t) = C(t)\underline{x}(t) + \underline{v}(t) + \underline{d}(t)f(t) \tag{5.53}$$

For both hypotheses $\underline{x}(t_0)$ is a Gaussian random variable with zero mean and covariance P_0.

Because the failure mode shape f(t) has not been specified, the hypothesis H_1 is not complete. In order that the test be robust to failure mode uncertainty, it would be desirable to allow f(t) to be completely arbitrary. However, this assumption does not lead to a well-posed problem. Therefore, some further assumptions must be made.

The approach that will be taken here is to represent the mode shape f(t) by a truncated series expansion with unknown coefficients. The motivation is that if the basis functions of the expansion are chosen properly, it should be possible to <u>approximately</u> represent a rich class of failure modes. Therefore, it is assumed that f(t) can be expressed as

$$f(t) = \sum_{i=1}^{p} a_{1i}\phi_{1i}(t) \tag{5.54}$$

where p is the number of basis functions, the a_{1i} are unknown coefficients, and the $\phi_{1i}(t)$ are the basis functions. Eq. (5-54) can be expressed more conveniently in vector form as

$$f(t) = \underline{\phi}_1^T(t)\underline{a}_1 \tag{5.55}$$

The subscript "1" indicates that this is an intermediate representation. Ultimately, we will be interested in a representation of the form

$$f(t) = \underline{\phi}^T(t_f - t)\underline{a}(t_f) \tag{5.56}$$

It cannot be overemphasized that the representation of f(t) in Eq. (5.55) is meant to be an approximation. There is no reason to believe that an actual failure mode will have this particular form.

Two important features of these hypotheses are that the failure hypothesis does not include a parameter representing the time of failure, and that the unknown parameters enter into the problem linearly. Hence, nonlinear estimation will not be required. As will be seen, this significantly reduces the amount of computation required relative to other GLR methods.

5.3.2 Derivation of the OSGLR Algorithm

The OSGLR test is derived in several steps. First, the test is derived based on the representation of f(t) given by Eq. (5.55). Next, the test is converted to a form that corresponds to a second intermediate representation of f(t). A special case of this representation is given in Eq. (5.56). In the process, the test statistic is converted from an integral representation to a differential equation representation. A more complete derivation may be found in Reference 10.

To determine the form of the test, we proceed as follows. A Kalman filter based on the unfailed system statistics (H_0), is used to generate the residual process $\underline{\gamma}(t)$. The filter equations are

$$\frac{d\underline{\hat{x}}(t)}{dt} = A(t)\underline{\hat{x}}(t) + K(t)\underline{\gamma}(t) \tag{5.57}$$

$$\underline{\hat{x}}(t_0) = \underline{0} \tag{5.58}$$

$$\underline{\gamma}(t) = \underline{y}(t) - C(t)\underline{\hat{x}}(t) \tag{5.59}$$

$$K(t) = P(t)C^T(t)R^{-1}(t) \tag{5.60}$$

$$\frac{dP(t)}{dt} = A(t)P(t) + P(t)A^T(t) + Q(t) - P(t)C^T(t)R^{-1}(t)C(t)P(t) \tag{5.61}$$

$$P(t_0) = P_0 \tag{5.62}$$

where $\hat{\underline{x}}(t)$ is the estimate of $\underline{x}(t)$, $P(t)$ is the covariance of the estimation error, and $K(t)$ is the Kalman gain matrix. The process $\underline{\gamma}(t)$ contains exactly the same information as $\underline{y}(t)$, because each can be determined unambiguously from the other. However, $\underline{\gamma}(t)$ is easier to work with than $\underline{y}(t)$ because it is a white noise process, whereas $\underline{y}(t)$ is correlated in time.

By the linearity of the Kalman filter and the system equations, the residual can be decomposed as

$$\underline{\gamma}(t) = \underline{\gamma}_0(t) + \underline{\gamma}_1(t) \tag{5.63}$$

where $\underline{\gamma}_0(t)$ is the residual process that results under H_0, and $\underline{\gamma}_1(t)$ is the part of the residual due to the failure. Again, due to the linearity of the filter and the system, $\underline{\gamma}_1(t)$ can be expressed as

$$\underline{\gamma}_1(t) = G_1(t)\underline{a}_1 \tag{5.64}$$

where the matrix $G_1(t)$ represents the influence of the vector of coefficients $\underline{a}_1$ on the residuals, and remains to be determined. Therefore, we can rewrite the two hypotheses as

$$H_0: \quad \underline{\gamma}(t) = \underline{\gamma}_0(t), \qquad t_0 \leq t \leq t_f \tag{5.65}$$

$$H_1: \quad \underline{\gamma}(t) = \underline{\gamma}_0(t) + G_1(t)\underline{a}_1 , \qquad t_0 \leq t \leq t_f \tag{5.66}$$

where $\underline{\gamma}_0(t)$ is a zero-mean, Gaussian process with the autocorrelation function

$$E[\underline{\gamma}_0(t_1)\underline{\gamma}_0^T(t_2)] = R(t_1)\delta(t_1-t_2) \tag{5.67}$$

Hence, the problem of deciding between H_0 and H_1 has been reduced to the problem of deciding whether or not a bias signal is present in the white residual process.

It can be shown that the information vector, defined by

$$\underline{\chi}_1(t_f) = \int_{t_0}^{t_f} G_1^T(t)R^{-1}(t)\underline{\gamma}(t)dt \tag{5.68}$$

is a sufficient statistic, i.e., that it contains all the information contained in the residual process regarding the hypotheses. Hence, it can be used in place of the entire time history of the residuals to determine whether a failure has occurred. Now, $\underline{\chi}_1(t_f)$ is a Gaussian random vector, because $\gamma(t)$ is a Gaussian random process. Hence, its probability density is completely specified by its mean and covariance. Under H_0, the mean of $\underline{\chi}_1(t_f)$ is zero since the residual has a mean value of zero. The covariance of $\underline{\chi}_1(t_f)$, known as the information matrix, is given by

$$S_1(t_f) = \int_{t_0}^{t_f} G_1^T(t)R^{-1}(t)G_1(t)dt \tag{5.69}$$

Under H_1, $\underline{\chi}_1(t_f)$ has the same covariance, but its mean is given by

$$E\left[\underline{\chi}_1(t_f)\middle|H_1\right] = S_1(t_f)\underline{a}_1 \tag{5.70}$$

The two hypotheses can be rewritten as

$$H_0: \ \underline{\chi}_1(t_f) \sim N(\underline{0}, S_1(t_f)) \tag{5.71}$$

$$H_1: \ \underline{\chi}_1(t_f) \sim N(S_1(t_f)\underline{a}_1, S_1(t_f)) \tag{5.72}$$

The problem of deciding between H_0 and H_1 has now been reduced to the problem of deciding whether the Gaussian random vector $\underline{\chi}_1(t_f)$ has zero mean or nonzero mean. Because the hypothesis H_1 is composite, an appropriate test to use is the GLR test.

The GLR decision function is defined by

$$DF(t_f) = \underline{\chi}_1^T(t_f)S_1^{-1}(t_f)\underline{\chi}_1(t_f) \tag{5.73}$$

Reference 10 contains a derivaton of the GLR test statistic. Then the GLR test is given by

$$DF(t_f) \underset{\text{decide } H_0}{\overset{\text{decide } H_1}{\gtrless}} T^2 \tag{5.74}$$

The threshold is written as T^2 because the decision function is a positive definite form. Therefore, a negative threshold would yield a trivial test that always decides that H_1 is true. Also, writing the threshold as T^2 rather than T will simplify the results of later sections.

To complete the derivation of the test, we must determine $G_1(t)$. It can be shown (Reference 10) that $G_1(t)$ is given by

$$G_1(t) = C(t)F_1(t) + \underline{d}(t)\underline{\phi}_1^T(t) \tag{5.75}$$

where

$$\frac{dF_1(t)}{dt} = [A(t) - K(t)C(t)]F_1(t) + [b(t) - K(t)\underline{d}(t)]\underline{\phi}_1^T(t) \tag{5.76}$$

and

$$F_1(t_0) = 0 \tag{5.77}$$

The above equations specify the OSGLR test for the failure as represented by Eq. (5.55). However, this representation has two weaknesses. First, because the basis functions $\phi_{1i}(t)$ were chosen arbitrarily, they may be highly correlated. The second problem is that the basis functions are defined relative to an absolute time scale, rather than with respect to the terminal time, t_f. For a number of reasons, it is desirable to define the basis functions relative to the time t_f, in which case the basis functions are $\phi_i(t_f-t)$ rather than $\phi_{1i}(t)$. For one thing, if the transformed basis functions are functions of t_f-t, then they will have the same shape on the time scale defined relative to the end of the observation interval, t_f. Also, if the system is time-invariant, the OSGLR equations will then be time-invariant in steady state.

Both of these problems can be remedied in the following way: A new set of basis functions will be defined that is the original set of basis functions orthogonalized over the interval $[t_0,t_f]$. This will eliminate the first of the problems discussed above. The second problem may be solved by judicious choice of the original set of basis functions. The vector of basis functions $\underline{\phi}_1(t)$ is transformed by an invertible linear transformation $\Gamma(t_1)$, so that

$$\underline{\phi}_2(t,t_f) = \Gamma(t_f)\underline{\phi}_1(t) \tag{5.78}$$

The transformation $\Gamma(t_f)$ is intended to orthogonalize the vector of basis function $\underline{\phi}_2(t)$ over the interval $[t_0,t_f]$, although it is not necessary that it do so. Based on this new vector of basis functions, a new information vector $\underline{\chi}(t_f)$, information matrix $S(t_f)$, and influence matrices $G(t_f)$ and $F(t_f)$ can be developed. These quantities are related to $\underline{\chi}_1(t_f)$, $S_1(t_f)$, $G_1(t_f)$, and $F_1(t_f)$ by the matrix $\Gamma(t_f)$. With the help of these relationships, differential equations for these new quantities can be derived. A useful definition is the following:

$$A_a(t_f) \triangleq - \Gamma^T(t_f) \frac{d\Gamma^T(t_f)}{dt_f} \tag{5.79}$$

The equations for the OSGLR algorithm then become

$$\frac{d}{dt_f}\underline{\chi}(t_f) = -A_a^T(t_f)\underline{\chi}(t_f) + G^T(t_f)R^{-1}(t_f)\underline{\gamma}(t_f) \tag{5.80}$$

with initial condition

$$\underline{\chi}(t_0) = \underline{0} \tag{5.81}$$

$$\frac{d}{dt_f}S(t_f) = - A_a^T(t_f)S(t_f) - S(t_f)A_a(t_f) + G^T(t_f)R^{-1}(t_f)G(t_f) \tag{5.82}$$

with initial condition

$$S(t_0) = 0 \tag{5.83}$$

$$G(t_f) = C(t_f)F(t_f) + \underline{d}(t_f)\underline{\phi}_2^T(t_f,t_f) \tag{5.84}$$

$$\frac{d}{dt_f} F(t_f) = [A(t_f) - K(t_f)C(t_f)]F(t_f)$$

$$+ [\underline{b}(t_f) - K(t_f)\underline{d}(t_f)]\underline{\phi}_2^T(t_f,t_f) - F(t_f)A_a(t_f) \tag{5.85}$$

with initial condition

$$F(t_0) = 0 \tag{5.86}$$

Now suppose that the basis functions are required to be shift invariant so that

$$\underline{\phi}_2(t,t_f) = \underline{\phi}(t_f - t) \tag{5.87}$$

Note that with the basis functions in this form, the failure mode f(t) has the form described in Eq. (5.56). It can be shown that the vector of basis functions $\underline{\phi}(\tau)$ satisfies the differential equation

$$\frac{d}{d\tau}\underline{\phi}(\tau) = A_\phi\underline{\phi}(\tau) \tag{5.88}$$

where A_ϕ is a constant matrix, and τ is a dummy variable defined by

$$\tau \triangleq t_f - t \tag{5.89}$$

A_ϕ is related to $A_a(t_f)$ by the equation

$$A_\phi = -A_a^T \tag{5.90}$$

That is, A_a is also a constant. τ may be thought of as defining a relative time scale that runs backward from the end of the observation interval, t_f. In some ways, the relative time τ is more natural for the failure detection problem than the absolute time t because it represents time relative to the current time (t_f), rather than relative to some arbitrary fixed initial time.

Note that the basis functions affect the OSGLR equations only through $A_a(t_f)$ and $\underline{\phi}_2(t_f,t_f)$. Therefore, if $\underline{\phi}_2(t_f,t_f)$ is required to be shift-invariant, the OSGLR equations will be functions only of the system matrices, A_ϕ, and $\underline{\phi}(0)$. In other words, there is no need to specify the underlying basis functions $\phi_{1i}(t)$ or the transformation $\Gamma(t_f)$. Since there is little motivation for using a basis which is not shift-invariant, this will be assumed to be true.

The OSGLR equations for continuous-time systems are summarized in Table 5.1.

After a failure has been detected, action must be taken by the FDI system to accommodate for the failure. Accommodation involves two distinct actions. First, the failed component, which is usually a sensor or an actuator, must be physically isolated from the system so that it can do no more harm. This aspect of accommodation is problem specific, and will not be discussed further here.

The other action the FDI system must take is to prepare to continue performing failure detection. A number of bookkeeping operations must be performed, such as changing the system models to account for the loss of the failed component, and reinitializing the information vector and information matrix to zero for each of the remaining components. The Kalman filter must be updated to account for the failure, so that monitoring of the other components can continue. More specifically, the filter estimate and covariance should be updated as follows:

$$\underline{\hat{x}}(t^+) = \underline{\hat{x}}(t^-) + F(t)\underline{\hat{a}}(t) \tag{5.91}$$

Table 5-1. Summary of continuous-time OSGLR equations.

Estimation error influence matrix propagation:

$$\frac{dF(t)}{dt} = [A(t) - K(t)C(t)]F(t) + [\underline{b}(t) - K(t)\underline{d}(t)]\phi^T(0) + F(t)A_\phi^T$$

$$F(t_0) = 0$$

Residual influence matrix:

$$G(t) = C(t)F(t) + \underline{d}(t)\phi^T(0)$$

Information vector propagation:

$$\frac{d\underline{\chi}(t)}{dt} = A_\phi \underline{\chi}(t) + G^T(t)R^{-1}(t)\underline{\gamma}(t)$$

$$\underline{\chi}(t_0) = \underline{0}$$

Information matrix propagation:

$$\frac{dS(t)}{dt} = A_\phi S(t) + S(t)A_\phi^T + G^T(t)R^{-1}(t)G(t)$$

$$S(t_0) = 0$$

Decision Function:

$$DF(t) = \underline{\chi}^T(t)S^{-1}(t)\underline{\chi}(t)$$

$$P(t^+) = P(t^-) + F(t)P_a(t)F^T(t) \qquad (5.92)$$

where t^- and t^+ are the times just prior to t and just after t, respectively.

5.3.3 OSGLR Performance Analysis

The performance of a failure detection and isolation (FDI) test depends on three types of events: false alarms, the detection of failures, and the (correct or incorrect) isolation of failures. A complete probabilistic description of these events, together with the distribution of failures, is required in general to determine the performance of a fault-tolerant system.

Unfortunately, it is generally quite difficult to evaluate the performance of an FDI test analytically. In principle, the performance of an FDI test could be determined by Monte Carlo simulation. However, the probability of false alarm, missed detection, or incorrect isolation is very small for an effective FDI test. The amount of simulation required to estimate these probabilities accurately by Monte Carlo methods is therefore prohibitive.

In Reference 10, a partial solution to the problem of evaluating the performance of the OSGLR test is given. The false-alarm performance of the OSGLR test is considered and an asymptotic expression for the steady-state false-alarm rate of the continuous-time OSGLR test is derived. Based on this analysis, an asymptotic bound is derived for the steady-state false-alarm rate of the discrete-time OSGLR test, and the conditions under which this bound is valid are discussed.

The derivation of the aforementioned performance criteria for the OSGLR algorithm are quite lengthy and complex. Therefore, only the resultant expressions obtained are presented here. For the continuous time case the false alarm rate, as a function of the threshold T, is

$$\lambda = \frac{-\mathrm{tr}[A_\phi]T^p}{\Gamma(\frac{p}{2}+1)2^{p/2}} e^{-T^2/2} \{1 - \frac{p}{T^2} + O(\frac{1}{T^4})\}, \quad T \to \infty \tag{5.93}$$

where Γ is the gamma function.

The bound for the discrete time case is

$$\lambda \leq \frac{-\ell n\ (\det\ \phi_\phi)T^p}{\Delta t\ \Gamma(\frac{p}{2}+1)\ 2^{p/2}} e^{-T^2/2} \{1 - \frac{p}{T^2} + O\ (\frac{1}{T^4})\}, \quad T \to \infty \tag{5.94}$$

The conditions under which this bound is valid are discused in Reference 10.

The asymptotic results obtained have been compared to exact results obtained numerically. As a practical matter, numerical results can be obtained only for the scalar case (p=1). Figure 5.1 shows the relative error in these approximations as a function of the threshold, T. (The relative error is defined by the error in the approximation divided by the actual value of the eigenvalue.) As might be expected, the two-term approximation is significantly better than the one-term approximation. The error in the two-term approximation is less than 1% for T larger than 4.0. Even the one-term approximation is accurate to within 5% for thresholds larger than 5.0. For practical purposes, determining the false-alarm rate to within 1% is probably adequate.

5.4 Results

The OSGLR and GLR tests ware applied to the problem of detecting failures in a C-130 transport aircraft. Simulation results are presented which allow a comparison of the performance of these two algorithms. The nominal flight condition is defined to be at an altitude of 304.8 m (1000 ft) with an airspeed of 77.2 m/s (150 knots). The turbulence level used

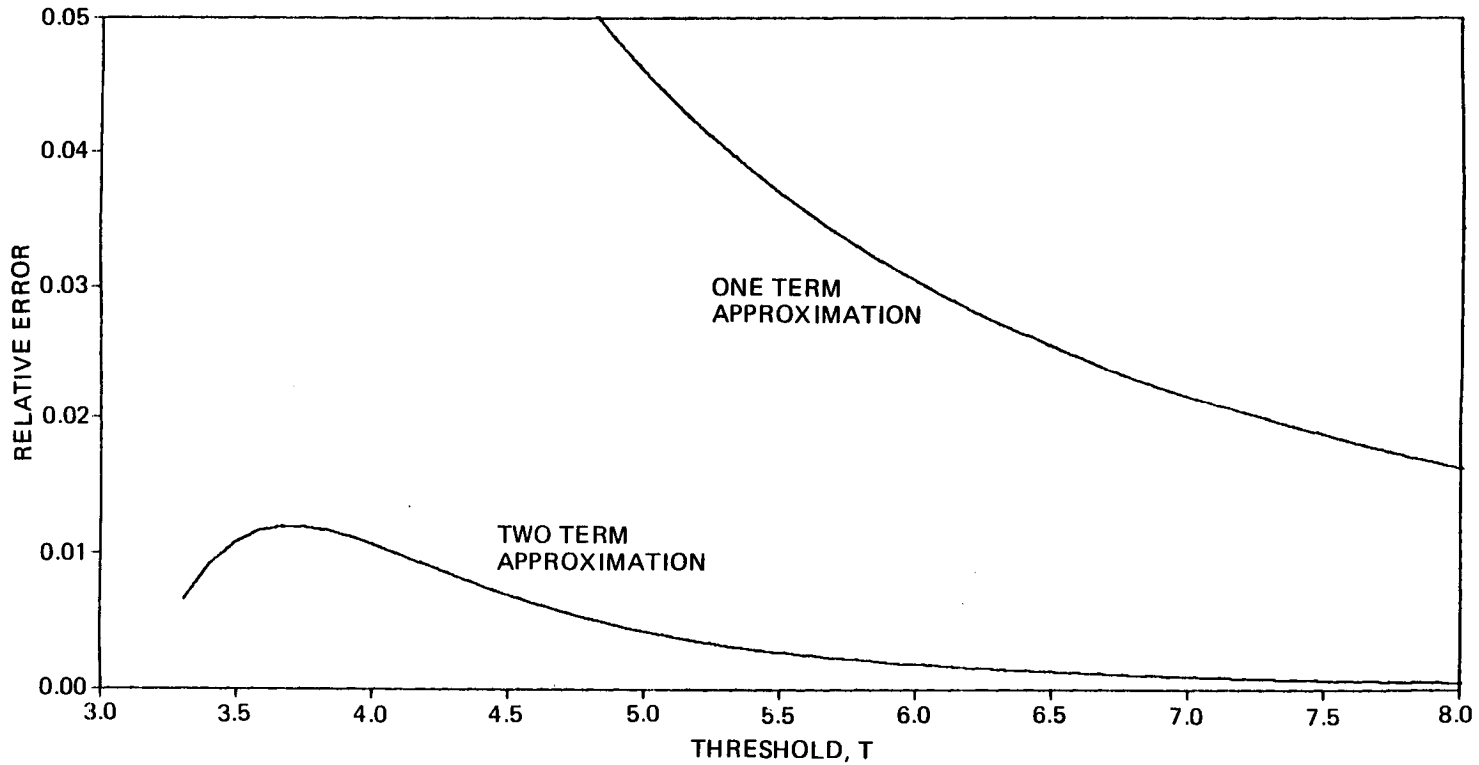

Figure 5.1. Relative error of the asymptotic expression for the false-alarm rate for the scalar case.

had a standard deviation of σ_ω = 6.5 ft/s, which corresponds to heavy turbulence. The control surfaces are defined as per Table 5-2 for this section of the report.

Table 5-2. C-130 control surface definition.

Input	Control Surface
1	elevator
2	right aileron
3	left aileron
4	rudder
5	right flap
6	left flap

Both tests were implemented in discrete time. The Kalman filter states are those listed in Table 2.1 of Section 2.2. In addition, five additional states were included in the Kalman filter to model the effects of turbulence. The measurements used are those described in Section 2.2. The measurements were assumed to be taken at a rate of 50 Hz.

The basis functions of the OSGLR failure hypotheses were determined by trial and error, so that good performance was achieved for many different failure modes. For each failure hypothesis, six basis functions were used in the truncated series expansion. Six basis functions were found to be adequate for all the failures simulated. The use of more than six sometimes caused numerical problems. The basis functions are the discrete-time equivalent of the Laguerre functions, with time constant

$$\tau = 3.0 \text{ s} \tag{5.95}$$

That is, the basis functions are obtained by orthonormalizing the (discrete-time) functions

$$\psi_i(k) = k^{i-1} z^k, \quad i = 1, 2, \ldots, 6 \tag{5.96}$$

where

$$z = e^{-\Delta t/\tau} \tag{5.97}$$

where $\Delta t = 0.02$s is the sampling interval. Other basis functions, such as the Legendre functions, were not tested. The results are not sensitive to the choice of time constant, so long as it is of the same order as the time scale over which the faiure is detected.

The assumed failure mode of each GLR failure hypothesis is a step function (or bias) of unknown magnitude occurring at time θ. The failure onset time θ is constrained to the data window $t - t_w \leq \theta \leq t$, where t_w is the length of the window. The GLR test was implemented using two different data windows: a 2 s (100 sample) window and a 5 s (250 sample) window. Most of the results presented in this section are for the 2 s data window.

The simulation results can be divided into two categories: those based on the linearized models and those based on the nonlinear simulation. For the most part, the simulation results presented are based on the linearized models. The reasons for this are twofold. First, the linear simulations demonstrate the characteristics of the OSGLR test unobscured by nonlinear effects. Second, the linear simulation requires considerably less computation than the nonlinear simulation. The nonlinear simulation is used to show the effects of nonlinearities and to generate test cases that are not easily generated using the linear simulation.

In order to determine the performance of the algorithms, a detection threshold must be set for each. Because no performance specifications have been given, the selection of the threshold is somewhat arbitrary. We will set the OSGLR threshold so that the resulting false-alarm rate of each OSGLR detector is 10^{-4} per hour or less. Using the results for discrete-time systems presented in Section 5.3.2 leads to

$$T^2 = 56.86$$

The false-alarm rate is very sensitive to the selection of the threshold. As a result, the threshold is not very sensitive to the specification of the false-alarm rate. For example, if we require that the false-alarm rate be decreased to 10^{-6} per hour, then the threshold must be increased to only $T^2 = 67.10$. Thus, the results presented here will not be sensitive to the exact value of the false-alarm rate specification.

It is somewhat more difficult to determine the threshold for the GLR test. In order to compare the GLR and OSGLR tests on a fair basis, we should select the threshold for the GLR test so that each GLR detector has the same false-alarm rate as the OSGLR detectors. Unfortunately, no analytic expression for the false-alarm rate of the GLR test exists. The false-alarm rate could be determined in principle by Monte Carlo simulation. However, the amount of simulation that would be required would be enormous, because of the very small rate at which false alarms occur. Therefore, we will simply set the GLR detection threshold to the same value as the OSGLR detection threshold.

5.4.1 Linear Simulation with No Failure

The C-130 linear simulation was used to generate Kalman filter residuals for the unfailed system. The duration of the simulation was 50 s.

Figure 5.2 shows the OSGLR detection decision functions for the six actuators for this simulation. Several features in the figure are noteworthy. First, since each of the decision functions can be shown to be a central chi-squared random variable with six degrees of freedom, the mean value of each decision function should be 6. This fact appears to be verified by the figure.

Second, some of the decision functions have peak values that approach 20. This is far below the detection threshold $T^2 = 56.86$, as would be expected for a simulation of such short duration.

The third noteworthy feature of Figure 5.2 is that the detection decision functions corresponding to the ailerons and flaps (DF_2, DF_3, DF_5, and DF_6) show a striking similarity. This is not unexpected, as we saw in previous sections that the failure of a given wing control surface (aileron or flap) is not easily distinguishable from the failure of any other wing control surface. This was due to the fact that these four surfaces have similar effects on the dynamics of the aircraft. Therefore, the OSGLR detectors for these surfaces are similar. Hence, the OSGLR decision functions for these surfaces are similar, even when there is no failure present. This is an effect that will be apparent in all of the simulations, whether a wing control surface has failed or not.

Figure 5.3 shows the GLR detection decision functions for the same simulation. For this case, the data window for the GLR test was 2 s long (100 samples). The general character of the GLR decision functions is somewhat different than that of the OSGLR decision functions. The decision functions seem to be somewhat noisier and to have a smaller mean value.

However, there are also some similarities between Figures 5.3 and 5.2. First, the GLR decision functions for the wing control surfaces (DF_2, DF_3, DF_5, and DF_6) are all similar, although the similarity is not

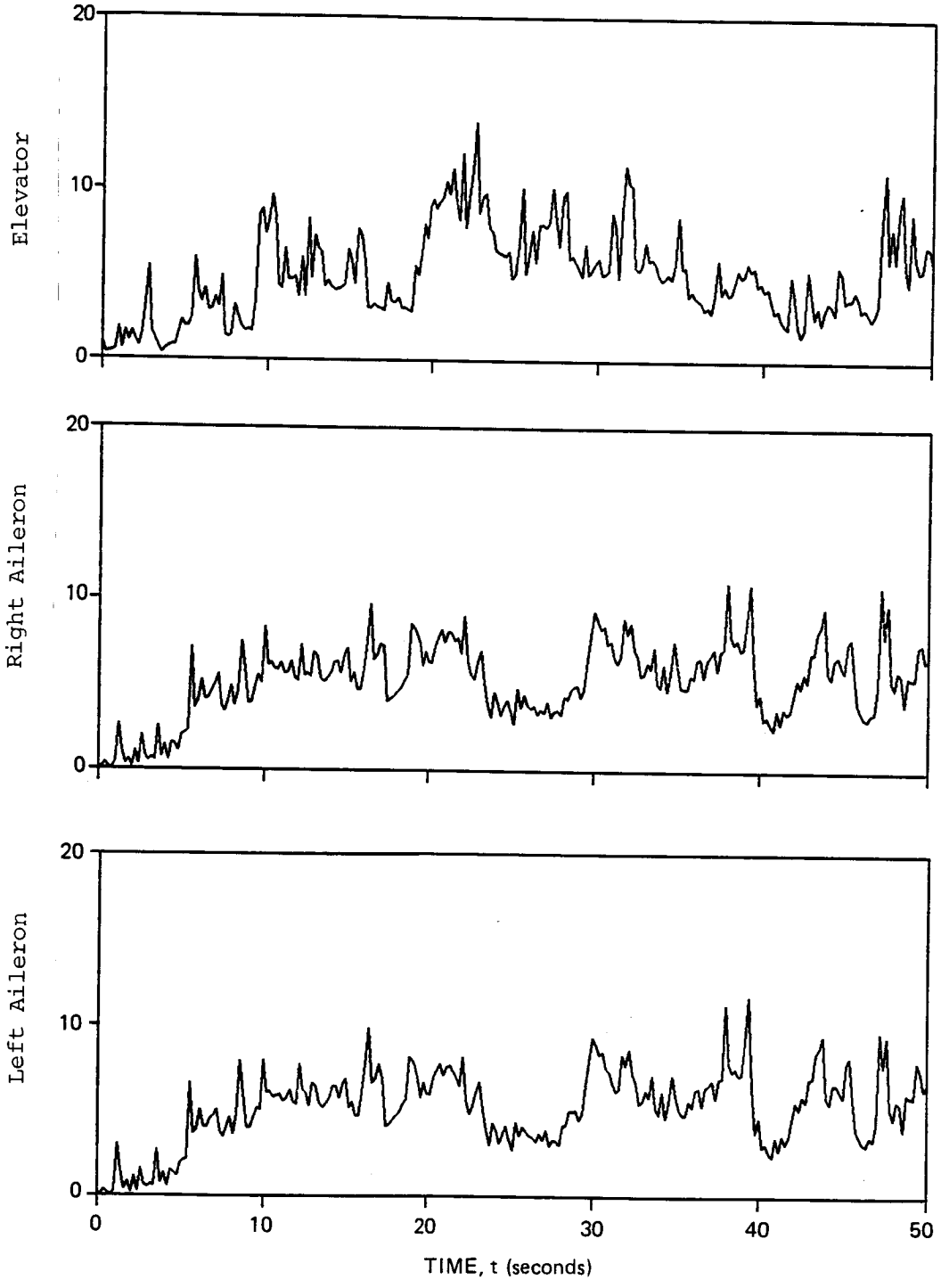

Figure 5.2. **OSGLR detection decision functions for the linear simulation with no failures**

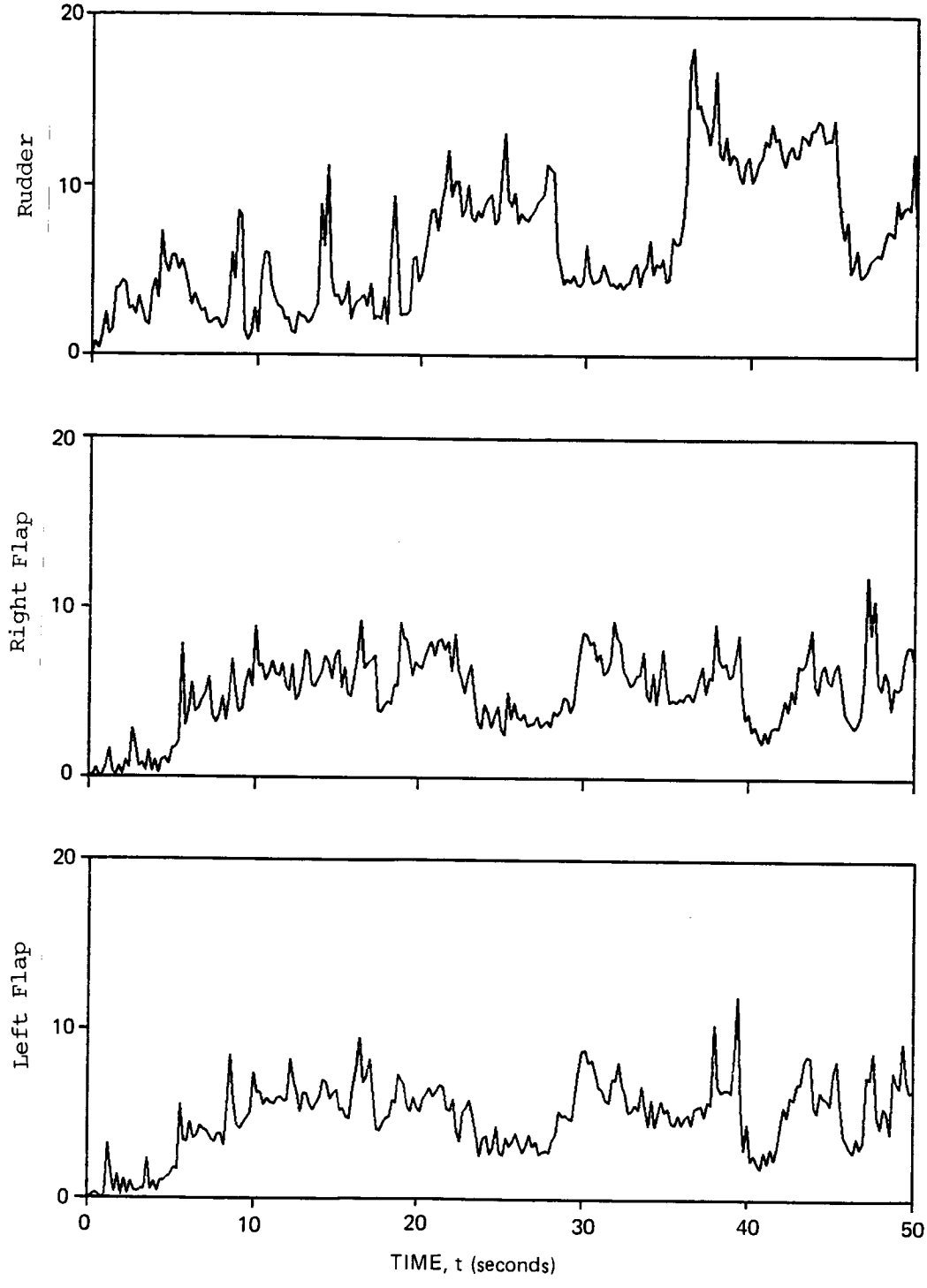

Figure 5.2. OSGLR detection decision functions for the linear simulation with no failures (Cont.)

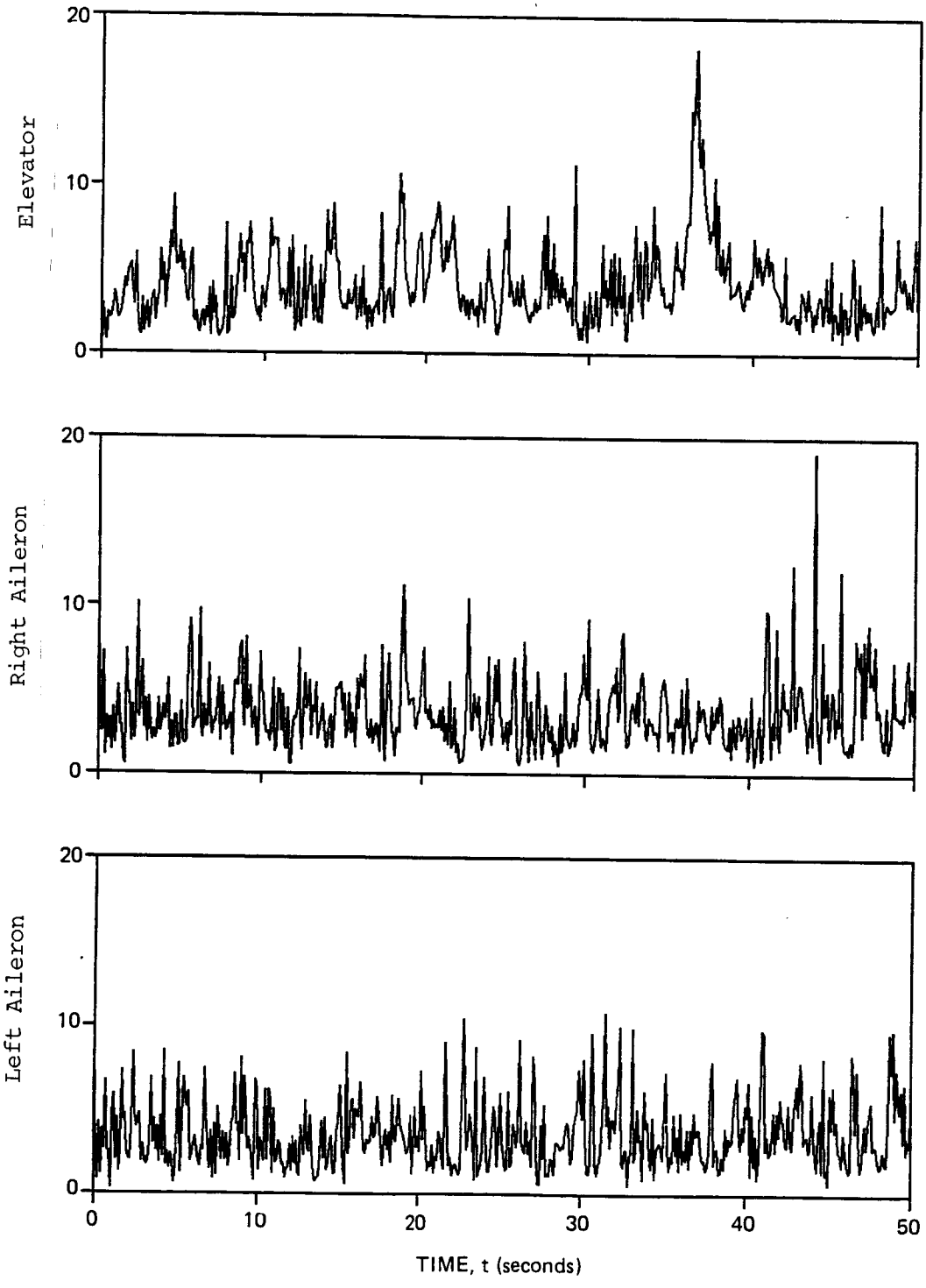

Figure 5.3. GLR detection decision functions for the linear simulation with no failures and a 2 s (100 sample) data window

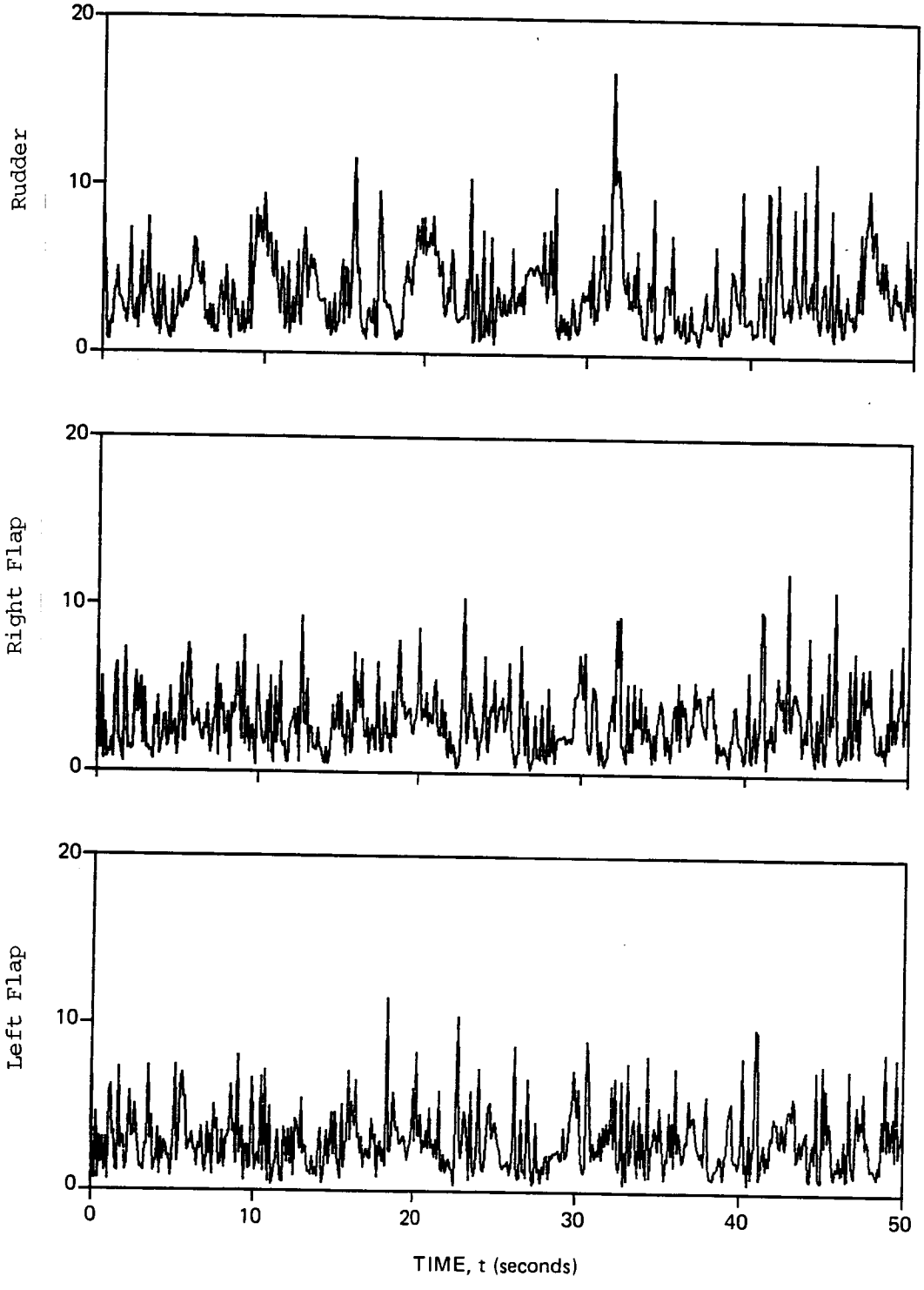

Figure 5.3. GLR detection decision functions for the linear simulation with no failures and a 2 s (100 sample) data window (Cont.)

as great as was the case for the OSGLR decision functions. Second, the peak values of some of the GLR decision functions are close to 20, as was the case with the OSGLR algorithm. From this we may conclude that the assumption that the GLR and OSGLR detection thresholds are the same is not unreasonable.

5.4.2 Elevator Bias Failure

In this case, a -0.01745 rad (-1°) bias of the elevator was simulated, using the linear simulation. The failure occurred at time t = 10 s of a 50 s simulation.

Figure 5.4 shows the OSGLR detection decision functions for the six control surfaces. The decision functions generally have the characteristics that we expect. Immediately following the onset of the failure, the decision function corresponding to the elevator, DF_1, increases rapidly, indicating a failure of the elevator. To a lesser extent, the other decision functions increase as well, although they are always much less than DF_1. For the detection threshold selected, detection occurs at t = 10.22 s, 0.22 s after the onset of the failure.

Several other features of the figure are noteworthy. First, the four decision functions DF_2, DF_3, DF_5, and DF_6 are very nearly equal. This is a characteristic that will be seen in all the simulations. It is simply a reflection of the fact that the four OSGLR detectors for the control surfaces on the wing are similar, because the effects of these surfaces on the aircraft are similar. Second, note that the elevator failure is easily isolated, because DF_1 is significantly larger than the other decision functions.

Figure 5.5 shows the GLR detection decision functions for the same simulation, using a 2 s (100 sample) data window. For the 2 s period immediately following the failure, the GLR detection functions closely resemble the OSGLR decision functions. The elevator decision function increases rapidly, crossing the detection threshold at t = 10.12 s.

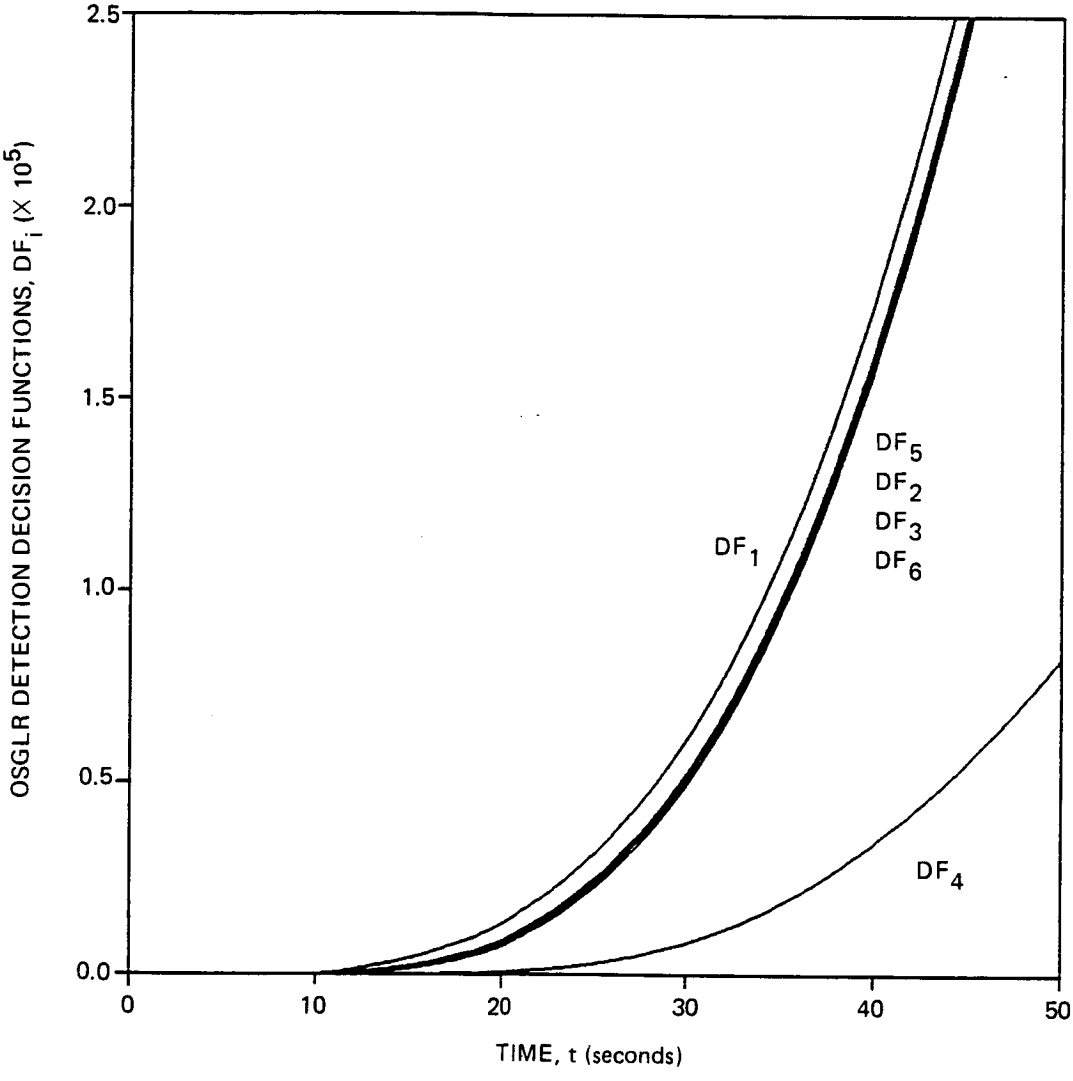

Figure 5.4. OSGLR detection decision functions for the linear simulation with a -0.01745 rad (-1°) bias failure of the elevator at time t = 10 s

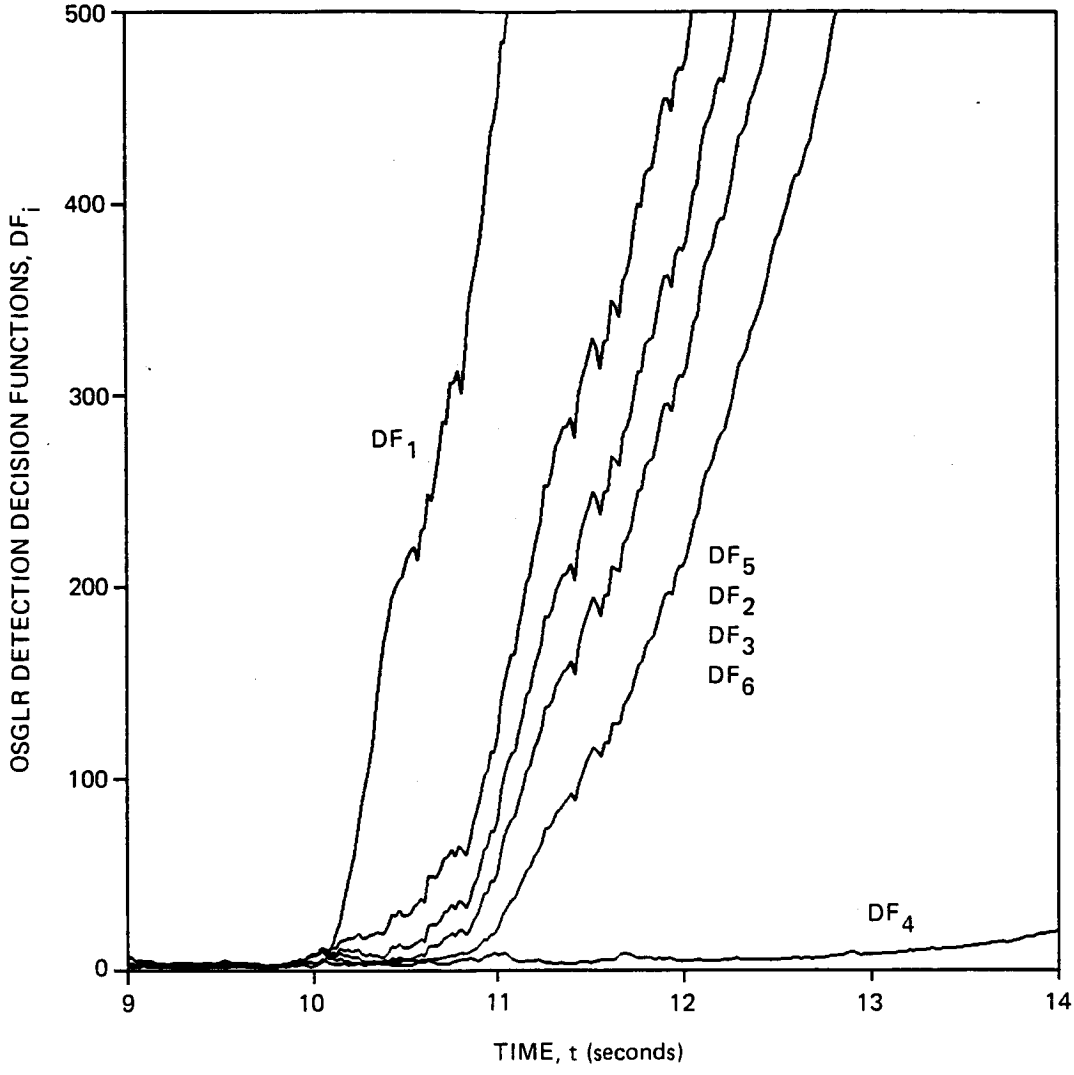

Figure 5.4. OSGLR detection decision functions for the linear simulation with a -0.01745 rad (-1^{o}) bias failure of the elevator at time t = 10 s (Cont.)

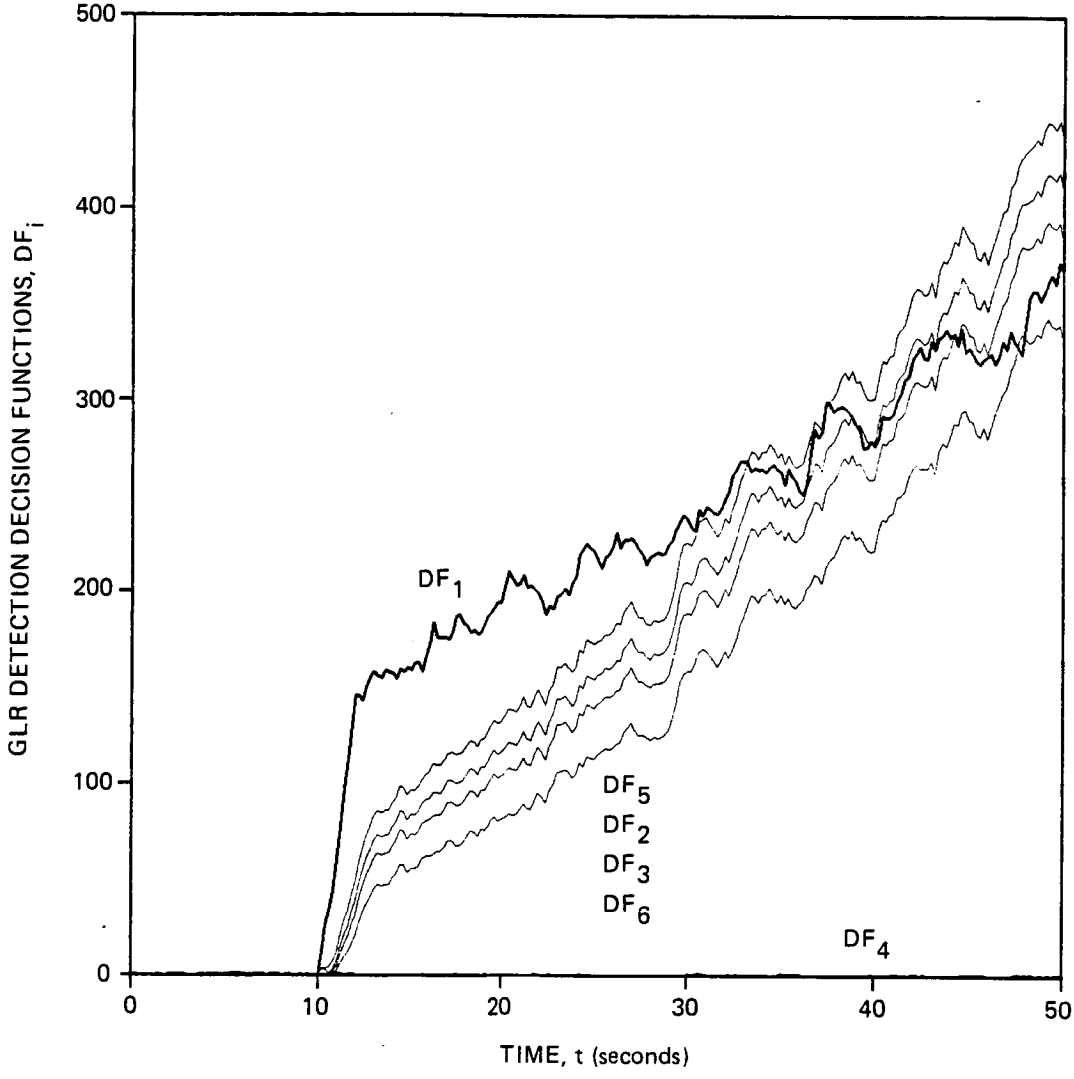

Figure 5.5. GLR detection decision functions for the linear simulation with a -0.01745 rad (-1°) bias failure of the elevator at time t = 10 s. A 100 sample (2 s) data window was used.

It is not surprising that the GLR detection time is less than that of the OSGLR test, because the GLR hypotheses can represent the failure mode exactly, whereas the OSGLR hypotheses can only approximate the failure mode. Also, the time scale of the basis functions is $\tau = 3$ s, which is considerably longer than the time required to detect the failure. If the time scale is reduced to $\tau = 0.5$ s, then the detection time for the OSGLR test is the same as for the GLR test. However, it was felt that the longer time scale was desirable to allow for failures that take longer to detect. Furthermore, the detection time of 0.22 s is probably acceptable.

Despite the good performance of the GLR test, the algorithm does display some undesirable characteristics. Note that at $t = 12$ s (2 s after the onset of the failure), the decision functions suddenly level off. This is due, of course, to the finite data window of the GLR test. The GLR algorithm accumulates data for only the length of the data window, which is 2 s long in this case. After that time, information about the failure is lost.

Furthermore, note that DF_5 exceeds DF_1 after $t = 33.2$ s. Had the threshold been larger, or the failure been smaller, the GLR test could have isolated the failure to the wrong component, namely, the right flap. The reason for this behavior is again related to the data window. After $t = 12$ s, the actual failure (a step failure at $t = 10$ s) is not one of the failures considered by the GLR test. Therefore, the behavior of the algorithm is unpredictable after $t = 12$ s.

The OSGLR test does not have the undesirable characteristics of the GLR test discussed above. The OSGLR hypotheses can represent the step failure, at least approximately, over a long time period, even though the approximation is somewhat inaccurate for a very short time period. Over a long time period, the OSGLR test continues to accumulate information about the failure. As a result, the OSGLR test does not display the characteristics of the GLR test which are associated with the finite data window.

5.4.3 Rudder Bias Failure

In this case, a 0.0349 rad (2°) bias of the rudder was simulated, using the linear simulation. The failure occurs at time t = 10 s of a 50 s simulation.

Figure 5.6 shows the resulting OSGLR detection decision functions. In many ways, this simulation resembles that of the elevator. The decision function corresponding to the failed component, DF_4, increases rapidly following the onset of the failure. The other decision functions increase also, but much more slowly than DF_4. The failure is detected at t = 13.06 s, 3.06 s after the beginning of the failure. The conclusion which can be drawn is that rudder failures are easily distinguishable from the other actuator failures. This is demonstrated by the extremely large difference between DF_4 and the other decision functions.

Figure 5.7 shows the GLR detection decision functions for this simulation, using a 2 s (100 sample) data window. After the onset of the failure, the rudder decision function, DF_4, increases quickly, indicating a failure of the rudder. The other five decision functions increase little, if any. The failure is detected at t = 11.80 s, when DF_4 exceeds the detection threshold. Shortly thereafter, at t = 12 s, DF_4 abruptly changes character. At this time, DF_4 levels off, except for wide fluctuations due to noise. Again, this behavior is attributable to the finite data window of the GLR test. Note that had the detection threshold been only slightly larger, say, $T^2 = 75$, then the detection time would have been greatly increased, from 1.08 s to 7.08 s.

Note that the detection time for the OSGLR test is somewhat longer than for the GLR test. The reason for this is as follows. The step failure in the rudder causes rapid changes in the mean values of some of the Kalman filter residuals. The OSGLR hypotheses are unable to accurately represent the discontinuities in the residuals. Therefore, some of the energy of the failure signature cannot be used by the OSGLR

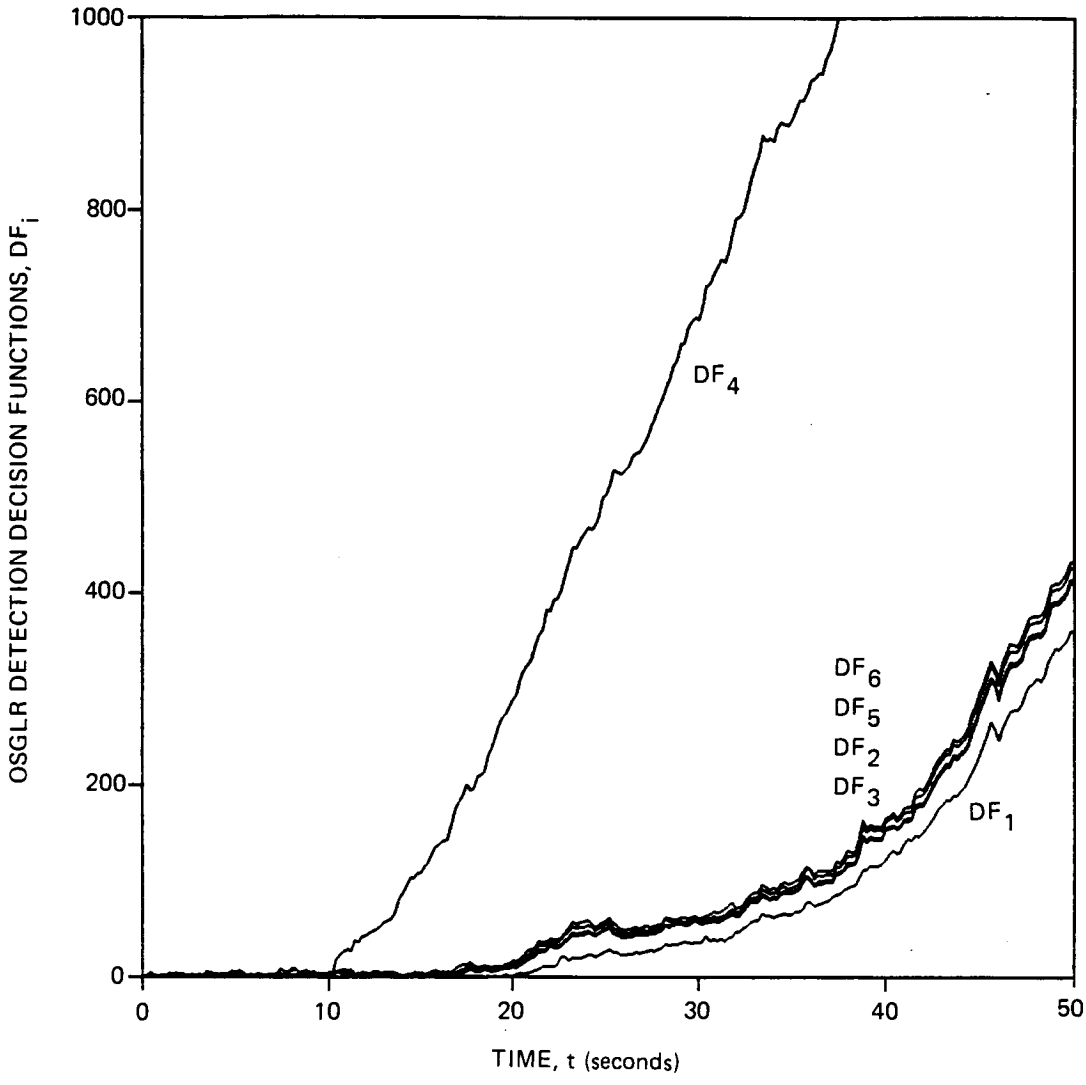

Figure 5.6. OSGLR detection decision functions for the linear simulation with a 0.0349 rad (2^{o}) bias failure of the rudder at time t = 10 s

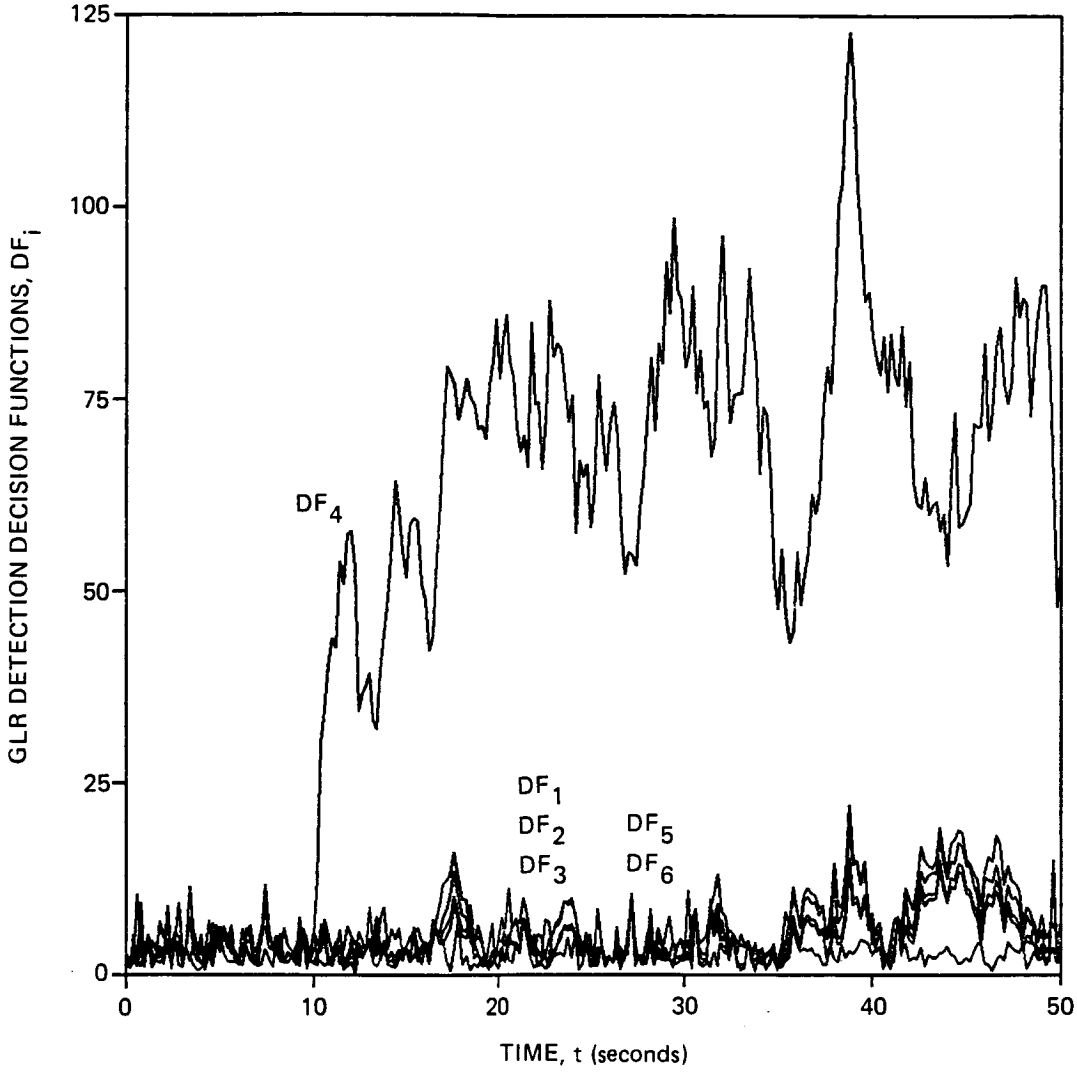

Figure 5.7. GLR detection decision functions for the linear simulation with a 0.0349 rad (2^{o}) bias failure of the rudder at time = 10 s. A sample (2 s) data window was used.

algorithm to detect the failure. On the other hand, the GLR hypotheses can represent the failure signature exactly within the data window.

The overall performance of the OSGLR test for this case is generally good. Although the detection time is slightly longer for the OSGLR test than for the GLR test, the OSGLR algorithm appears to be more robust than the GLR algorithm.

5.4.4 Right Aileron Bias Failure

In this case, the linear simulation was used to simulate a 0.0175 rad (1°) bias failure of the right aileron. The failure occurred at time t = 10 s of a 50 s simulation.

Figure 5.8 shows the OSGLR detection decision functions for this simulation. Immediately following the failure, these four decision functions corresponding to the wing control surfaces (DF_2, DF_3, DF_5, and DF_6) begin to rise steadily. To the scale of the plot, these four decision functions cannot be distinguished. The elevator decision function (DF_1) also rises steadily following the failure. On the plot, DF_1 appears to be close to the four decision functions of the ailerons and flaps. On an absolute scale, however, this difference is large. Finally, the rudder decision function (DF_4) also increases somewhat, although not nearly so much as the other five decision functions. For the detection threshold given, the detection occurs 0.56 s after the onset of the failure.

In order to determine which of the four detection decision functions of the wing control surfaces is largest following the failure, (some of) the OSGLR isolation decision functions are plotted in Figure 5.9. The isolation decision function DF_{ij} is defined to be

$$DF_{ij} = DF_i - DF_j \tag{5.96}$$

Shown in the figure are DF_{23}, DF_{25}, and DF_{26}. Following the failure, all

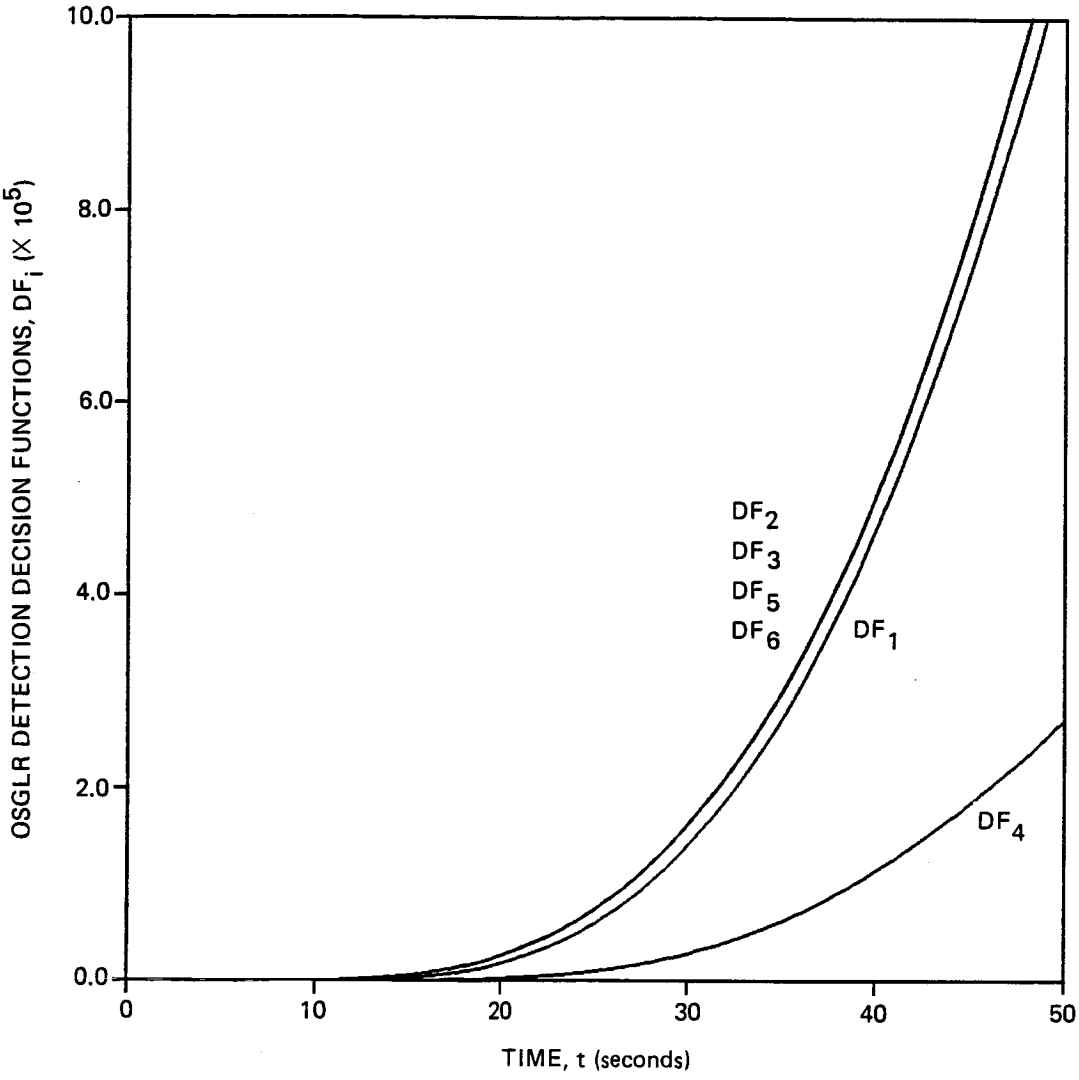

Figure 5.8. OSGLR detection decision functions for the linear simulation with a 0.01745 rad (1°) bias failure of the right aileron at time t = 10 s

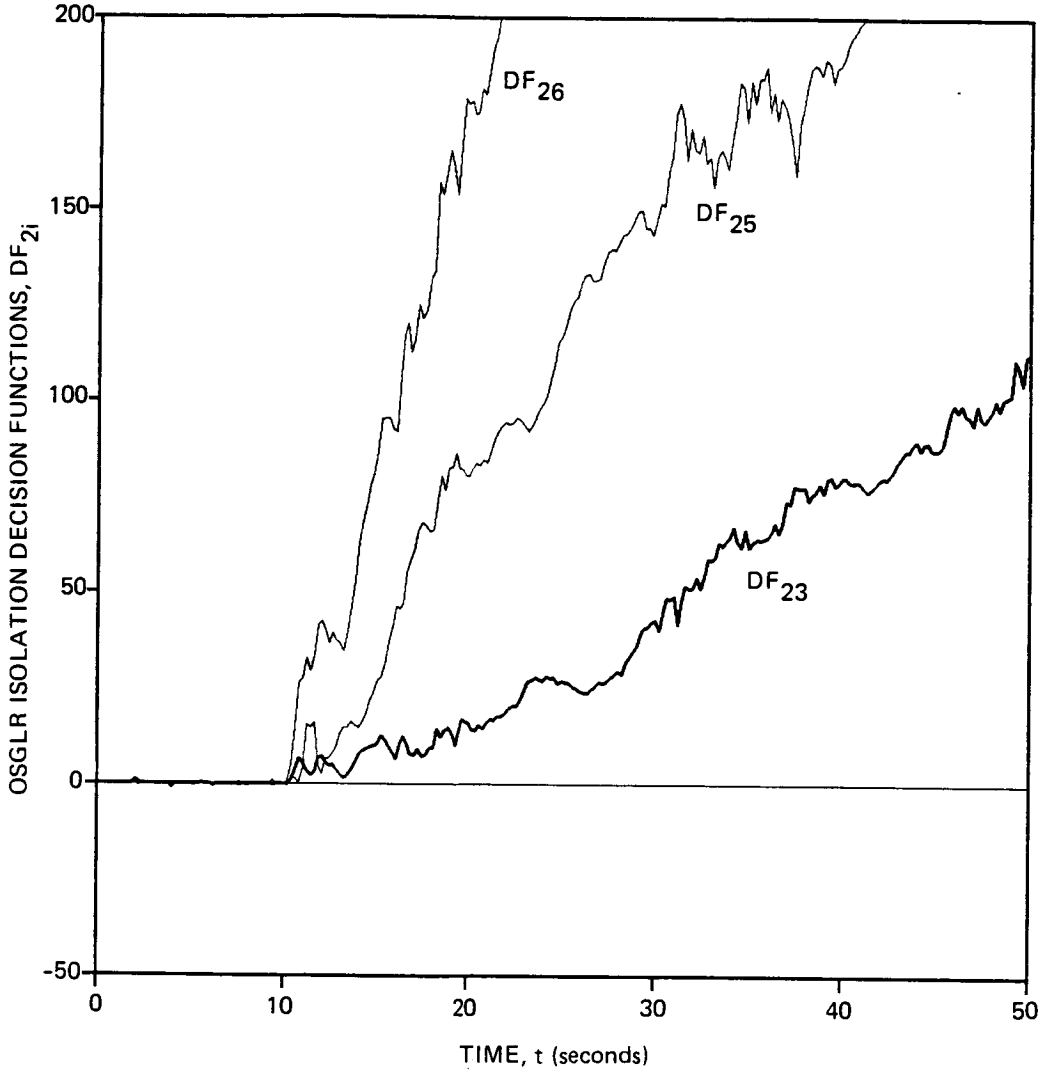

Figure 5.9. OSGLR isolation decision functions for the linear simulation with a 0.01745 rad (1°) bias failure of the right aileron at time t = 10 s

three of these isolation decision functions are positive, correctly indicating that the right aileron is the surface that has failed. Also, except for a brief period immediately following the failure,

$$DF_{26} > DF_{25} > DF_{23}$$

These results imply that it is relatively easy to distinguish between failures of the right aileron and the elevator or rudder, but progressively more difficult to distinguish a right aileron failure from the failure of the left flap, the right flap, and the left aileron.

Note that because the failure of the right aileron is barely distinguishable from failures of the other three wing control surfaces, it would be wise to use an isolation threshold for this system to prevent incorrect isolations. We have not attempted to determine an isolation threshold for this study. However, it is clear that an isolation threshold that is large enough to be effective at preventing incorrect isolations will cause a significant delay in the isolation of the failure, perhaps 10 s or more.

Figure 5.10 shows the GLR detection decision functions for this simulation. (Note the difference in scale from Figure 5.9.) In many respects, Figure 5.10 resembles Figure 5.8. Immediately following the failure, the aileron and flap decision functions increase rapidly. At t = 12 s, however, the rate of increase of these decision functions slows, due to the finite data window. To a lesser degree, the elevator and rudder decision functions increase also. Detection occurs 0.48 s after the failure.

Figure 5.11 shows the GLR isolation decision functions DF_{23}, DF_{25}, and DF_{26}. Note that the GLR isolation decision functions are somewhat smaller than the OSGLR isolation decision functions (cf Figure 5.9). Once again, this is because the finite data window limits the amount of information that can be accumulated about the failure. Also

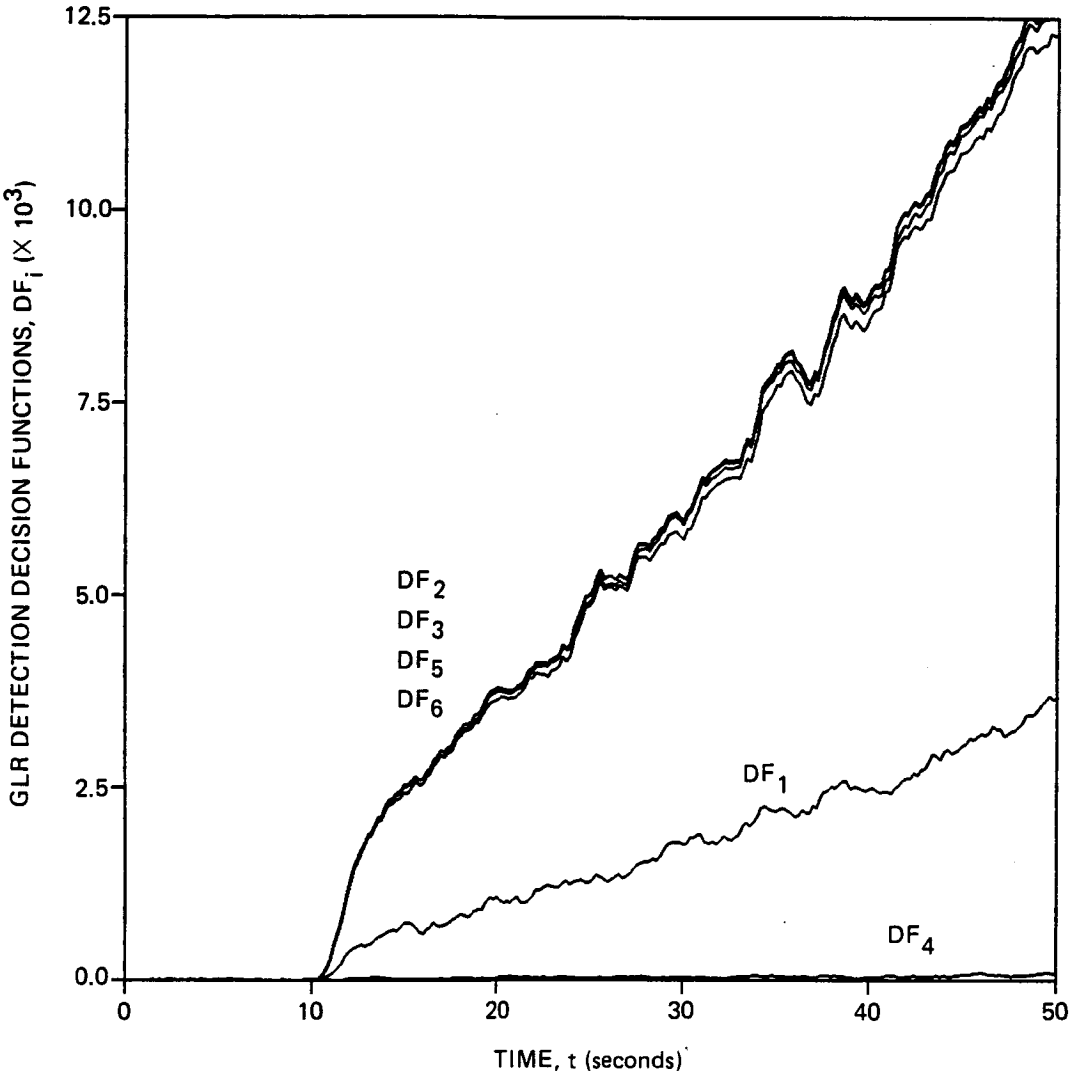

Figure 5.10. GLR detection decision functions for the linear simulation with a 0.01745 rad (1°) bias failure of the right aileron at time t = 10 s. A 100 sample (2 s) data window was used.

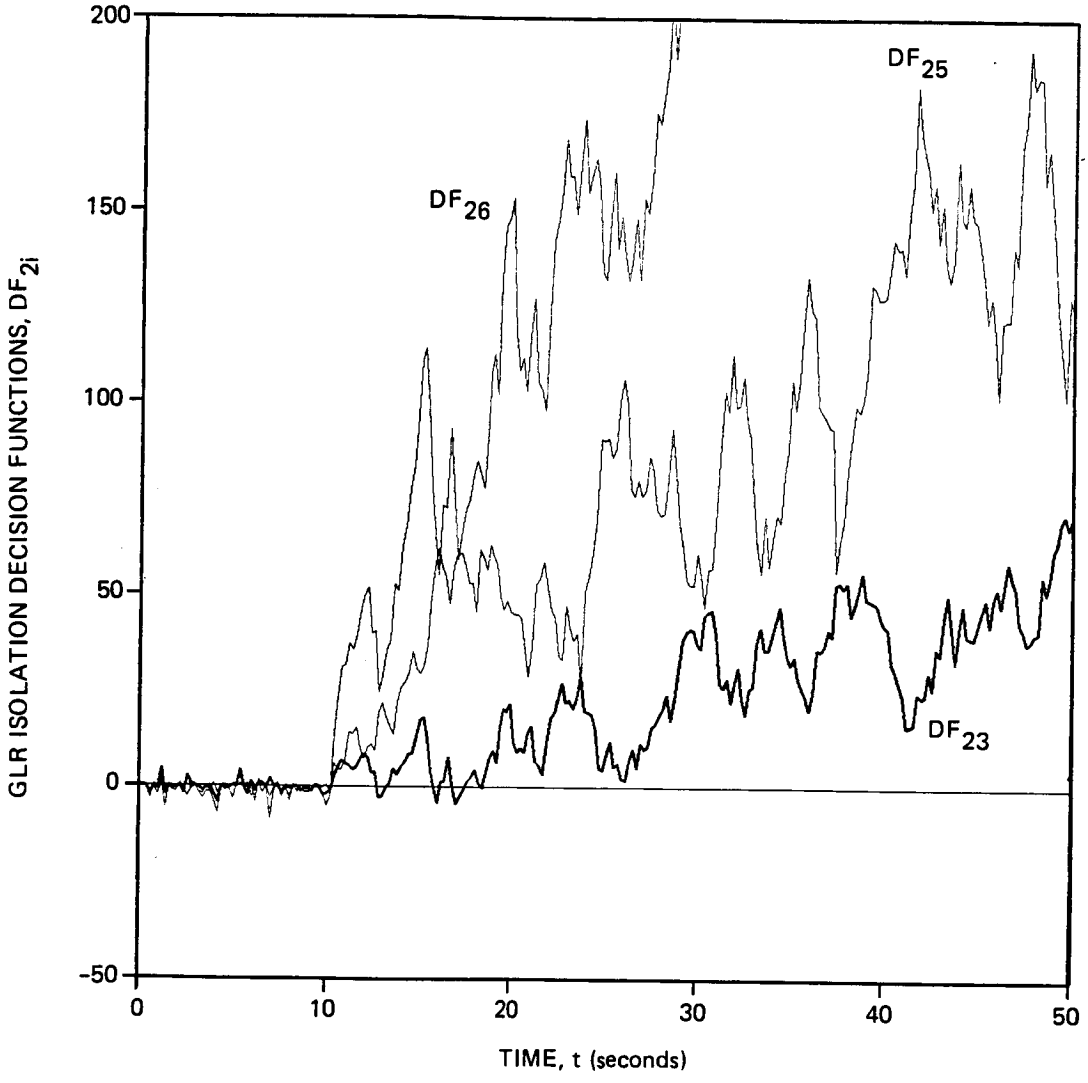

Figure 5.11. GLR isolation decision functions for the linear simulation with a 0.01745 rad (1^{o}) bias failure of the right aileron at time t = 10 s.

note that even as late as 7.5 s after the failure, DF_{23} is occasionally negative, indicating that the failure is in the left aileron, rather than the right aileron. Even at t = 26 s, 16 s after the failure, DF_{23} is close to zero. Thus, the behavior of the OSGLR test seems to be more robust for this case.

5.4.5 Rudder Ramp Failure

The failures simulated thus far have all been step bias failures. This puts the GLR test at an advantage, since the GLR test assumes a bias failure mode, whereas the OSGLR test assumes a more general failure mode shape. To see how these tests perform with a different failure mode, a ramp failure of the rudder was simulated, using the linear simulation. The ramp begins at t = 10 s, and the ramp increases at a rate of 0.001745 rad/s (0.1 deg/s).

Figure 5.12 shows the resulting OSGLR decision functions. The decision functions change very little until about t = 15 s. At that time, the rudder decision function begins to increase, albeit slowly at first. As the magnitude of the failure increases, DF_4 increases more rapidly. DF_4 crosses the detection threshold at t = 23.08 s, so that the time to detection is 13.08 s. Meanwhile, the other five decision functions increase only slightly until about t = 24 s, at which time these decision functions begin to increase. Thus, this failure is easily detected using the OSGLR test.

Figure 5.13 shows the GLR detection decision functions for this simulation, using a 2 s (100 sample) data window. This figure is similar to Figure 5.12, except that the decision functions are generally smaller than for the OSGLR test. Also, DF_4 seems to be quite a bit noisier. The detection time for the GLR test is 18.88 s, which is significantly longer than for the OSGLR test. The major reason for this is that the data window is too short to allow enough data to be accumulated to detect the failure.

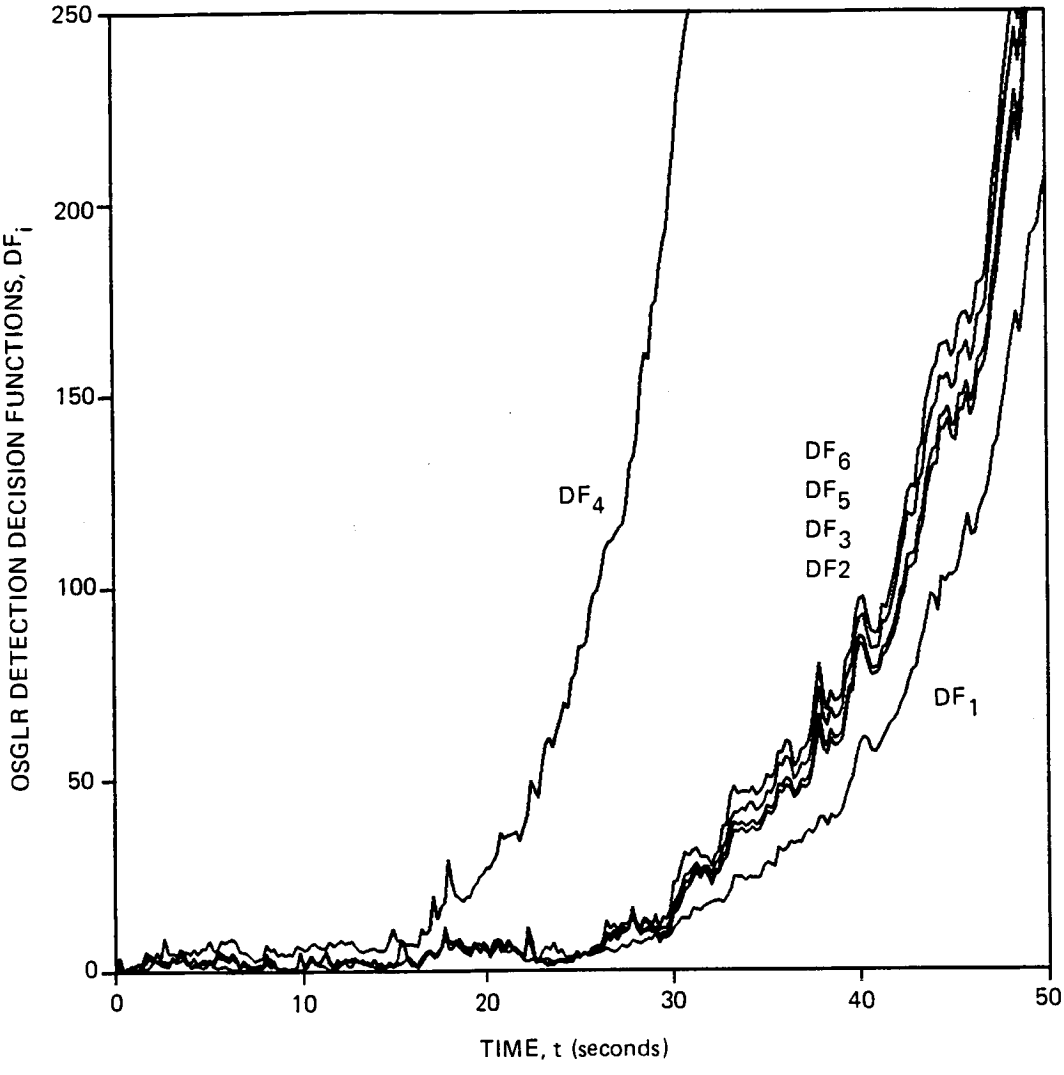

Figure 5.12. OSGLR detection decision functions for the linear simulation with a 0.001745 rad/s (0.1°/s) ramp failure of the rudder at time = 10 s

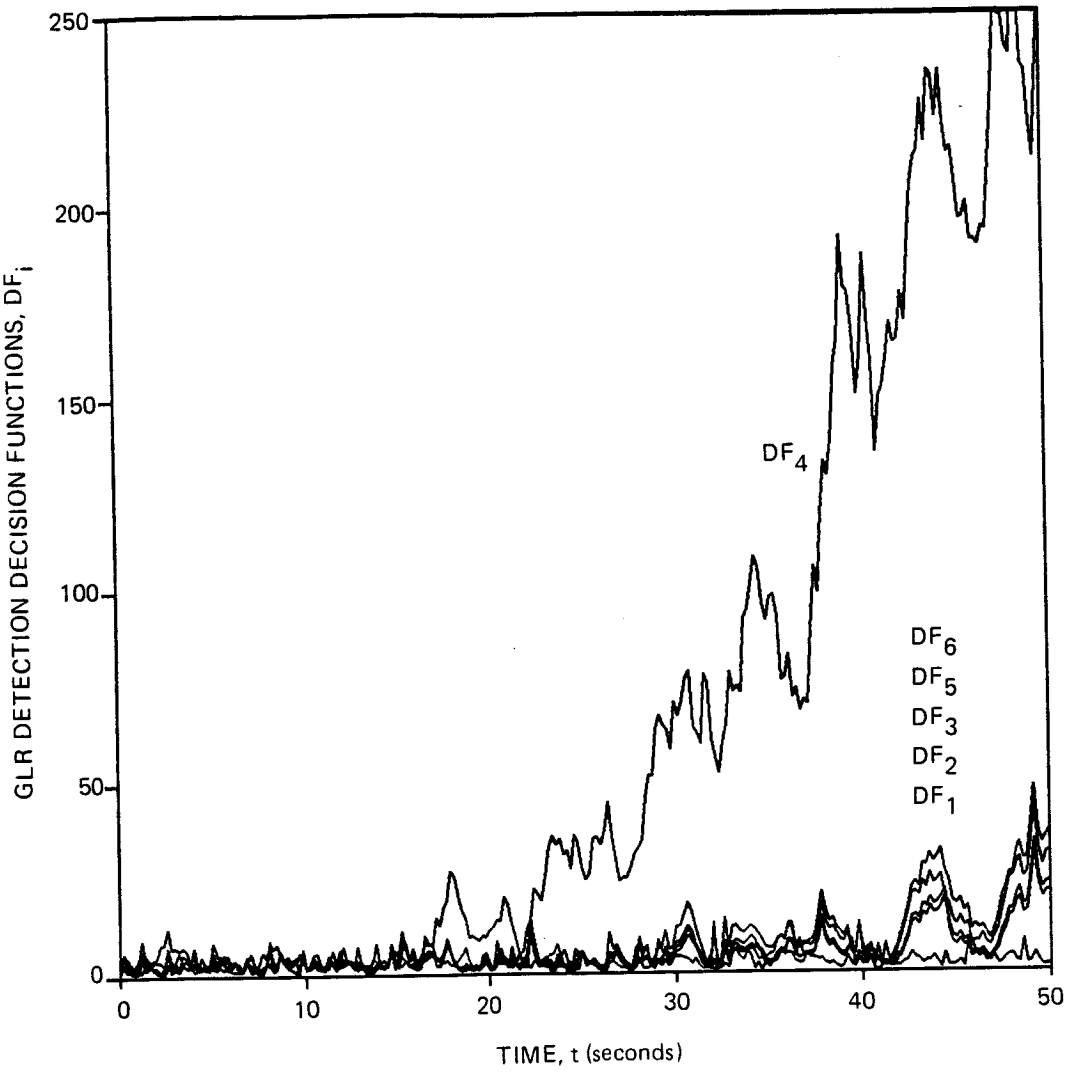

Figure 5.13. GLR detection decision functions for the linear simulation with a 0.001745 rad/s (0.1°/s) ramp failure of the rudder at time t = 10 s. A 100 sample (2 s) data window was used.

To demonstrate this last point, the GLR data window was increased to 5 s (250 samples) (Figure 5.14). In this case, DF_4 increases more rapidly than with the 2 s data window. The detection time for this case is 14.90 s, which compares favorably with the OSGLR test, although the OSGLR test still performs slightly better than the GLR test in this case.

5.4.6 Nonlinear Simulation with No Failure

This simulation is similar to that of Section 5.4.1, except that the nonlinear simulation was used instead of the linear simulation. In this case, it was necessary to implement the Kalman filter in order to generate the residuals.

Figure 5.15 shows the OSGLR detection decision functions for the nonlinear simulation with no failures. Ideally, the decision functions should resemble those of Figure 5.2. However, the decision functions in this case are quite different. Specifically, the decision functions for the wing control surfaces (DF_2, DF_3, DF_5, and DF_6) have peak values of approximately 500, which is a factor of 25 larger than the peaks seen in Figure 5.2. This effect is due to the differences between the nonlinear model and the linearized model generated from it. It was determined that the greatest source of error is due to mismodeling of the aerodynamic moments about the roll axis. This produces a bias in the estimate of roll rate, which is small compared to the standard deviation of the estimation error. However, this bias is integrated by the Kalman filter to produce a very large bias in the estimate of the bank angle. This in turn caused the residual associated with the bank angle measurement to be significantly biased. Because the four wing control surfaces primarily affect the roll axis, the decision functions associated with these surfaces are the ones most affected by this modeling error. The decision function associated with the elevator is also affected, because elevator deflections cause a moment about the roll axis, due to coupling between the longitudinal and the lateral dynamics. To a lesser extent,

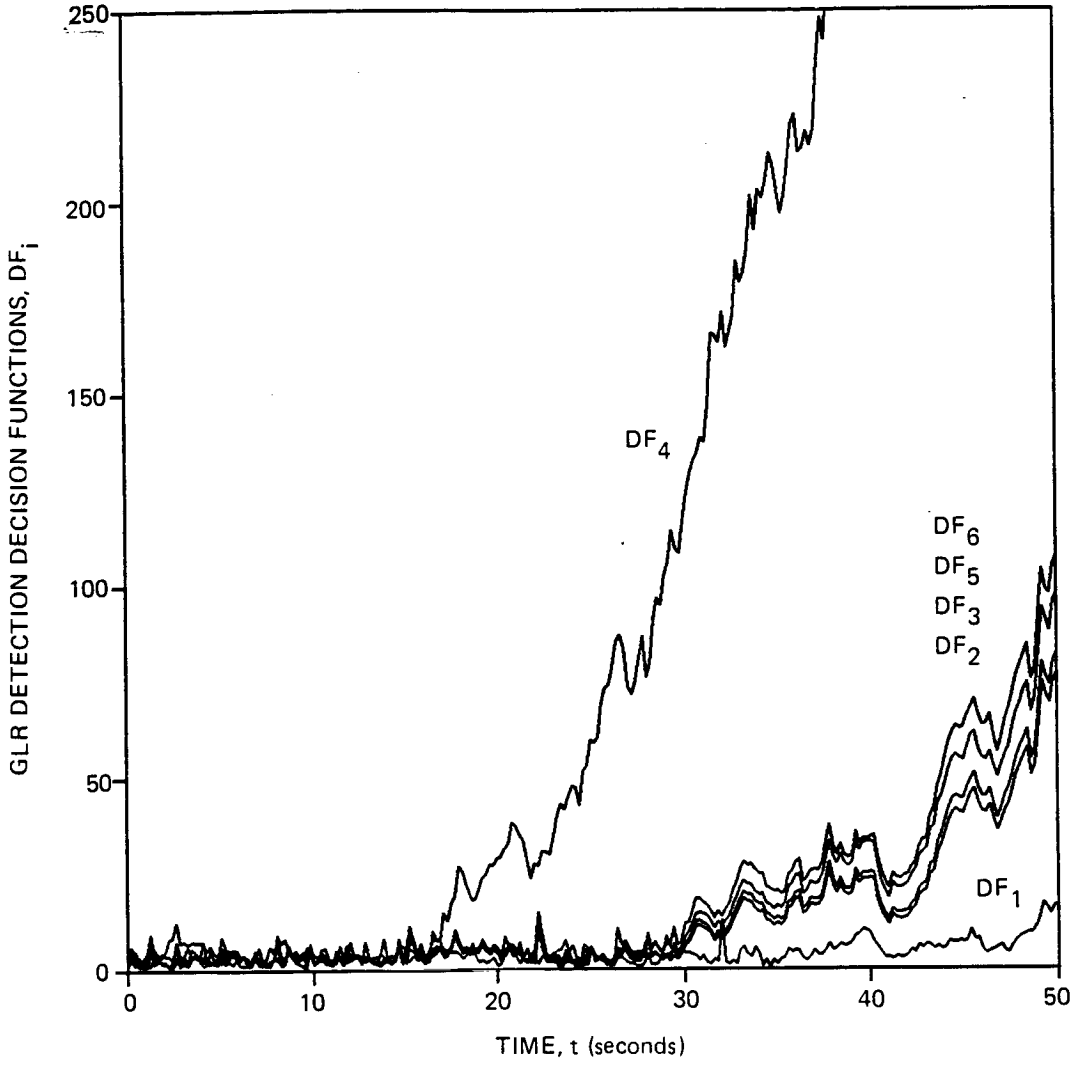

Figure 5.14. GLR detection decision functions for the linear simulation with a 0.001745 rad/s (0.1°/s) ramp failure of the rudder at time t = 10 s. A 250 sample (5 s) data window was used.

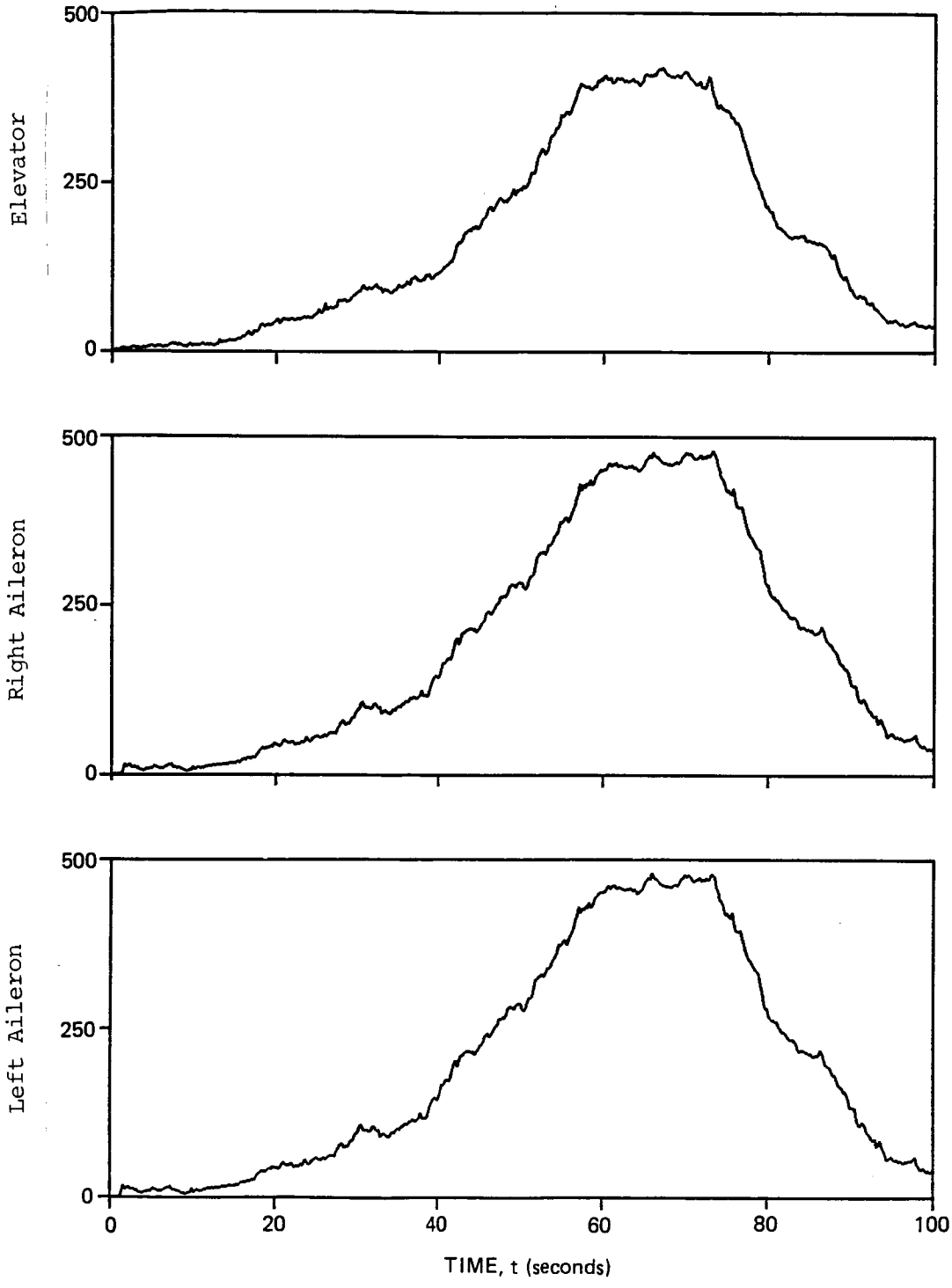

Figure 5.15. **OSGLR detection decision functions for the nonlinear simulation with no failures**

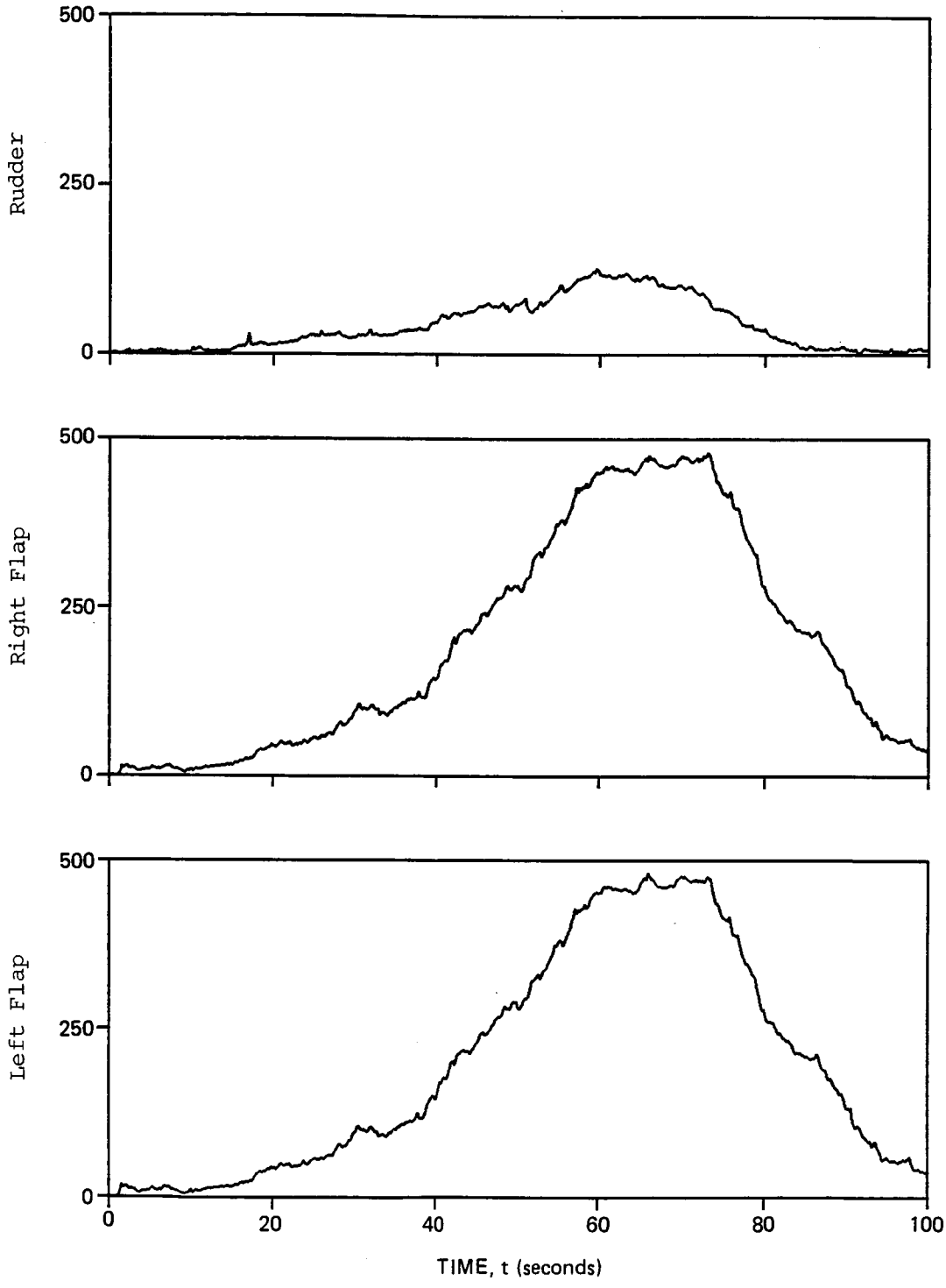

Figure 5.15. **OSGLR detection decision functions for the nonlinear simulation with no failures** (Cont.)

the rudder decision function is also affected, because the rudder can produce motion in the roll axis. However, the rudder is not as effective in producing rolling moments as the flaps, ailerons, or elevator (at this flight condition). Therefore, the rudder decision function is not as large as the others.

Figure 5.16 shows the GLR detection decision functions for the same simulation. Again, a 2 s (100 sample point) data window was used. As was the case with the OSGLR algorithm, the GLR decision functions are larger for the nonlinear simulation than for the linear simulation. In this case, the decision functions corresponding to the control surfaces on the wing reach peak values of approximately 35. This is much lower than the peak values of the OSGLR decision functions. There are two reasons for this. First, the GLR data window is relatively short. The energy in the residuals due to the biases in the estimation error is correlated over a time period much longer than 2 s. Hence, we might expect that a GLR detector with a longer data window would produce much larger decision functions. In fact, this is the case, as shown by Figure 5.17, which shows the GLR detection decision functions using a 5 s (250 sample) data window. (Note the difference in scale from Figure 5.16). In this case, the decision functions corresponding to the control surfaces on the wings have peak values of approximately 75, which is about twice as large as the peak values using a 2 s window.

The other reason that the GLR decision functions are smaller than the OSGLR decision functions is more subtle. Essentially, each GLR or OSGLR detector finds the failure input f(t) which generates a mean process in the residuals that most closely matches the observed residual process. However, the GLR algorithm considers (in this case) only step failures, whereas the OSGLR algorithm considers more general failure modes. Hence, the OSGLR algorithm can find among its hypotheses a failure input time history that matches the observed residuals more closely than does any of the step failures considered by the GLR algorithm. Thus, the same property of the OSGLR algorithm that makes it robust to failure mode uncertainty also makes it more sensitive to modeling errors.

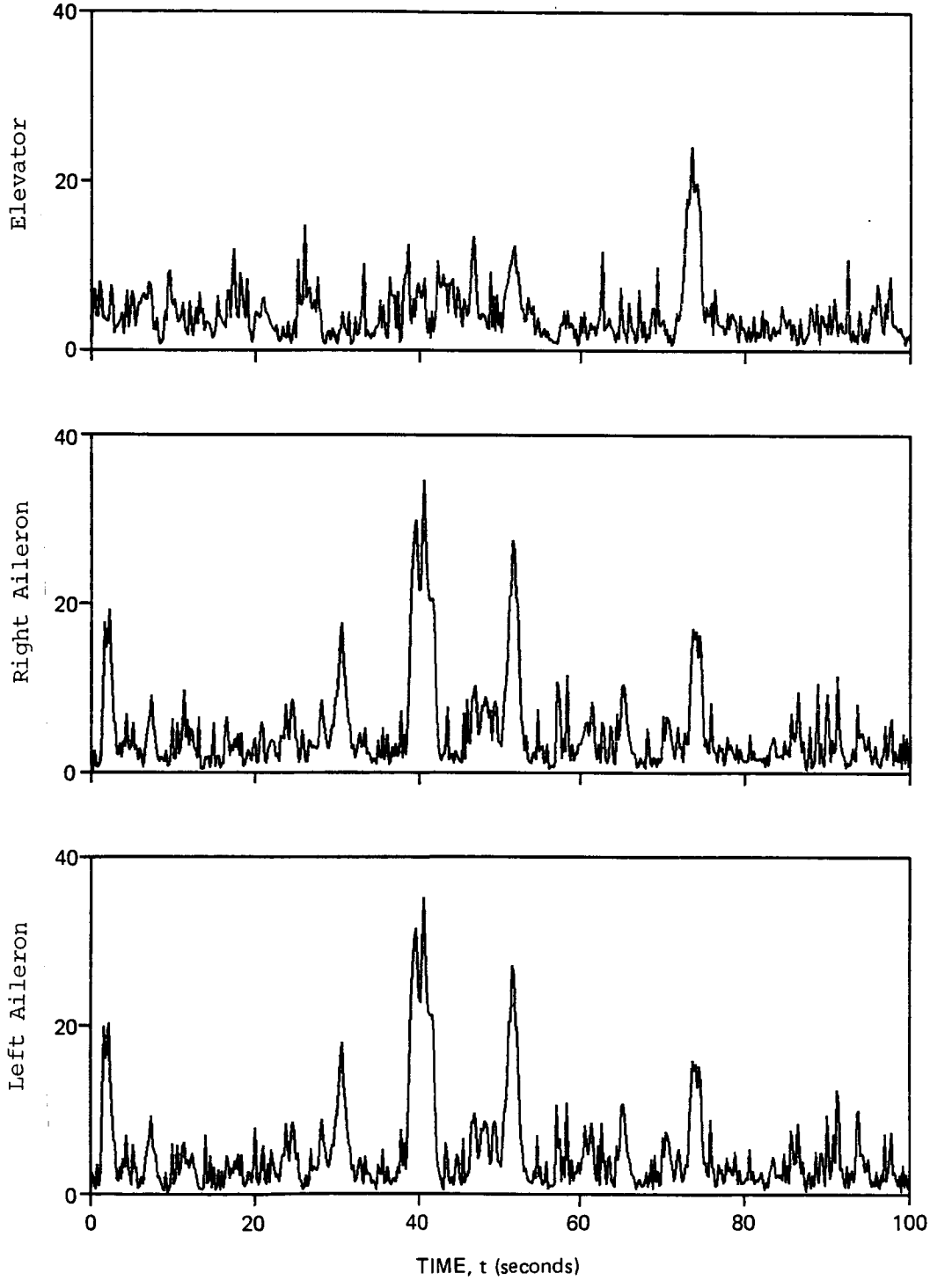

Figure 5.16. GLR detection decision functions for the nonlinear simulation with no failures and a 2 s (100 sample) data window

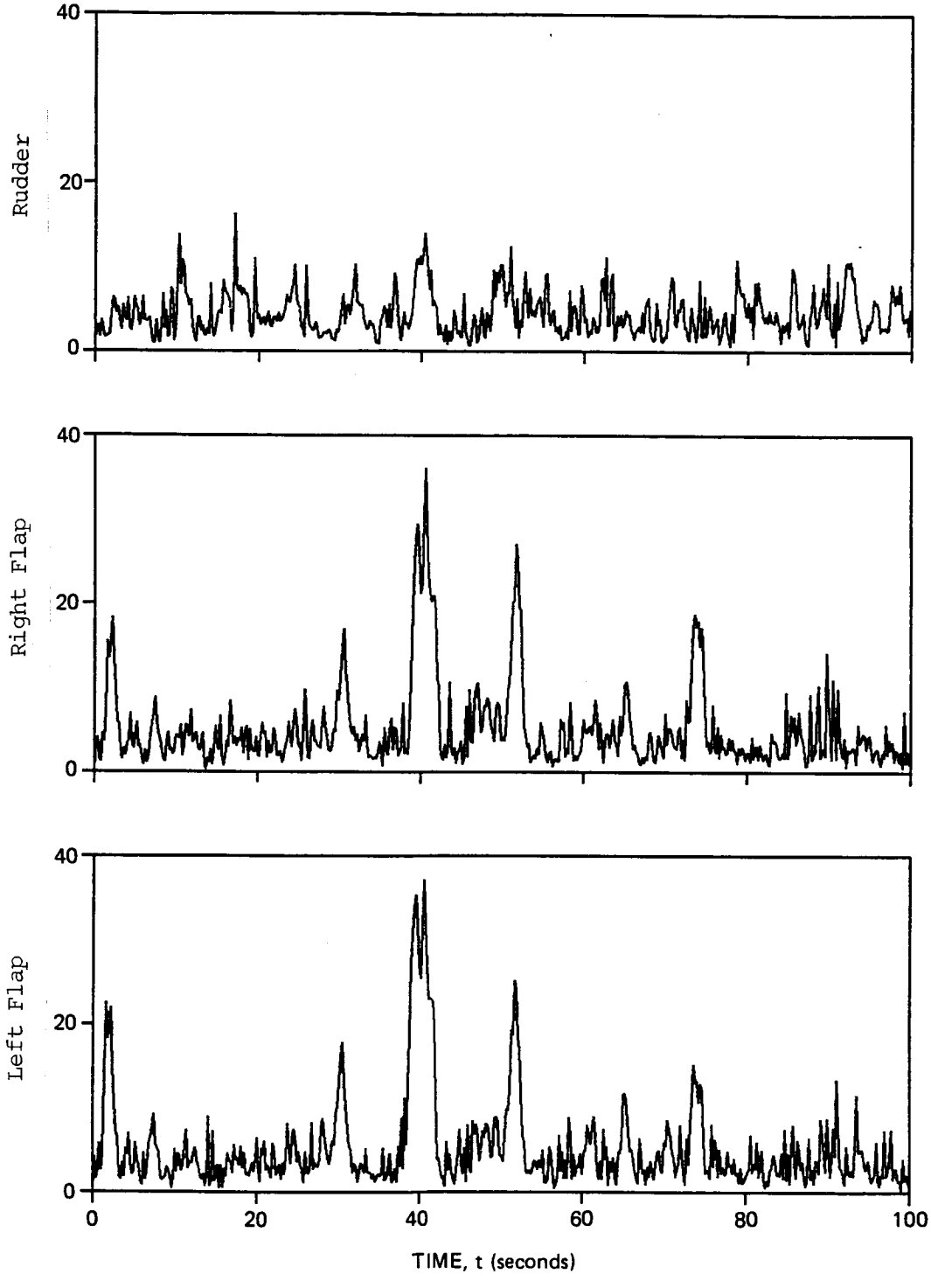

Figure 5.16. GLR detection decision functions for the nonlinear simulation with no failures and a 2 s (100 sample) data window (Cont.)

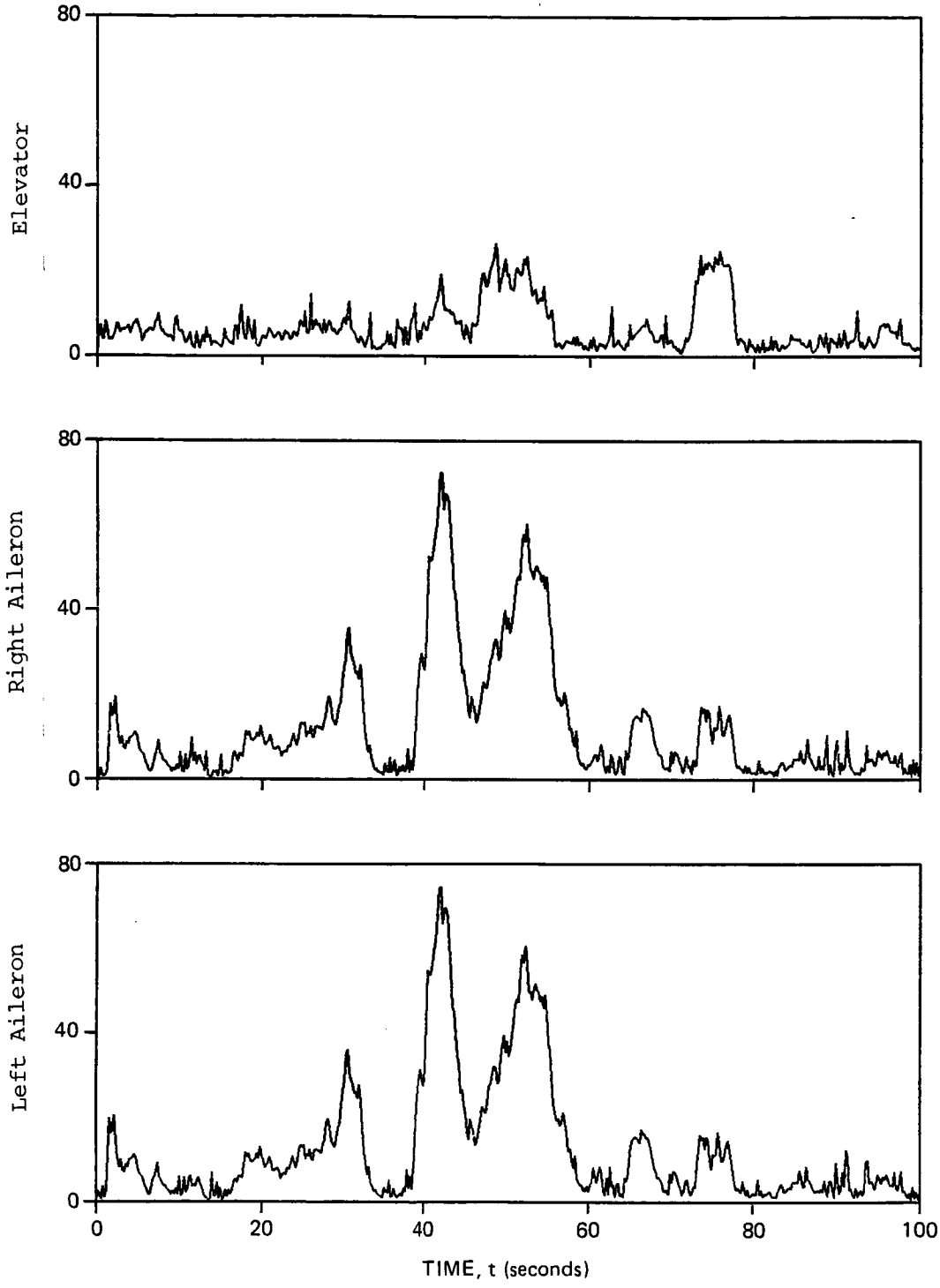

Figure 5.17. GLR detection decision functions for the nonlinear simulation with no failures and a 5 s (250 sample) data window

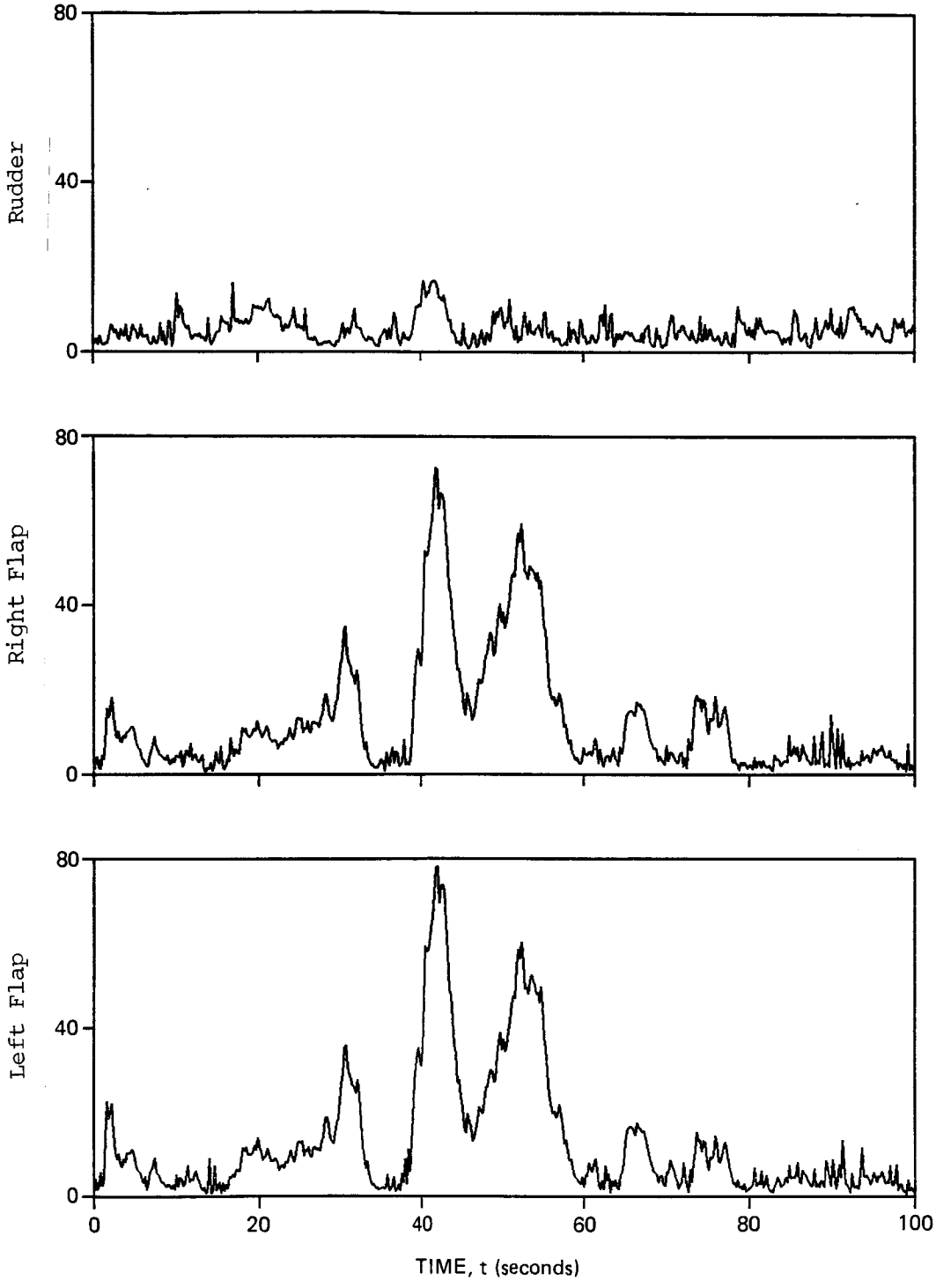

Figure 5.17. GLR detection decision functions for the nonlinear simulation with no failures and a 5 s (250 sample) data window (Cont.)

5.4.7 Stuck Elevator

In this case, the nonlinear simulation was used to simulate a stuck elevator. Such a failure might be caused, for example, by a jam of a mechanical linkage. The elevator was struck at δ_E = 0.0977 rad (0.56°). By comparison, the trim valve of the elevator deflection is approximately δ_E= 0.020 rad (1.15°). The failure occurred at time t = 10 s of a 50 s simulation. Figure 5.18 shows the resulting error in the elevator position, i.e., the difference between the actual elevator position and the commanded elevator position. Note that the history of the error does not fit into any easily characterized category, such as a bias or ramp failure.

Figure 5.19 shows the resulting OSGLR detection decision functions. The OSGLR test performs quite well in this case, despite the complexity of the failure input. Approximately 1 s after the onset of the failure, the elevator decision function, DF_1, increases rapidly, indicating a failure. The other five decision functions also increase, but they are always significantly smaller than DF_1. For the threshold selected earlier, the failure is detected at t = 11.94 s. (Note, however, that this threshold would not be used unless the problem of modeling errors had been addressed.)

Figure 5.20 shows the GLR detection decision functions for this case, using a 2 s (100 sample) data window. For the 3 s immediately following the onset of the failure, the GLR decision functions resemble the OSGLR decision functions. (cf. Figure 5.19.) DF_1 increases rapidly, indicating a failure of the elevator. For the threshold selected, the detection of the failure occurs at t = 12.14 s, 2.14 s after the onset of the failure. This is not significantly different from the OSGLR test.

However, this result is somewhat misleading. Note that at about t = 13 s, DF_1 begins to <u>decrease</u> for the GLR test, until at t = 15 s it is at about the same value that it had before the failure. For a brief time, the four decision functions corresponding to the control surfaces

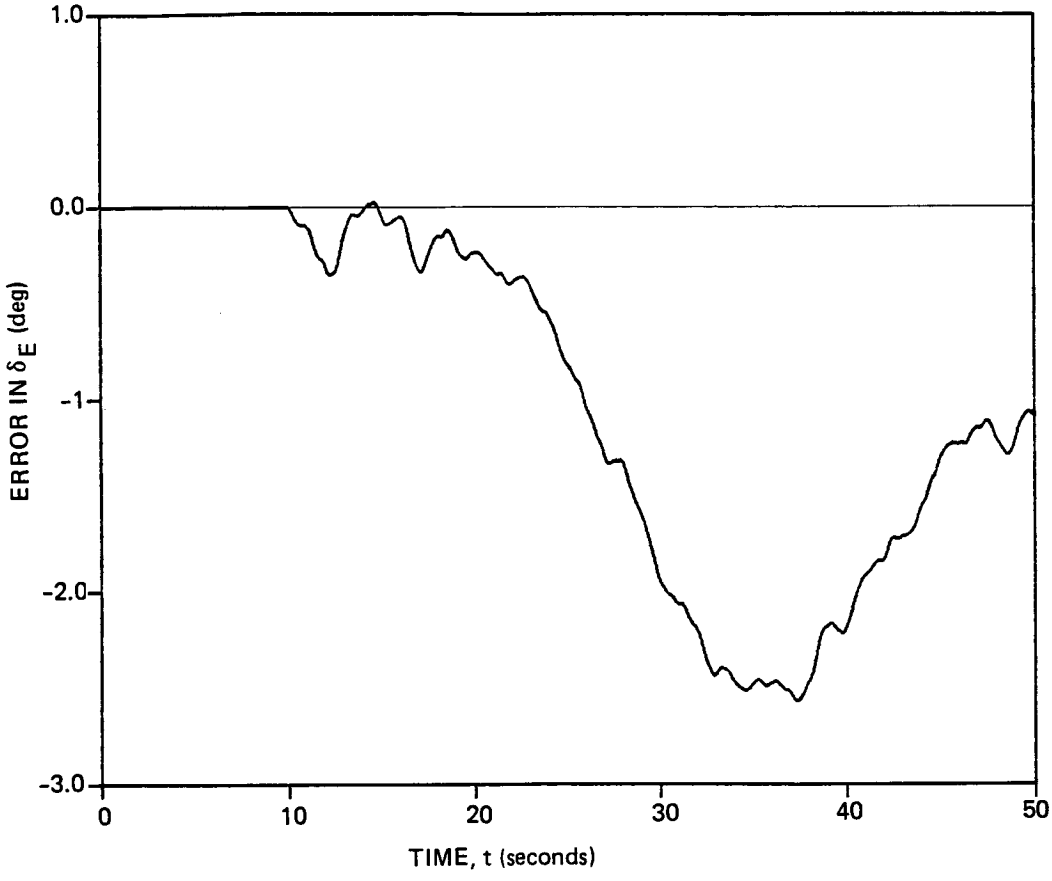

Figure 5.18. Error in elevator deflection due to stuck elevator

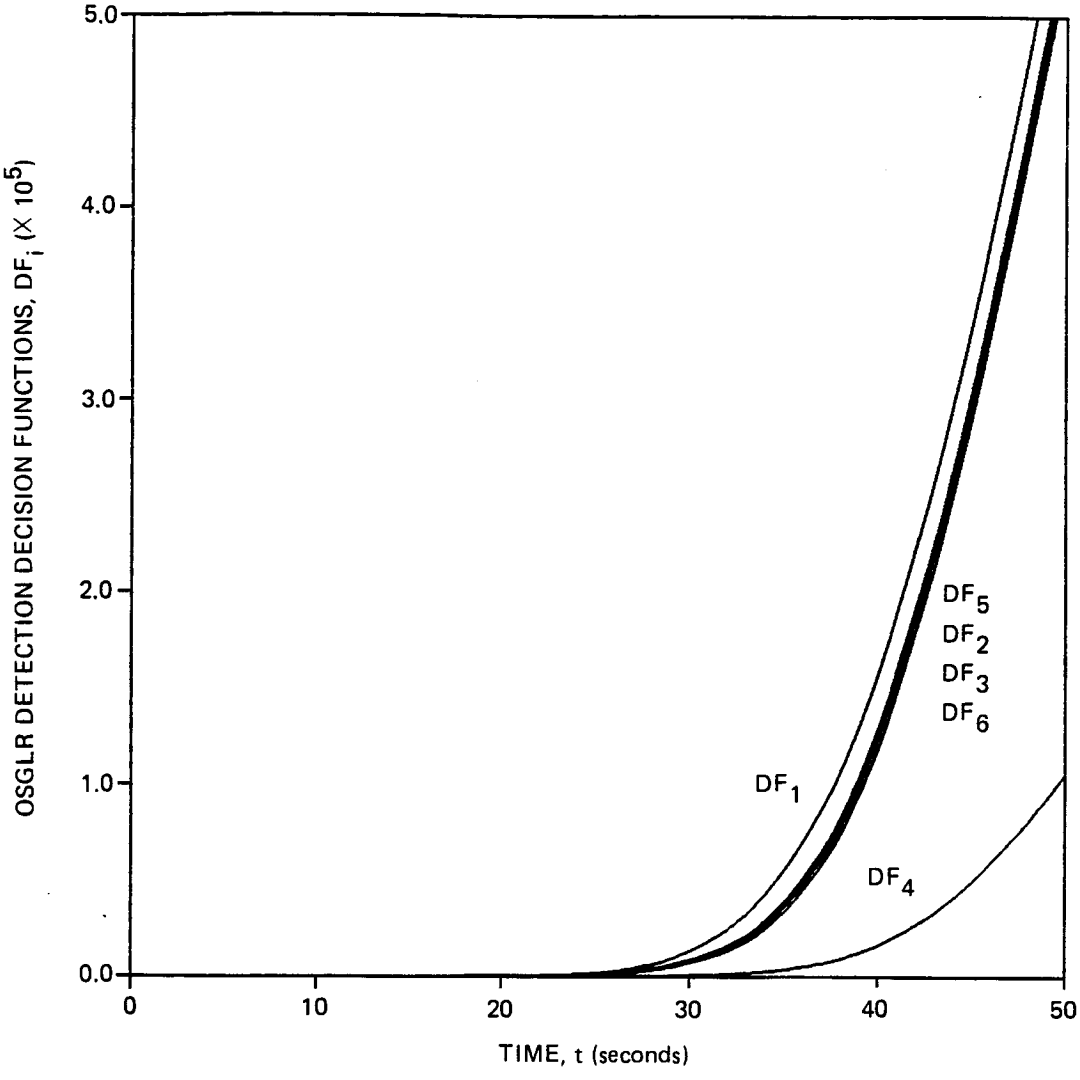

Figure 5.19. OSGLR detection decision functions for the nonlinear simulation with a stuck elevator at time t = 10 s

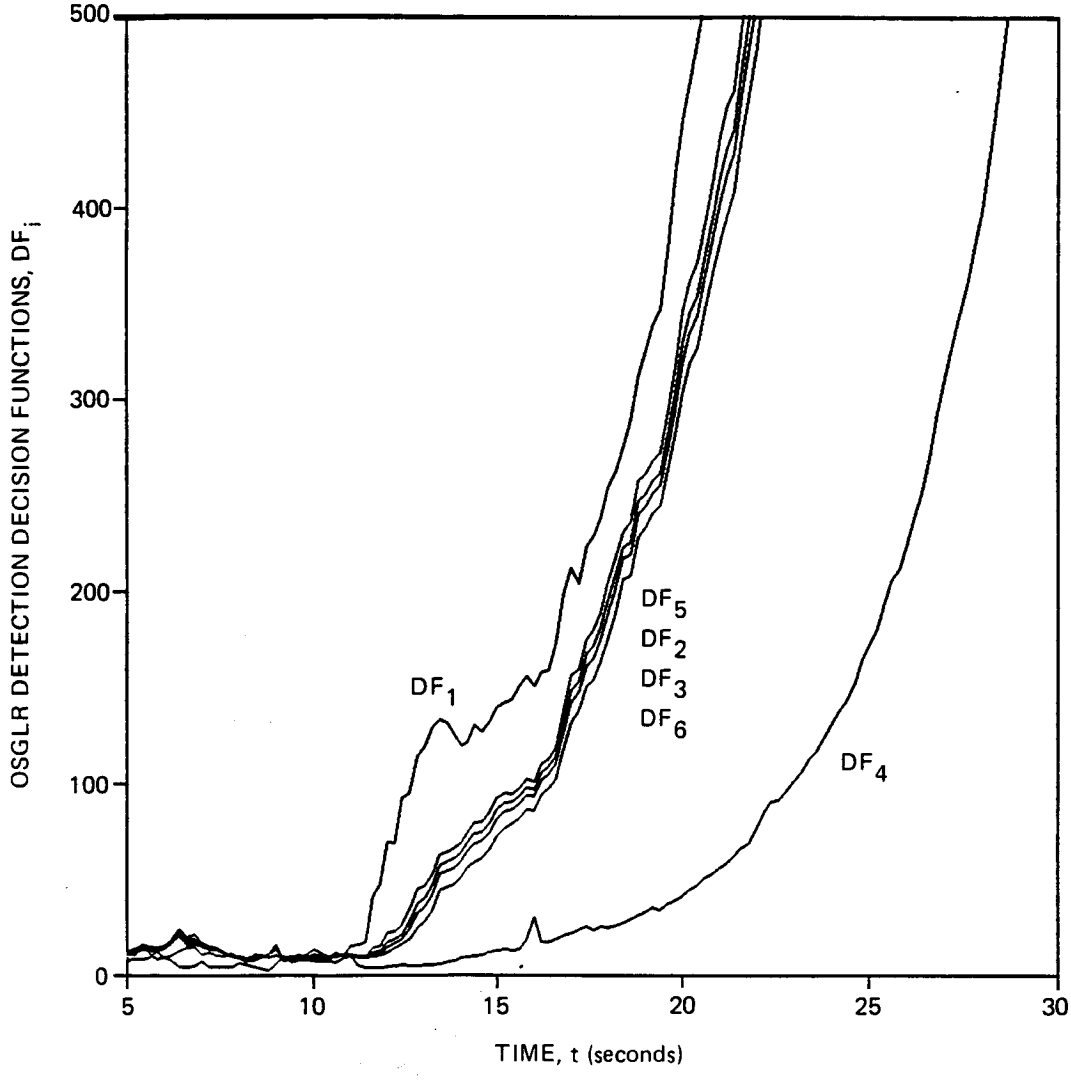

Figure 5.19. OSGLR detection decision functions for the nonlinear simulation with a stuck elevator at time t = 10 s. Note the expanded time scale in the vicinity of t = 10 s (Cont.)

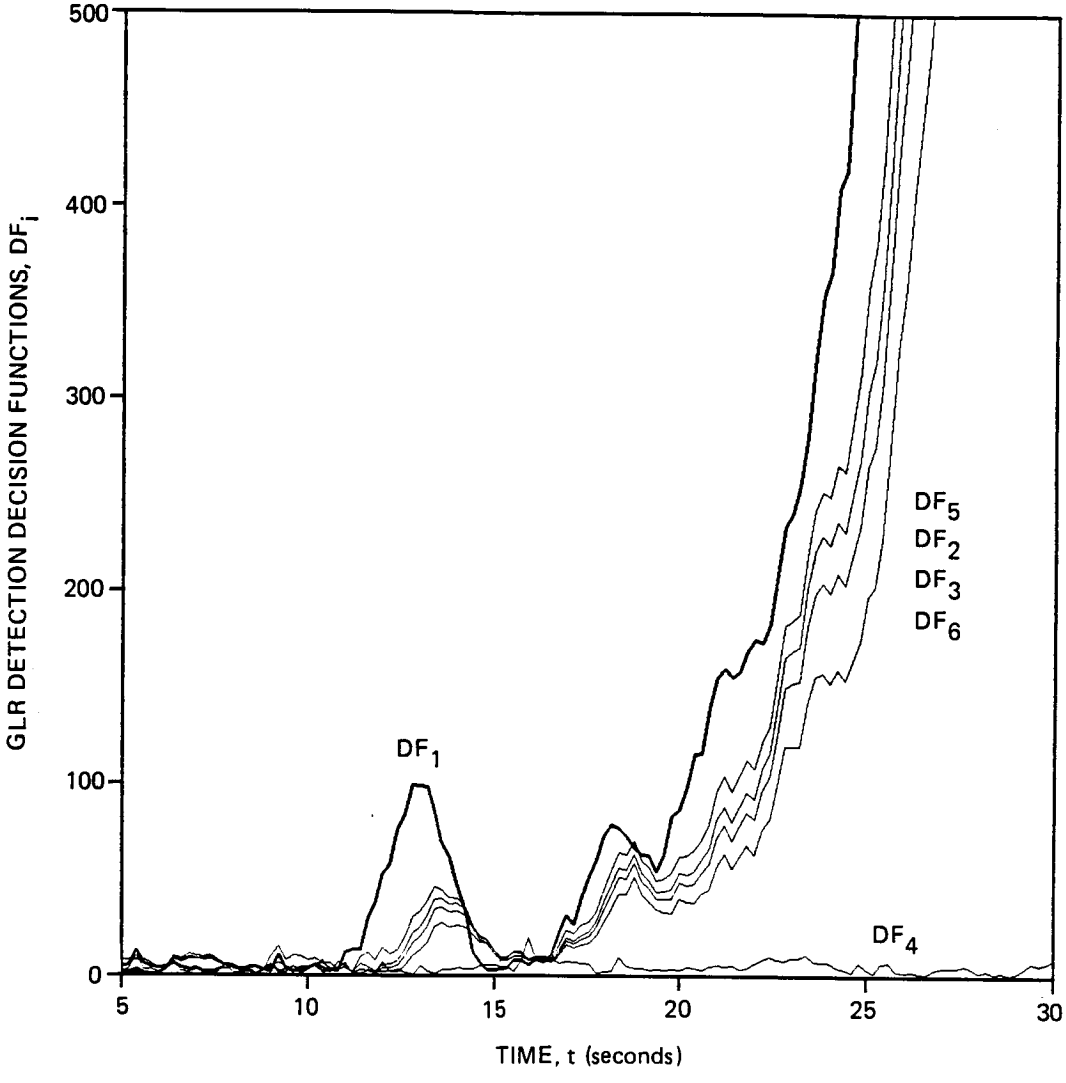

Figure 5.20. GLR detection decision functions for the nonlinear simulation with a stuck elevator at time t = 10 s. A 2 s (100 sample) data window was used.

on the wing exceed DF_1. At t = 16 s, DF_1 again increases until t = 18 s, where once again DF_1 decreases slightly. At about t = 19 s, DF_5 exceeds DF_1 slightly. Shortly thereafter, DF_1 begins to increase steadily and is always greater than the other decision functions.

Also, note that if the detection threshold is increased (e.g., to account for modeling errors), then the decision time is likely to increase significantly. For example, if the threshold is set to $T^2 = 200$, then the time of the detection would be t = 22.52 s, 12.52 s after the failure. On the other hand, the time to detection for the OSGLR test for this threshold is only 6.82 s.

This behavior is caused by two separate effects. The first is the relatively short (2 s) data window. Thus, when the failure input subsides in the vicinity of t = 15 s (Figure 5.18), the GLR decision functions also decrease.

The other reason for this behavior is that the actual failure mode does not agree with any of the hypothesized failure modes of the GLR algorithm. As a result, the results of the test are unpredictable. In particular, DF_1 is sometimes less than the other decision functions. As a result, we see that the GLR test is not robust. On the other hand, the failure mode can be represented, at least approximately, by the OSGLR failure hypotheses. As a result, the OSGLR test is robust to failure mode uncertainty, and does not have the undesirable properties of the GLR test displayed in Figure 5.20.

Finally, note that increasing the length of the GLR data window to 5 s (250 samples) improves the performance of the GLR test only slightly (Figure 5.21). Immediately following the failure, the behavior of the decision functions is the same as for the GLR test with a 2 s data window. Following time t = 12.5 s, however, DF_1 declines only slightly, whereas DF_5, DF_2, DF_3, and DF_6 continue to increase. At about t = 17.5 s, these four decision functions all exceed DF_1. It is not until t = 19 s that DF_1 again is the maximum decision function. With the

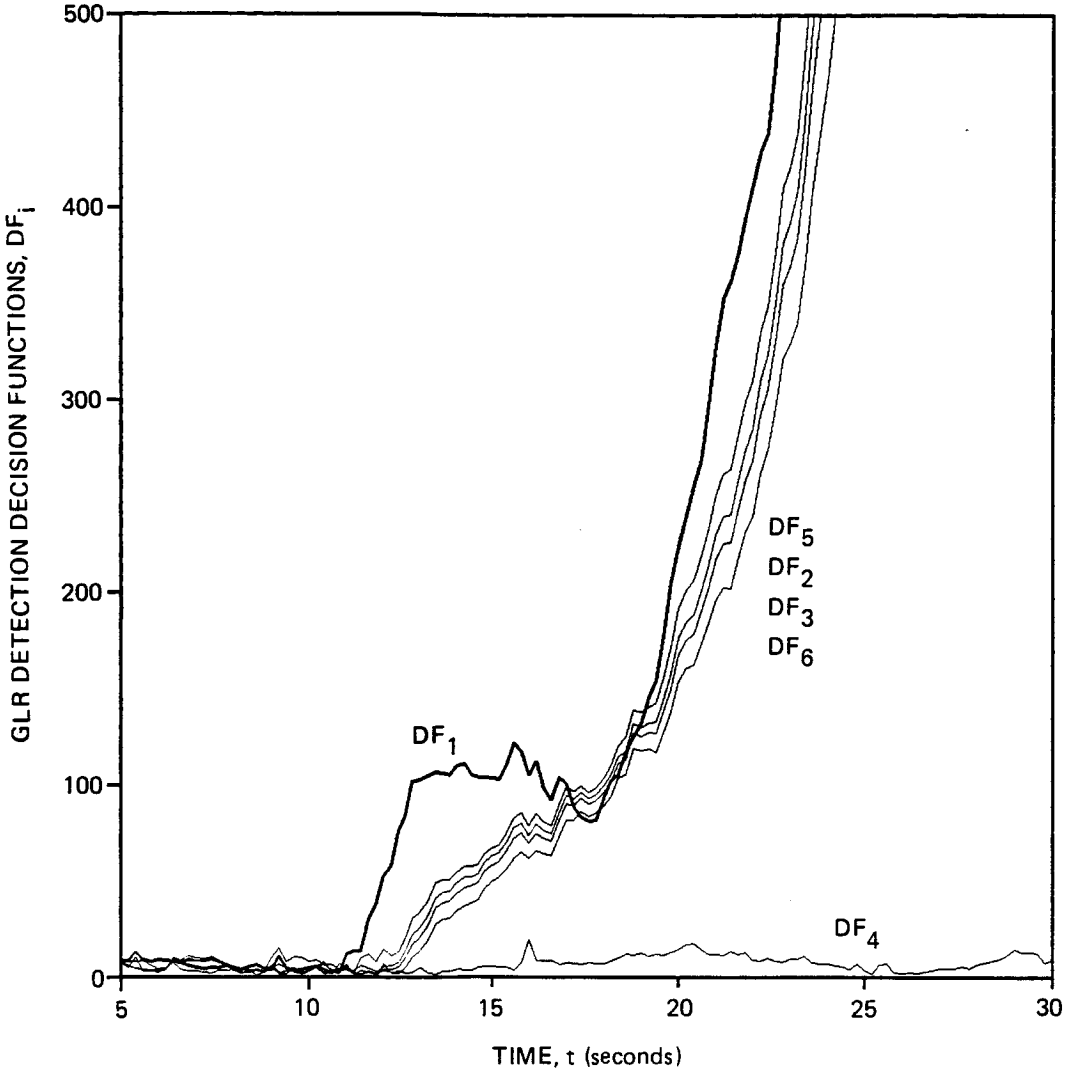

Figure 5.21. GLR detection decision functions for the nonlinear simulation with a stuck elevator at time t = 10 s. A 5 s (250 sample) data window was used.

threshold $T^2 = 56.86$, the detection time is 2.14 s, which compares favorably with the OSGLR test. However, for the threshold $T^2 = 200$, the detection time is 9.79 s, which is somewhat longer than the detection time for the OSGLR test with that threshold.

5.4.8 Summary

As measured by the time required to detect a failure, it would appear that the performance of the OSGLR test is roughly comparable to that of the GLR test. Table 5.3 summarizes the detection times of the two tests for the control surface failures simulated. Generally, the performance of the GLR tests is better when the failure mode simulated is the same as one of those hypothesized in the GLR failure hypotheses. For other failure modes, the OSGLR test performs better. Nevertheless, the detection times are comparable for all of the failures.

However, the results presented in Table 5.3 are somewhat misleading. In almost all of the test cases, the GLR test exhibited nonrobust behavior. This is caused by two features of the GLR test. First, in order to make the GLR test computationally feasible, it is necessary to restrict the hypothesized time of failure by using a data window. As a result, if detection does not occur when the time of the failure is within the data window, then information about the failure is lost. Second, the GLR test assumes a particular failure mode. Consequently, the behavior of the test is not predictable when a different failure mode occurs.

Table 5.3. Summary of the detection performance of the OSGLR and GLR tests.

Failure Mode Simulated	Time to Detect Failure (s)		
	OSGLR	GLR	
		2 s Data Window	5 s Data Window
-0.01745 rad(-1.0°) Elevator Bias	0.22	0.12	0.12
0.0349 rad(2.0°) Rudder Bias	3.06	1.80	1.80
0.01745 rad(1.0°) Right Aileron Bias	0.56	0.48	0.48
0.001745 rad/s (0.1°/s) Ramp Rudder	13.08	18.88	14.90
Stuck Elevator	1.94	2.14	2.14

On the other hand, the OSGLR test does not exhibit these undesirable characteristics. The test can continue to accumulate information about a failure for as long as the truncated series expansion of the OSGLR failure hypothesis can adequately represent the failure. Also, the series expansion can represent, at least approximately, many different failure modes. Therefore, the OSGLR test is robust to failure mode uncertainty, whereas the GLR test is not.

Furthermore, the OSGLR test requires far less computation than does the GLR test, at least in this case. Table 5.4 summarizes the computational requirements of the two tests. Each number in the table is the ratio of the CPU time required to run a particular test to the length of the simulation for which the test was implemented. The tests were implemented in FORTRAN on a Digital Equipment Corporation VAX 11/780.

For each test, six detectors were implemented, corresponding to the six control surfaces. The GLR test requires 18.5 or 46.2 times more computation than the OSGLR test, depending on whether a 2 s or 5 s data window is used for the GLR test.

Table 5.4. Computational requirements of the OSGLR and GLR algorithms.

Ratio of CPU Time to Simulation Time		
OSGLR	GLR	
6 Basis Functions	2 s Data Window	5 s Data Window
0.686	12.66	31.66

One disadvantage of the OSGLR test is that it appears to be more sensitive to modeling errors than the GLR test.

CHAPTER 6

DISTINGUISHABILITY OF FAILURES

6.1 Introduction

In some systems, the failure of one component may closely mimic the effects of the failure of another component. In such systems, it may be impossible to distinguish between different types of failures, regardless of the FDI algorithm used. Therefore, quantitative measures would be desirable to indicate to what extent the failures of different components are distinguishable. The measures would serve two purposes: First, they could be used to alert the system designer that a change in the system is needed to achieve fault tolerance. Such a change could be, for example, the addition of more sensors or the change in location of an actuator. Second, the measures may be used to determine whether the inability of a particular FDI algorithm to isolate failures is a deficiency of the algorithm or a property of the system.

In this section, two measures of distinguishability are proposed (Reference 10). The first of these is interpreted as the distance between two failure hypotheses, assuming that one failure mode is fixed and that the other failure mode is allowed to take on its worst-case value. Based on a geometric interpretation of this distance, a second measure of distinguishability is defined, which is interpreted as the angle between the hypotheses.

6.2 Distance Measure

The distinguishability measure presented below will measure how closely the failure of one component, say component j, can mimic the failure of another component, component i, when the failure mode of component i is given. If the failure mode of component j is thought of as an unknown control, and "how closely" is interpreted as implying a cost function, then this formulation could be expected to lead to some sort of optimal control problem. As shown below, this is indeed the case.

We will formulate the problem as follows: First, it is assumed that the observation interval $[t_0, t_f]$ is fixed. Next, the failure mode of component i is specified to be some function, $f_i(t)$. For the time being, it is assumed that the failure mode $f_j(t)$ is specified as well. Note that for either failure, the onset time of the failure, θ, may be anywhere in the interval $[t_0, t_f]$. Then the problem of determining which component has failed is a binary hypothesis testing problem, with hypotheses

$$H_i: \quad \frac{d\underline{x}(t)}{dt} = A(t)\underline{x}(t) + \underline{w}(t) + \underline{b}_i(t)f_i(t) \tag{6.1}$$

$$\underline{y}(t) = C(t)\underline{x}(t) + \underline{v}(t) + \underline{d}_i(t)f_i(t) \tag{6.2}$$

$$H_j: \quad \frac{d\underline{x}(t)}{dt} = A(t)\underline{x}(t) + \underline{w}(t) + \underline{b}_j(t)f_j(t) \tag{6.3}$$

$$\underline{y}(t) = C(t)\underline{x}(t) + \underline{v}(t) + \underline{d}_j(t)f_j(t) \tag{6.4}$$

Note that because the failure modes $f_i(t)$ and $f_j(t)$ are assumed known, these hypotheses are simple, rather than composite.

The data $\{\underline{y}(t),\ t_0 \leq t \leq t_f\}$ will be reduced to a sufficient statistic which contains all the information about the two hypotheses. To begin, the data are filtered using a Kalman filter based on the unfailed (H_0) system equations

$$H_0: \quad \frac{d\underline{x}(t)}{dt} = A(t)\underline{x}(t) + \underline{w}(t) \tag{6.5}$$

$$\underline{y}(t) = C(t)\underline{x}(t) + \underline{v}(t) \tag{6.6}$$

The hypotheses H_i and H_j can then be written as

$$H_i: \quad \underline{\gamma}(t) = \underline{\gamma}_0(t) + \underline{m}_i(t) \tag{6.7}$$

$$H_j: \quad \underline{\gamma}(t) = \underline{\gamma}_0(t) + \underline{m}_j(t) \tag{6.8}$$

where $\underline{\gamma}(t)$ is the Kalman filter residual, and $\underline{\gamma}_0(t)$ is a zero-mean, white Gaussian process with intensity $R(t)$. $\underline{m}_i(t)$ and $\underline{m}_j(t)$ are the means in the residual $\underline{\gamma}(t)$ under H_i and H_j, respectively.

The sufficient statistic for this problem is given by

$$\chi = \int_{t_0}^{t_f} [\underline{m}_j(t) - \underline{m}_i(t)]^T R^{-1}(t)\underline{\gamma}(t)\, dt \tag{6.9}$$

Because $\underline{\gamma}(t)$ is a Gaussian random process, χ is a Gaussian random variable. The mean of χ under H_i is given by

$$\begin{aligned} \chi_i &= E[\chi | H_i] \\ &= \int_{t_0}^{t_f} [\underline{m}_j(t) - \underline{m}_i(t)]^T R^{-1}(t)\underline{m}_i(t)\, dt \end{aligned} \tag{6.10}$$

Similarly, the mean of χ under H_j is given by

$$\chi_j = E[\chi | H_j]$$

$$= \int_{t_0}^{t_f} [\underline{m}_j(t) - \underline{m}_i(t)]^T R^{-1}(t) \underline{m}_j(t)\, dt \qquad (6.11)$$

The variance of χ under H_i is given by

$$S = E[(\chi - \chi_i)^2 | H_i] \qquad (6.12)$$

The final expression for the variance is

$$S = \int_{t_0}^{t_f} [\underline{m}_j(t) - \underline{m}_i(t)]^T R^{-1}(t) [\underline{m}_j(t) - \underline{m}_i(t)]\, dt \qquad (6.13)$$

The variance of χ under H_j is also given by S.

Thus, the problem of deciding whether H_i or H_j is true has been reduced to that of deciding whether the Gaussian random variable χ has mean χ_i or χ_j. The parameter that determines the performance that can be achieved under these circumstances is the signal-to-noise ratio, defined by

$$d^2 = \frac{(\chi_j - \chi_i)^2}{S} \qquad (6.14)$$

But it can be shown that

$$\chi_j - \chi_i = S \qquad (6.15)$$

Therefore,

$$d^2 = S \tag{6.16}$$

So the distance between the hypotheses is defined to be

$$d = S^{1/2} \tag{6.17}$$

The distance d is simply the number of standard deviations that separate the conditional means χ_1 and χ_2.

Up to this point, it has been assumed that both failure modes $f_i(t)$ and $f_j(t)$ are known. However, what we really want is to find the failure mode $f_j(t)$ that most closely mimics the failure mode $f_i(t)$. In other words, we want to find the distance between the hypotheses for the worst-case $f_j(t)$. Therefore, the distinguishability measure $\Delta_{ij}(f_i(\cdot), t_f)$ is defined by

$$\Delta_{ij}(f_i(\cdot), t_f) = \min_{\substack{f_j(t) \\ t_0 \leq t \leq t_f}} d \tag{6.18}$$

or alternatively,

$$\Delta_{ij}^2(f_i(\cdot), t_f) = \min_{\substack{f_j(t) \\ t_0 \leq t \leq t_f}} \int_{t_0}^{t_f} [\underline{m}_j(t) - \underline{m}_i(t)]^T R^{-1}(t)[\underline{m}_j(t) - \underline{m}_i(t)]\, dt \tag{6.19}$$

The problem of determining Δ_{ij}^2 has two interpretations. The obvious interpretation is as an optimal control problem and the problem may be recognized as being equivalent to the optimal linear quadratic tracking problem. A less obvious interpretation is that the cost function to be minimized is the same as that which is minimized to solve the optimal least-squares filtering problem. In this case, $f_j(t)$ is

interpreted as infinite variance noise driving the state $\underline{e}(t)$, rather than as a control input.

6.3 Geometric Interpretation

In this section, a geometric interpretation of the distance measure Δ_{ij} will be provided. Based on that interpretation, a relative measure of distinguishability will be defined.

Consider the continuous-time case. The set of square-integrable, m-dimensional vector functions on the interval $[t_0, t_f]$ is denoted by $L_2^m[t_0, t_f]$, or simply L_2^m. L_2^m is a complete, infinite-dimensional vector space. A valid inner product for L_2^m is defined by

$$\langle \underline{m}_1(\cdot), \underline{m}_2(\cdot) \rangle = \int_{t_0}^{t_f} \underline{m}_1^T(t)\, R^{-1}(t)\, \underline{m}_2(t)\, dt \qquad (6.20)$$

where R(t) is a symmetric, positive definite matrix. If the norm for L_2^m is defined by

$$\left|\left| \underline{m}(\cdot) \right|\right| = \langle \underline{m}(\cdot), \underline{m}(\cdot) \rangle^{1/2} \qquad (6.21)$$

then L_2^m is a Hilbert space.

Given this background, the problem of determining Δ_{ij} may be succinctly stated as

$$\Delta_{ij} = \min_{\underline{m}_j \in V_j} \left|\left| \underline{m}_j - \underline{m}_i \right|\right| \qquad (6.22)$$

where V_j is the subspace of L_2^m that is the set of all valid $\underline{m}_j(\cdot)$. By the orthogonal projection theorem, the minimizing $\underline{m}_j(\cdot)$, denoted by $\underline{m}_j^*(\cdot)$, is the unique $\underline{m}_j^*(\cdot) \in V_j$ such that

$$\langle \underline{m}_i(\cdot) - \underline{m}_j^*(\cdot), \underline{m}_j(\cdot) \rangle = 0 \qquad \text{for all } \underline{m}_j(\cdot) \in V_j \qquad (6.23)$$

In other words, $\underline{m}_j^*(\cdot)$ is the projection of $\underline{m}_i(\cdot)$ onto V_j, and the representation error

$$\underline{m}_i(\cdot) - \underline{m}_j^*(\cdot) \tag{6.24}$$

is orthogonal to the subspace V_j. In particular,

$$\langle \underline{m}_i(\cdot) - \underline{m}_j^*(\cdot), \underline{m}_j(\cdot) \rangle = 0 \tag{6.25}$$

That is, the representation error is orthogonal to $\underline{m}_j^*(\cdot)$. This situation is represented graphically in Figure 6.1. In the figure, the vector space L_2^m is depicted as being spanned by $\underline{e}_1$, $\underline{e}_2$, $\underline{e}_3$, whereas the subspace V_j is spanned by $\underline{e}_1$ and $\underline{e}_2$. Δ_{ij} is simply the length of the vector $m_i(\cdot) - \underline{m}_j^*(\cdot)$.

Based on this geometric interpretation, a relative measure of distinguishability, $\alpha_{ij}(f_i(\cdot), t_f)$, will be defined as the <u>angle</u> between $\underline{m}_i(\cdot)$ and $\underline{m}_j^*(\cdot)$. Because the representation error is orthogonal to the projection, α_{ij} is given by

$$\alpha_{ij} = \sin^{-1} \frac{\left|\left| \underline{m}_i(\cdot) - \underline{m}_j^*(\cdot) \right|\right|}{\left|\left| \underline{m}_i(\cdot) \right|\right|} \tag{6.26}$$

But by definition,

$$\Delta_{ij} = \left|\left| \underline{m}_i(\cdot) - \underline{m}_j^*(\cdot) \right|\right| \tag{6.27}$$

Therefore,

$$\alpha_{ij} = \sin^{-1} \frac{\Delta_{ij}}{\left|\left| \underline{m}_i(\cdot) \right|\right|} \tag{6.28}$$

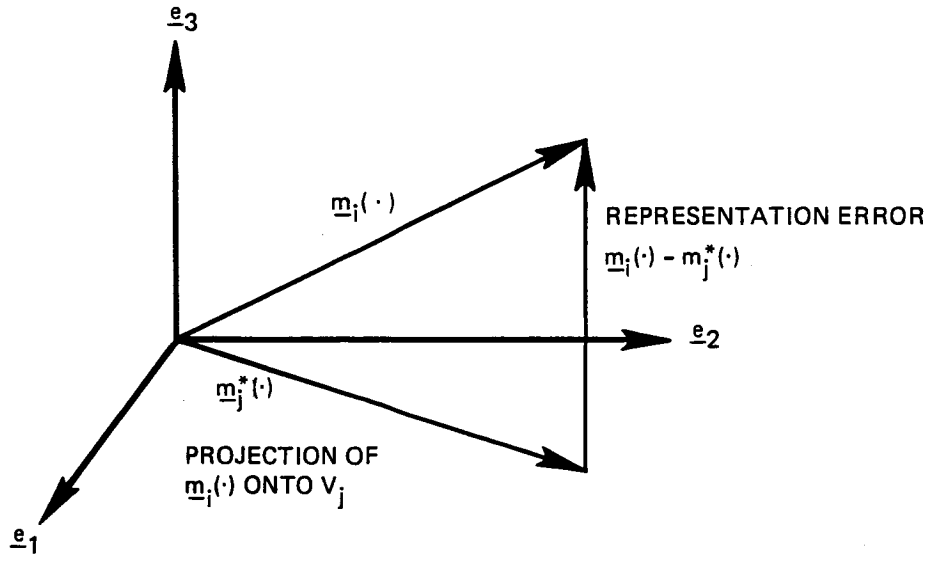

Figure 6.1. Geometric interpretation of the orthogonal projection theorem.

As a practical matter, both α_{ij} and Δ_{ij} are useful measures of the distinguishability of failures. As noted earlier, if $\Delta_{ij}/2$ is small, say on the order of unity or less, then it will not be possible to isolate a failure of component i or j (with failure mode $f_i(\cdot)$ or $f_j(\cdot)$) reliably. If $\Delta_{ij}/2$ is small, but α_{ij} is large (say, greater than 0.349 rad or 20°), the problem is that the energy in the failure signature $\underline{m}_i(\cdot)$ is small, not that the two failure types are similar.

On the other hand, if $\Delta_{ij}/2$ is large, but α_{ij} is small (say, less than 0.08725 rad or 50°), then isolation should be possible, given knowledge of $f_i(\cdot)$ and $f_j(\cdot)$, and given that the system model is accurate. However, the isolation performance is likely to be sensitive to failure mode uncertainty, modeling uncertainty, and of course to the actual (sequential) FDI test used.

6.4 Results

The distinguishability measures just defined will be used to determine the degree to which failures of the control surfaces for the C-130 aircraft system are distinguishable from one another.

Recall that the distance between two hypotheses H_i and H_j, Δ_{ij}, and the angle between two hypotheses, α_{ij}, are functions of the (assumed) failure mode of H_i, $f_i(t)$. For the purposes of this section, only one type of failure mode was assumed, namely, a step bias failure occurring at time θ. Note that because the system is time-invariant and the Kalman filter is (assumed to be) operating in steady state, the time origin may be shifted arbitrarily. Therefore, the distinguishability measures are functions of $t - \theta$, the length of time since the onset of the failure.

Figure 6.2 shows the distinguishability measures Δ_{1j} and α_{1j} for a 0.01745 rad (1°) bias failure of the elevator. The subscripts i and j refer to the vehicle control surfaces as defined by Table 5.2. The five α_{1j}'s are greater than 0.61075 rad (35°) for 10 s after the failure, and are larger than 0.61075 rad (35°) soon after the failure. This indicates that on a relative basis, an elevator bias failure is

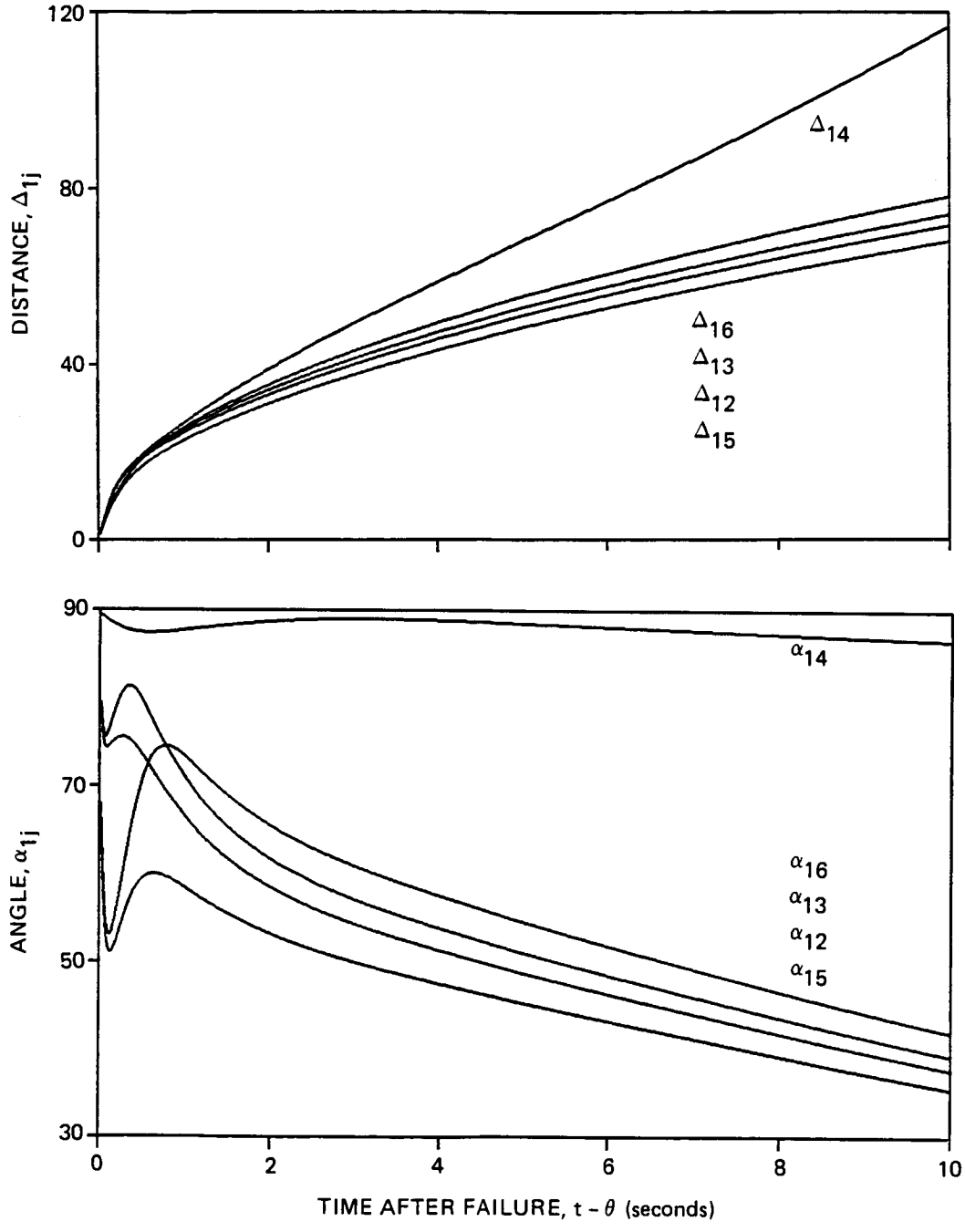

Figure 6.2. Distinguishability measures for a 0.01745 rad (1^{o}) bias failure of the elevator

easily distinguishable from the failure of any other control surface. On an absolute basis, all the Δ_{1j}'s are larger than 21 by time $t - \theta = 1$ s, which is quite large. Therefore, we expect that for a well-designed FDI test, failure detection and isolation of a 0.01745 rad (1°) bias failure of the elevator should take less than 1 s.

Figure 6.3 shows the distinguishability measures for a 0.01745 rad (1°) bias failure of the rudder. Note that all the α_{4j}'s are greater than 1.2564 rad (72°) for the entire time of the plot. That is, the failure signature of a rudder failure is nearly perpendicular to any failure signature that can be generated by any other control surface failure. On the other hand, the Δ_{4j}'s are relatively small. At $t - \theta = 2$ s, the five Δ_{4j}'s are about 4.0, which is small. This is simply a reflection of the fact that the signal-to-noise ratio (d^2) of the rudder failure (when tested against the hypothesis that no failure has occurred) is small. The conclusion is that if a rudder failure is large enough to be detected, then it will be easily distinguishable from failures of the other control surfaces.

Figure 6.4 shows the distinguishability measures for a 0.01745 rad (1°) bias failure of the right aileron. This figure is quite different from the previous two. In particular, the distinguishability measures associated with the left aileron, the right flap, and the left flap (corresponding to the subscripts 3, 5, and 6, respectively) are small. Except for the first 1.0 s following the failure, α_{26} is less than 0.26175 rad (15°), α_{25} is less than 0.1745 rad (10°), and α_{23} is less than 0.08725 rad (5°). α_{23}, α_{25}, and α_{26} all decrease as the time after failure, $t - \theta$, increases. Therefore, a failure of the right aileron is not very distinguishable from failures of another wing control surface (flap or aileron) based on the relative measure α_{2j}.

The failure that most closely resembles the right aileron failure is, not surprisingly, a failure of the left aileron. As indicated by the distance measure Δ_{23}, a failure of the right aileron is barely distin-

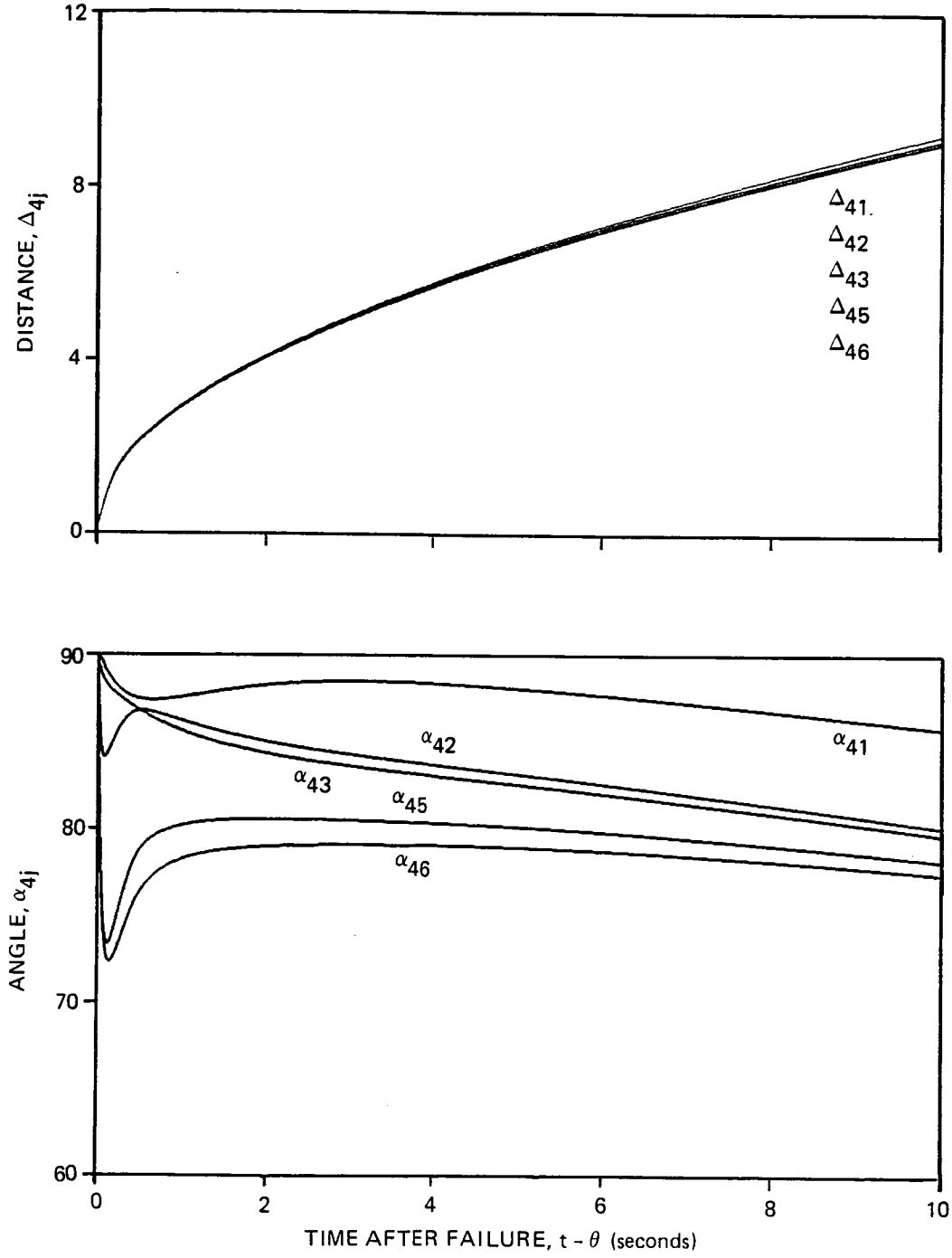

Figure 6.3. Distinguishability measures for a 0.01745 rad (1^{o}) bias failure of the rudder

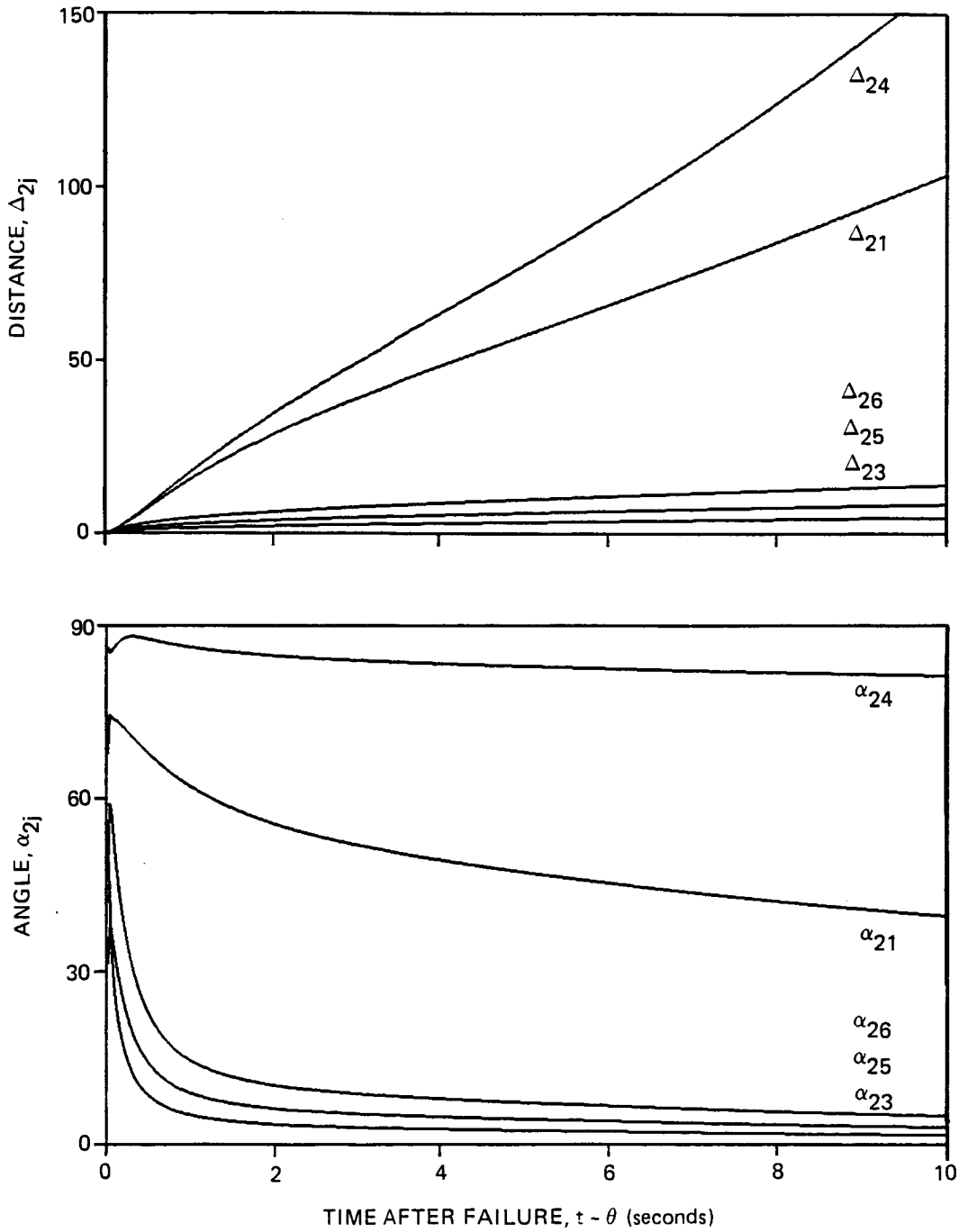

Figure 6.4. Distinguishability measures for a 0.01745 rad (1^{o}) bias failure of the right aileron

guishable from a failure of the left aileron. Even after 10 s, Δ_{23} is only 4.6, which is too small to ensure reliable isolation, even by a well-designed FDI test. Of course, if the failure were larger than 0.01745 rad (1°) Δ_{23} would scale proportionally. Nevertheless, these results indicate that aileron failures are difficult to isolate. This was clearly evident in the simulation results.

Figure 6.5 shows the distinguishability measures for a 1 percent bias failure of the right flap. This figure is qualitatively similar to Figure 6.4. That is, the distinguishability measures associated with the other three wing control surfaces (in this case, the left flap, and the right and left ailerons) are small. In this case, the failure that most resembles the right flap failure is a failure of the right aileron. However, the failure of the right flap is somewhat more distinguishable (as measured by α_{52}) than was the failure of the right aileron (as measured by α_{23}). 10 s after the onset of a failure, $\alpha_{52} = 2.98$, whereas $\alpha_{23} = 1.63$.

The results presented in this section may be explained in terms of the aircraft's dynamics. The elevator's primary effect is to produce a moment about the pitch axis. The other control surfaces do not produce significant moments about the pitch axis. Therefore, an elevator failure is easily distinguished from failures of the other control surfaces. Similarly, the rudder's primary effect is to produce a yawing moment, whereas none of the other control surfaces produce significant moments about the yaw axis. Therefore, rudder failures are easily distinguished from other failures.

On the other hand, the primary effect of the ailerons is to produce a moment about the roll axis. Furthermore, even though their purpose is to produce lift, flaps produce significant rolling moments when operated differentially. In that regard, they behave very much like ailerons. Therefore, it is not surprising that a failure of one of these four control surfaces is not very distinguishable from failures of the other three.

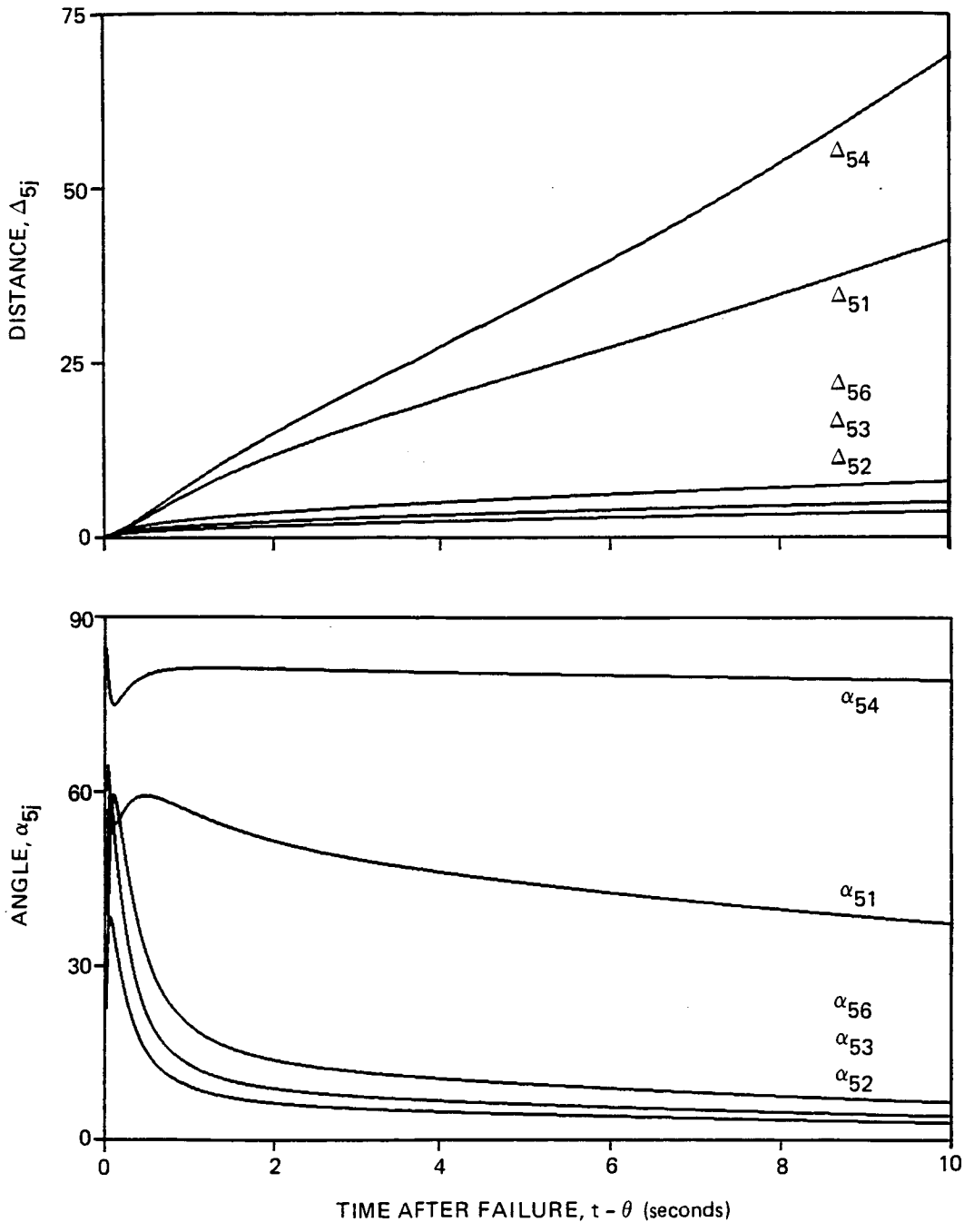

Figure 6.5. Distinguishability measures for a 0.01745 rad (1^{o}) bias failure of the right flap

Furthermore, the results concerning distinguishability are consistent with the FDI simulation results presented for the detection filter and likelihood ratio tests. They suggest that the ability to detect and isolate failures is more a function of the physics of the problem and less algorithm specific.

SECTION 7

A COMPARISON OF FDI ALGORITHMS

7.1 Introduction

The purpose of this section is to make qualitative comparisons of the FDI algorithms being evaluated for the Restructurable Control System application. These comparisons are based on the test cases used to evaluate each algorithm. Thresholds were not selected in all cases and a general detection and isolation logic was not developed. Only a limited number of flight conditions and environments were simulated. Yet we believe that a sufficiently accurate picture of the capabilies of each algorithm was obtained, allowing the algorithms to be qualitatively compared. In comparing the four algorithms evaluated, the following issues have been considered:

- Failure modes (bias, stuck, ramp, etc.) that can be detected.
- Type of failure (rudder, elevator, etc.) that can be detected and isolated.
- Magnitude (or degree) of failures that can be detected.
- False alarm performance.
- Detection time (time delay between failure and detection).
- Computational burden
- Robustness
- Maturity

These issues will now be addressed individually.

7.2. Failure Modes

Failure modes describe the behavior of the failed surface. Some of the important failure modes for restructurable control applications are stuck, hardover, and bias failures and the loss of part or all of a surface. The ability of the algorithms to detect these and other failure modes will be considered here. Note that bias failures were used most extensively to test the algorithms in this evaluation. Therefore, the ability of each algorithm to detect other failure modes was based on its theoretical capabilities in certain instances.

The GLR test uses models of failure modes to detect failures. It is therefore, most capable of detecting the modes that are modeled. However, each mode modeled requires a separate bank of filters which makes modeling even a small number of possible modes computationally costly. The bias failure mode is the easiest mode to model that is applicable to control surface failure detection and isolation. The ability of the GLR test with only the bias failure mode modeled to detect failure modes other than a bias was considered in Section 5.4.5. A 0.001745 rad/s (0.1 deg/s) rudder ramp failure was detected in 14.90 s with a 5 s data window.

The OSGLR algorithm is similar to the GLR algorithm except that the failure modes are represented by a truncated series expansion rather than a fixed function. The series expansion chosen and the number of terms used determine how well a particular failure mode can be represented. In addition, representing the high-frequency portion of the actuator or control surface failure is not necessary as the plant is a low-pass filter. Using the first six terms in the expansion, the OSGLR test was able to detect bias failures. These same six terms should be adequate to detect most other failure modes. This was demonstrated for a 0.001745 rad/s (0.1 deg/s) rudder ramp failure which was detected in 13.08 s.

One advantage of both the unmodified and the modified detection filter is that all failure modes should be detectable as the residual direction is independent of the failure mode, depending only on the

surface which failed. However, for the unmodified detection filter the planar test used to detect failures assumed that the failed control surface was not oscillating about the desired control surface position. Even with this restriction, the unmodified detection filter should still be able to detect most failure modes.

7.3 Type of Failure

All four algorithms were able to detect elevator, rudder, right and left aileron, and right and left flap failures. The left and right elevators were assumed to move together as a unit. Elevator failures could be isolated by all four algorithms as could rudder failures. However, isolating wing surface (aileron and flap) failures was difficult for all of the algorithms. The modified detection filter seemed to display some ability to distinguish between wing surfaces for moderate failures (0.0349 rad (2°) aileron bias, 10% flap bias) in minor turbulence. Based on the few test cases simulated, the modified detection filter could isolate a wing surface failure to one of two possible surfaces. The detection filter algorithm could eliminate one wing surface from consideration at most. It was demonstrated that false isolation could result with the GLR algorithm. Isolation to a specific wing surface is possible with the OSGLR algorithm with a significant delay of perhaps 10 s or more.

7.4 Magnitude of Failure

The magnitude of the failures that can be detected depends on the sensor noise, disturbances, and modeling errors. The GLR and OSGLR algorithms were able to detect moderate (0.01745 rad(1°) elevator, rudder and aileron) bias failures in the presence of noise and severe turbulence (σ_ω = 1.98 m/s or 6.5 ft/s). The OSGLR algorithm appears to be more sensitive to modelling errors than does the GLR algorithm.

Turbulence and modeling errors significantly degraded the ability of the detection filter to detect failures. Moderate (-0.0349 rad or -2° elevator, aileron, and 10% flap) failures could be detected in minor turbulence (σ_ω = 0.3 m/s or 1 ft/s). However, detecting moderate failures in severe turbulence was more difficult. While hardover failures were not tested, they should be easily detected even in severe turbulence. Modeling errors also degraded the ability of the detection filter to detect moderate failures. In fact, some moderate aileron failures were no longer detectable. Detection of hard failures, though, should still be possible.

The modified detection filter could also detect moderate failures in minor turbulence. The detection of failures in severe turbulence or with modeling errors would require dynamic thresholds or a method of estimating the nominal no-failure residuals caused by severe turbulence and modeling errors.

7.5 False Alarm Performance

False alarm rates for the GLR test and the detection filter can only be determined via simulation because analytic estimates are not available. Some analytic estimates which assume Gaussian noise, no disturbances, and no mismodeling are available for the OSGLR algorithm. Still, the false alarm rates for the OSGLR algorithm due to disturbances and mismodeling would have to be determined by simulation. However, determining even large false alarm rates using simulation is difficult because of the limited number of conditions that can be tested and the large computational burden.

Specific false alarm rates were not determined for all of the algorithms. Thresholds were not selected in all cases and even if they had been, the simulation test cases were of insufficient number to be able to estimate any false alarm rates. Instead, the false alarm per-

formance of each of the algorithms will be qualitatively assessed by its sensitivity to noise, turbulence, and modeling errors. Algorithms that are sensitive to these effects can be expected to have larger false alarm rates than algorithms that are less sensitive.

The OSGLR and GLR algorithms were least sensitive to noise and turbulence. This is true for two reasons: the system model incorporated into these algorithms included a turbulence model, and a Kalman filter is used to provide an estimate of the state. The OSGLR test was more sensitive to modeling errors than the GLR test.

The unmodified detection filter is sensitive to turbulence and modeling errors. The modified detection filter is sensitive to modelling errors and very sensitive to turbulence. As mentioned previously, the modified detection filter would require dynamic thresholds or a method of estimating the nominal no-failure residuals caused by severe turbulence and modeling errors to compensate for its sensitivity to these errors and disturbances.

7.6 Detection Time

The failure detection times depend on the magnitude of the failure, the sensor noise, the disturbances present, and the thresholds selected. While the detection times were comparable for all of the algorithms, the GLR and OSGLR algorithms were tested in severe turbulence as opposed to the detection filter algorithms which were tested in minor turublence. Detection times for the GLR and OSGLR algorithms were on the order of a half-second or less for .01745 rad (1°) elevator and right aileron bias failures in severe turbulence for the thresholds selected (cf. Table 5.3).

Higher thresholds would probably be required to provide adequate false alarm performance. Even with higher thresholds, detection times should be on the order of a second. If the same thresholds are used for detecting rudder failures as for other control surface failures,

detection times would be much longer since the rudder decision functions are smaller than the other control surface decision functions for the same magnitude failure. However, as the effects of mismodeling affect the rudder decision functions less than the other decision functions, smaller thresholds could be used, allowing the rudder detection times to be on the same order.

Detection times for both the modified and unmodified detection filters also depend on the filter eigenvalue chosen and the time constant of the low-pass filter, if any, required to suppress noise in the residual. Thresholds were not chosen for the detection filter. The detection times were estimated based on the time delay between failure onset and a clear indication that a failure has occurred. For the unmodified detection filter, approximately two seconds would be required to detect a 0.0349 rad (2°) elevator or right aileron failure in minor turbulence with the residual being low-pass filtered with a time constant of one second. A 0.0349 rad (2°) rudder failure would take a second longer. Harder failures could be detected faster as much less, if any, filtering would be necessary. On the other hand, the detection and isolation of small magnitude failures would require heavy low-pass filtering for noise suppression which would impact the failure detection time because of the relatively long time required to reach steady state. Detection times for the modified detection filter would be on the same order as for the unmodified detection filter.

7.7 Computational Burden

The computational burden of all of the algorithms has not been quantitatively determined. Yet, some approximate comparisons will be made here. Each of the algorithms consists of a filter of the system to generate a residual, some type of residual processing, and a test for failures. The filter portion of each algorithm is computationally equivalent. Therefore, the relative computational burden can be deter-

mined by examining the computations required to process the residual and to test for the failure.

The least additional computations are required by the unmodified detection filter. The residual processing would likely consist of several banks of low-pass filters to give the algorithm the ability to quickly detect hard failures and still detect soft failures. To test for a failure, the residual must be projected onto the failure signature plane segment for each control surface.

The modified detection filter requires slightly more computational processing than the detection filter. The additional computations result from the secondary filtering of the residual which restores the property of a unidirectional residual in response to a control surface failure. However, fewer computations are required to project the residual onto a signature direction than onto plane segments.

The relative computational burden of the OSGLR algorithm is primarily determined by the number of actuators or control surfaces and by the number of terms in the series used to represent the possible failure modes. The residual is used to drive an additional filter for each actuator to produce an information vector. The dimension of each of these information vectors is the number of terms used in the series expansion to represent the failure mode. The test for a failure in each actuator or control surface is the information vector weighted by an information matrix. For the time-invariant case considered here, the information matrix is a constant matrix. For a large number of both actuators and terms used in the series, the computational burden would be very heavy. However, keeping only the first six terms of the series expansion was found to be adequate in the present application. In addition, only six control surfaces were considered in this evaluation. Still, for this case, the computational burden of the OSGLR algorithm is at least 50% greater than the unmodified detection filter.

The relative computational burden for the GLR algorithm is mainly a function of the number of actuators, the number of failure modes modeled, and the data window chosen. Each actuator requires N correlation receivers for each failure mode modeled where N is the length of the data window divided by the time step. For a half second window and a 0.02 second time step, 25 correlation receivers would be required per actuator per failure mode. For six actuators and only modeling the bias failure mode, 150 correlation receivers were required for this application. With 150 correlation receivers, the GLR algorithm was more computationally costly than the OSGLR algorithm. However, a half second window was too short for adequate FDI performance. A realistic data window of two seconds perhaps would make the GLR algorithm computationally very expensive. Table 5.4 indicates that it requires approximately 18 times more computation than the OSGLR test.

7.8 Robustness

As each of the algorithms considered here relies upon a linear model of the system to detect and isolate failures, these algorithms will be sensitive to modeling errors. The OSGLR test was shown to be more sensitive to modelling errors than the GLR test in Section 5.4.6. The unmodified detection filter was unable to detect a right aileron (0.0349 rad or 2° bias) failure with the aircraft flying at an off-nominal cruise condition. Modeling errors caused the modified detection filter to produce large residual projections.

Another source of modeling errors for the GLR and OSGLR algorithms are the failure mode models incorporated into each of the algorithms. The OSGLR algorithm is likely to be robust to actuator failure mode modeling errors as the model is sufficiently general to represent most modes adequately. However, the GLR algorithm required specific models of failure modes such as bias failures. As only bias failures were modeled in the present application, the GLR algorithm is likely to be less robust to other failure modes than the other three algorithms.

7.9 Maturity

The GLR algorithm is mature in both theory and in application. The OSGLR algorithm is almost as mature in theory as the GLR algorithm. However, as the OSGLR test is a recently developed FDI algorithm, there is very little experience in applying it.

Detection filter theory is mature for restructurable controls application to linear, time-invariant systems with no input-to-output coupling. However, no theory exists for applying the detection filter to time-varying systems. In addition, for systems with input-to-output coupling, systematic methods of using the extra degrees of freedom in the gain matrix calculation (which result from having more measurements than states) and scaling to improve detection filter performance are needed. Finally, there is limited experience in applying the detection filter with only a couple of applications having been reported.

The modified detection filter, developed for this application, needs additional investigation to be considered mature in both theory and application. The problems of time-varying systems, improving performance through scaling, and the extra degrees of freedom in the gain matrix calculation mentioned above for the detection filter also apply to the modified detection filter.

7.10 Conclusions

The eight issues addressed in this memorandum are summarized in Table 7.1. The GLR and OSGLR algorithms performed the best, especially in severe turbulence. However, the computational burden of the GLR algorithm is heavy and its ability to isolate wing surface failure modes is uncertain. An additional advantage of the OSGLR algorithm is that analytic false alarm rate results are available. The most significant advantage of the detection filter algorithms is their relatively low computational processing requirements. If the sensitivity of the

Table 7.1. Comparison of FDI Algorithms*

ALGORITHM		GLR	OSGLR	DETECTION FILTER	MODIFIED DETECTION FILTER
Failure Modes Detectable		Bias, Ramp**	Most failure modes	All (Only bias tested)	All (Only bias tested)
Type of Failure	Detect	All	All	All	All
	Isolate	Elevator, Rudder, False isolation of wing surface failures possible	Elevator, Rudder, Wing surface with a moderate time delay	Elevator, Rudder	Elevator, Rudder
Magnitude		0.01745 rad(1°) bias in severe turbulence and no modeling errors	0.01745 rad(1°) bias in severe turbulence and no modeling errors	0.0349 rad(2°) bias in minor turbulence and no modeling errors	0.0349 rad(2°) bias in minor turbulence and no modeling errors; larger failures in heavier turbulence and modeling errors
False Alarm Performance		Insensitive to turbulence; sensitive to modeling errors	Analytic results available; insensitive to turbulence; very sensitive to modeling errors	Sensitive to turbulence and modeling errors	Very sensitive to turbulence; sensitive to modeling errors

*The comparison is based on the test cases used to evaluate each algorithm during the course of this study. Only a limited number of flight conditions and environments were simulated. Also, the comparison is qualitative as thresholds were not chosen in all cases and a general detection and isolation logic was not selected.

**A bias failure mode was assumed in the GLR hypotheses.

Table 7.1. Comparison of FDI Algorithms (Cont.)

ALGORITHM	GLR	OSGLR	DETECTION FILTER	MODIFIED DETECTION FILTER
Detection Time	Less than 0.5 seconds for 0.01745 rad(1°) bias failure in severe turbulence	Less than a half second for 0.01745 rad (1°) bias failure in severe turbulence	Approximately two seconds for 0.0349 rad (2°) bias failure in minor turbulence; longer in severe turbulence	Approximately two seconds for 0.0345 rad(2°) bias failure in minor turbulence; probably longer in severe turbulence
Computation Burden	Heavy	Moderate	Light	Light
Robustness	Poor; less robust to failure mode uncertainty than the other three algorithms	Poor; worse than GLR	Poor	Poor
Maturity in Theory	Mature	Mature	Mature for linear time-invariant systems with no input-to-output coupling	Needs more investigation
Experience in Application	Much	No previous experience	Some	No previous experience

detection filter algorithms to turbulence could be reduced, their performance might be comparable to the GLR and OSGLR algorithms. However, until this is accomplished, the OSGLR algorithm is the most promising of these four algorithms evaluated.

SECTION 8

AUGMENTATION OF ANALYTIC FDI SCHEMES FOR IDENTIFYING FAILURES IN FUNCTIONALLY REDUNDANT CONTROL SURFACES

8.1 Introduction

A second program task is to develop a system monitoring strategy to implement the failure detection and isolation techniques which identifies the mix of sensors and analytic redundancy required. Issues associated with this second task are discussed in this section. It has been shown that analytic FDI schemes can have difficulty in fully isolating failures among control surfaces that are functionally redundant. Thus, it was difficult to decide between flap and aileron as the failed wing surface. The quantitative measures developed to determine the maximum discrimination of such failures showed the inherent difficulty. It can be expected then that any intentional maneuvering for the purpose of isolating failures of such surfaces using analytic FDI would be of only limited value, even if practical otherwise.

The value of actually isolating a failure of a surface that is functionally redundant might be questioned to some degree. After a surface fails, it is required that sufficient capability remain to end the flight in an acceptable way. If there is sufficient capability (and if this can be appropriately determined) then complete failure isolation might be considered optional. But there could be reasons why isolation to a specific surface would be preferred. It is likely that a failure could be more quickly and appropriately compensated if it were fully isolated. Moreover, full isolation might allow for more flexibility and confidence in continuing a flight after a failure has occurred.

There should be thorough investigation of the merits of dispensing with complete isolation when functional capability can be reasonably assured. There has been some consideration of in-flight dynamics testing (Reference 14) and at least a limited demonstration (Reference 15). Pre-flight dynamic testing has been standard for military aircraft (Reference 15). Dynamic testing could eventually provide information quickly and accurately on functional capability of the aircraft while in flight. In what follows, however, full isolation capability is taken as the simpler and more desirable option.

A discussion of fault tolerance in current aircraft actuation systems and of the role of analytic FDI schemes follows. Augmenting analytic schemes with direct measurements of control surface position is also considered.

8.2 Fault Tolerance in Current Aircraft Actuators

Direct duplication of actuation has been the practice for most military and large commercial aircraft for quite some time. Whole actuation channels may be duplicated several times. There have been several methods devised for dealing with failures of elements in these channels. The subsystems and channels must be substantially identical in order to give the same control inputs and to enhance the performance of the system. Some differences are inevitable because of tolerances, and these must be taken into account so that disengagement of a channel will occur only under genuine failure conditions. The performance of the subsystems and channels is continuously adjusted, in a process called equalization (Reference 16). As a part of equalization, inter-channel differences are minimized through feedback. If a difference is too great, then the failed channel is disengaged or bypassed. Frangible elements (shear pins, for example) have also been used, allowing a jammed actuator to be broken by the others. Thus, a large degree of actuator FDI (and reconfiguration) already takes place on a local level, before the surface has actually been moved. This can be expected to continue.

8.3 The Role of Analytic FDI

Analytic FDI schemes, such as those evaluated in this program, look for control surface failure signatures in the whole-system dynamics. That they detect failures at the system level (ultimately the most important one) is what makes these schemes potentially of great value. They can be considered most useful in the context of aircraft actuator FDI in identifying failures that the lower-level FDI schemes have missed. Such failures might include inaccuracy or breakdown of the local schemes and actual physical damage to the control surface itself. Outputs from the local automatic schemes might be of some use in augmenting the analytic algorithms for the purpose of identifying certain types of failures. However, it can be expected that this information could be of limited value in detecting and isolating some significant failures.

8.4 Augmentation of Analytic FDI Schemes with Actuator Position Measurements

The concern here is with failures that manifest themselves in some way in the system dynamics. It is reasonable to assume that the local FDI scheme, having failed to identify and compensate, is not an independent source of information to the overall FDI strategy. Such "failures" as actuator bias, jamming, or inappropriate overall actuation gain might be identifiable through use of surface position transducers.

Position sensors mounted on or near the control surface itself could be considered to provide failure information on a level just below that of the whole system. Information from these transducers can be expected to be reasonably easy to obtain and use. Position transducers of the synchro, potentiometer, and linear variable differential (LVDT) types have been extensively used and are simple (Reference 17). To have these position transducers be an independent source of information on any type of failure, however, they should not be part of the actual flight control loop.

Since WWII, position transducers have provided feedback in aircraft flight control systems (Reference 18). They have typically been mounted on primary or secondary actuation output shafts. There, they could be used for limiting and nulling control as actuator positioning commands were satisfied. The currently favored Control Augmentation and Fly-By-Wire flight control systems have as a primary characteristic that the flight control loops are no longer closed using actuator position information but using information from aircraft attitude and position sensors (Reference 18). Depending upon the extent of their continued use in the flight control system, actuator position sensors could serve as more or less independent sources of FDI information.

Flight control systems in which control loops are closed using aircraft dynamic information will automatically compensate for some actuator failures, such as small surface bias errors. To identify larger biases, comparing actuator position expected (using a reference model) with that actually measured by position transducers might suffice to isolate a failed surface. Alternately, in a separate actuator positioning flight control mode in secure flight conditions, commanding the surface to move to some absolute position or to more a certain fixed amount could suffice to detect and isolate biases or incorrect gains. If the surface is jammed, FDI using outputs from position transducers is also possible, using similar tests.

Employing an FDI scheme based on surface position measurements involves additional hardware and perhaps the design of separate flight or test modes. It should be stressed, too, that position transducers would still be of only limited use in identifying certain types of failures, such as actual control surface damage.

Position sensors could be used as a primary source of FDI information, with position measurements obtained continually. Actuator position information could also be used on some lower FDI decision level. If a sensitive whole-system FDI scheme were available, however - and this

would ideally be preferred - then direct surface position sensors could be used in augmentation to provide information for complete failure isolation, eliminating the uncertainties inherent in fully identifying the failure of a functionally redundant surface. Only a limited number of transducers might then be required, and limited use made of their information. Use of position sensors to augment analytic FDI schemes also implies that each scheme could serve as a limited check on the other.

8.5 Conclusions

It has been shown that analytic FDI schemes can have difficulty in isolating failures among functionally redundant control surfaces. Complete isolation might not be needed if the presence of adequate functional capability can be determined quickly and accurately. This point deserves more investigation. Full isolation might lead to simpler or better compensation for a failure, however. Then, depending upon the type of usage of control surface position transducers in the flight control system, they can be used to provide information for identifying actuator failures. Analytic FDI schemes will always be of great value as they detect failures based on whole-system dynamics. Where they cannot fully isolate a failure, actuator position information could be useful.

Whether actuator position transducers can provide useful augmentation to analytic FDI schemes for the C-130 should be investigated. The role that such transducers now have in the flight control system should first be determined. Then, if they are not a primary part of the flight control loop, selective addition of the sensors should be considered, starting with the wing surfaces so that their failures can be fully isolated.

SECTION 9

SUMMARY AND CONCLUSIONS

This report has described work performed with regard to the evaluation of FDI algorithms for application to aircraft restructurable control systems. Three algorithms were evaluated: the detection filter, the Generalized Likelihood Ratio test and the Orthogonal Series Generalized Likelihood Ratio test. In addition, a modification to the detection filter, to produce unidirectional failure residuals for systems with direct input-output coupling, was also investigated. This modification is relevant since the use of accelerometer measurements for FDI in aircraft systems results in direct input-output coupling. The algorithms were evaluated and compared using results from a nonlinear simulation of a C-130 aircraft. The issue of the distinguishability of failures was also addressed and measures defined which permit an a priori determination of the ability to do this for a specific system. Considerations in the development of a system monitoring strategy were also discussed.

The major conclusion which may be drawn from the results of this study is that algorithmic failure detection and isolation may be feasible for restructurable control applications. This conclusion must be qualified by the results obtained during this study, which have been basically limited to a single operating condition and to the investigation of a small subset of the potential failures. In particular, failure detection does not appear to be a problem. Each of the algorithms was able to detect small elevator, rudder, aileron and flap failures for the C-130 aircraft in turbulence. The isolation of control surface failures was

not a problem for elevator and rudder failures. However, difficulties arose in the isolation of wing surface, i.e., aileron and flap, failures. These failures have a similar effect on the responses of the aircraft system. The OSGLR algorithm performed best in this regard and the isolation of these failures was possible, although a relatively long time was required to do this. It was difficult to isolate these failures with the other algorithms, at best, and it was shown that false isolation may occur with the GLR test. This conclusion highlights the potential need to augment the analytic FDI algorithms with the direct measurement of failures using, for example, position sensors for some of the control surfaces.

The OSGLR algorithm performed best of those evaluated. The nature of the algorithm and its basis upon a series expansion implies that most failure modes should be detectable. All failure types investigated during this study were detected and were isolated, although there was a long time delay associated with the wing surface failures. Bias failures on the order of a degree of surface deflection were detected in less than a half a second for a system without modeling errors. The computational burden associated with this algorithm is moderate relative to the others, its false alarm rate can be analytically estimated and the theory associated with it is mature. On the negative side, the robustness properties of the OSGLR test are poor but so are those of the other algorithms. In addition, the OSGLR algorithm has not been previously applied to any system.

The GLR algorithm also performed well in the C-130 application. The major drawbacks associated with it are its heavy computational burden and the uncertainty associated with its ability to isolate wing surface failures. The most significant advantage of the detection filter algorithms is their relatively low computational processing requirements. If the sensitivity of these algorithms to turbulence could be reduced, their performance might be comparable to the GLR and OSGLR algorithms.

REFERENCES

1. Montoya, R.J., W.E. Howell, W.T. Bundick, A.J. Ostroff, R.M. Heuschen, and C.M. Belcastro, Restructurable Controls, NASA Conference Publication 2227, NASA Langley Research Center, Hampton, Virginia, September 21-22, 1982.

2. Ostroff, A.J., and R.M. Heuschen, "Investigation of Control Law Reconfigurations to Accommodate a Control Element Failure on a Commercial Aircraft," Proceedings of the 1984 Automatic Control Conference, San Diego, CA, June 6-8, 1984.

3. Looze, D.P., S.M. Krolewski, J.L. Weiss, J.S. Eterno, and S.W. Gully, "An Approach to Restructurable Control System Design," Proceedings of the 23rd Conference on Decision and Control, Las Vegas, NV, December, 1984.

4. "National Transportation Safety Board Accident Report of the American Airlines DC10 Crash at Chicago - O'Hare International Airport, May 25, 1979," NTSB-AAR-79-17, December, 1979.

5. McMahan, J., "Flight 1080," Air Line Pilot, July, 1978.

6. Beard, R.V., "Failure Accommodation in Linear Systems Through Self-Reorganization," Ph.D. Thesis, Dept. of Aeronautics and Astronautics, MIT, Cambridge, MA, February, 1971.

7. Jones, H.L., "Failure Detection in Linear Systems," Ph.D. Thesis, Dept. of Aeronautics and Astronautics, MIT, Cambridge, MA, August, 1973.

8. Meserole, Jr. J.S., "Detection Filters for Fault-Tolerant Control of Turbofan Engines," Ph.D. Thesis, Dept. of Aeronautics and Astronautics, MIT, Cambridge, MA, June, 1981.

9. Willsky, A.S. and H.L. Jones, "A Generalized Likelihood Ratio Approach to the Detection and Estimation of Jumps in Linear Systems," IEEE Transactions on Automatic Control, Vol. AC-21, No. 1, pp. 108-112, February, 1976.

10. Hall, S.R., "A Failure Detection Algorithm for Linear Dynamic Systems," Sc.D. Thesis, Department of Aeronautics and Astronautics, Massachusetts Institute of Technology, Cambridge, MA, June, 1985 (also CSDL-T-874, June, 1985)

11. Chalk, C.R., et al, "(1969) Background Information and User Guide for MIL-F-8785B (ASG), Military Specification - Flying Qualities of Piloted Airplanes," Technical Report AFFDL-TR-69-72, Air Force Flight Dynamics Laboratory, Wright-Patterson Air Force Base, Ohio, August, 1969.

12. Vander Velde, W.E., "Application of Failure Detection Filter Theory to Reliable Longitudinal Control of Guideway Vehicle," Report for U.S. Department of Transportation Contract No. DOT-TSC-1445, Massachusetts Institute of Technology, Cambridge, MA, March, 1979.

13. Noble, B. and J. W. Daniel, Applied Linear Algebra, Prentice-Hall, Inc., Englewood Cliffs, N.J., 1977, p. 337.

14. Plice, W.A., "Built-in Test Techniques for Digital Flight Control Systems," paper 13 in Integrity in Electronic Flight Control Systems, AGARDograph No. 224, April 1977.

15. Towill, D.R., "Pre-Flight Dynamic Checkout," paper 14 in Integrity in Electronic Flight Control Systems, AGARDograph No. 224, April 1977.

16. Pallett, E.H.J., Automatic Flight Control, Granada, 1983, pp. 264-270+.

17. Weirather, L.H., "Transducers," Chapter 4 in Basic Principles of Flight Test Instrumentation Engineering, Vol. 1, AGARDograph No. 160, April 1974.

18. Earley, B.H., "Objectives for the Design of Improved Actuation Systems," paper 18 in Integrity in Electronic Flight Control Systems, AGARDograph No. 224, April 1977.

APPENDIX A

C-130 LINEAR MODEL DEVELOPMENT

A.1 Introduction

Each of the FDI algorithms investigated under the Restructurable Controls Program requires a linear model of the nonlinear system for design or implementation. The linearization technique used to generate linear models of the C-130 aircraft dynamics is described and some comparisons of the linear model and the nonlinear system are presented.

A.2 Linearization Technique

The nonlinear system consists of dynamics which describe the motion of the aircraft and output equations which describe the measurements as functions of the states and the controls. The nonlinear dynamics can be functionally represented by

$$\underline{\dot{x}} = \underline{f}(\underline{x},\underline{u}) \tag{A.1}$$

The output equations are of the form

$$\underline{y} = \underline{g}(\underline{x},\underline{u}) \tag{A.2}$$

The outputs of the linear model were chosen to be airspeed, acceleration at the cg along the y and z body axes, angular velocity about the body axes, attitude, and altitude. The inputs of the linear model are a subset of the inputs for the nonlinear model. The inputs

chosen for the linear model include the elevator, rudder, left and right aileron, and left and right flap where each aileron and each flap is allowed to move independently of the other aileron or flap. Elevator trim tabs and engine throttle setting were not included as elevator trim tab and engine failures were not considered. The states chosen for the linear model differ slightly from the nonlinear system. Airspeed, angle of attack, and sideslip angle were selected to be states of the linear model instead of the velocities along each of the body axes. The reason for choosing airspeed, angle of attack, and sideslip angle was that there is a closer relationship between these three variables and the first three measurements mentioned previously (airspeed and the acceleration along the y and z body axes).

To develop a linear model, the nonlinear system is expanded in a Taylor series about a nominal point $(\underline{x}_o, \underline{u}_o)$, neglecting second and higher order terms.

$$\dot{\underline{x}} = \underline{f}(\underline{x}_o, \underline{u}_o) + \frac{\partial \underline{f}}{\partial \underline{x}}(\underline{x}_o, \underline{u}_o)(\underline{x} - \underline{x}_o) + \frac{\partial \underline{f}}{\partial \underline{u}}(\underline{x}_o, \underline{u}_o)(\underline{u} - \underline{u}_o) \quad (A.3)$$

$$\underline{y} = g(\underline{x}_o, \underline{u}_o) + \frac{\partial \underline{g}}{\partial \underline{x}}(\underline{x}_o, \underline{u}_o)(\underline{x} - \underline{x}_o) + \frac{\partial \underline{g}}{\partial \underline{u}}(\underline{x}_o, \underline{u}_o)(\underline{u} - \underline{u}_o) \quad (A.4)$$

To put Eq. (A.3) and (A.4) in more standard form, define

$$\Delta \underline{x} \equiv \underline{x} - \underline{x}_o \quad (A.5)$$

$$\Delta \underline{u} \equiv \underline{u} - \underline{u}_o \quad (A.6)$$

$$A \equiv \frac{\partial \underline{f}}{\partial \underline{x}}(\underline{x}_o, \underline{u}_o) \quad (A.7)$$

$$B \equiv \frac{\partial \underline{f}}{\partial \underline{u}}(\underline{x}_o, \underline{u}_o) \quad (A.8)$$

$$C \equiv \frac{\partial \underline{g}}{\partial \underline{x}} (\underline{x}_o, \underline{u}_o) \tag{A.9}$$

$$D \equiv \frac{\partial \underline{g}}{\partial \underline{u}} (\underline{x}_o, \underline{u}_o) \tag{A.10}$$

Also, differentiate Eq. (A.5), assuming the nominal point remains fixed.

$$\dot{\Delta \underline{x}} = \dot{\underline{x}}$$

Combining Eq. (A.3) through (A.11) results in the form

$$\dot{\Delta \underline{x}} = \underline{f}(\underline{x}_o, \underline{u}_o) + A\Delta \underline{x} + B\Delta \underline{u} \tag{A.11}$$

$$\underline{y} = \underline{g}(\underline{x}_o, \underline{x}_o) + C\Delta \underline{x} + D\Delta \underline{u} \tag{A.12}$$

The A, B, C, and D matrices which describe the linear model can either be calculated by analytically determining the partial derivatives and then evaluating the partial derivates or by numerically approximating the partial derivatives about the nominal point. As the C-130 nonlinear dynamics contain many lookup tables as opposed to explicit functions of the states and the controls, the partial derivatives were numerically approximated in the following manner. Define x_i to be the ith state, $f_i(\underline{x},\underline{u})$ to be the nonlinear function which describes the derivative of the ith state, and $\underline{\eta}_i$ to be a column vector with unity in the ith row and zero in the other rows. Let a_{ij} be the element in the ith row and the jth column of the A matrix. Then a_{ij} is numerically approximated by

$$a_{ij} \equiv \frac{\partial f_i}{\partial x_j} (\underline{x}_o, \underline{u}_o) \approx \frac{f_i(\underline{x}_o + \underline{\eta}_j x_{j_p}, \underline{u}_o) - f_i(\underline{x}_o - \underline{\eta}_j x_{j_p}, \underline{u}_o)}{2x_{j_p}} \tag{A.13}$$

where x_{j_p} is a perturbation in jth state from the nominal. This perturbation must be chosen to produce a good approximation to the partial derivative. The B, C, and D matrices were calculated similarly.

A.3 Results

Figures A.1 and A.2 present simulation runs which compare the linear and nonlinear system responses. The nominal point used to generate the linear model is with the C-130 aircraft flying straight and level with an airspeed of 77.2 m/s (150 knots) at an altitude of a 304.8 m (1000 ft). Figure A.1 investigates the quality of the A matrix linearization by perturbing only the states. The nonlinear and linear response for perturbations in airspeed, angle of attack, sideslip angle, and the angular velocity of the vehicle expressed in the body coordinate system are compared. The dynamics are well represented although the linear and nonlinear models begin to diverge after about 60 s. There are, however, nonlinear dynamics which are poorly represented. In the nonlinear system, a perturbation in the lateral dynamics also excites the longitudinal dynamics while the linear model is unable to represent this cross-coupling because of the nonlinearities involved.

Figure A.2 presents comparisons of linear and nonlinear responses for a perturbation in the rudder control input. Note the small changes in most of the states and outputs. The quality of the linear response is dependent on roll. Once roll becomes "large", the cross-coupling between the lateral and longitudinal dynamics causes the linear response to diverge from the nonlinear response.

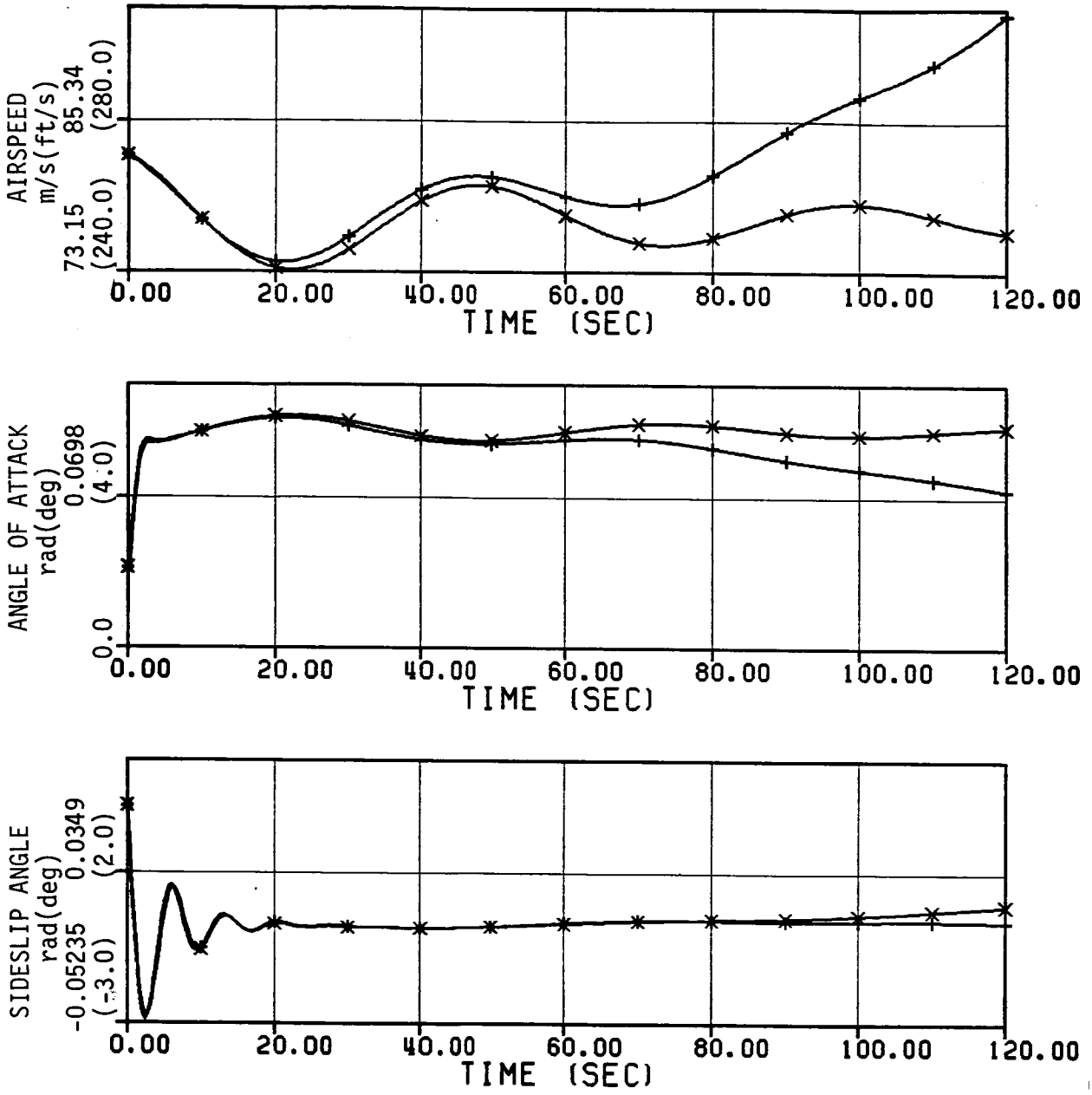

Figure A.1. Linear and nonlinear response for perturbations in airspeed, angle of attack, sideslip angle, and the angular velocities

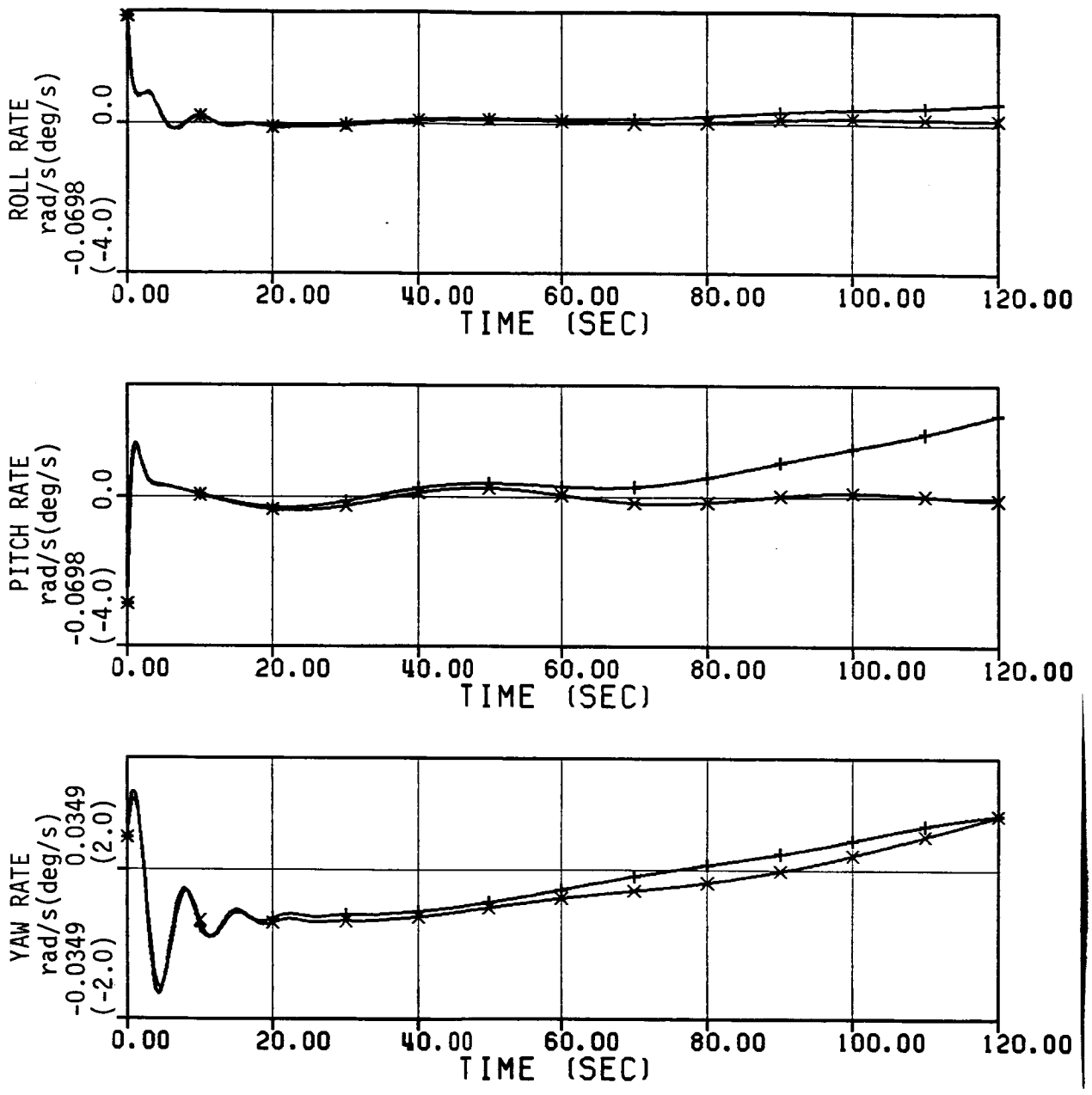

Figure A.1. Linear and nonlinear response for perturbations in airspeed, angle of attack, sideslip angle, and the angular velocities (Cont.)

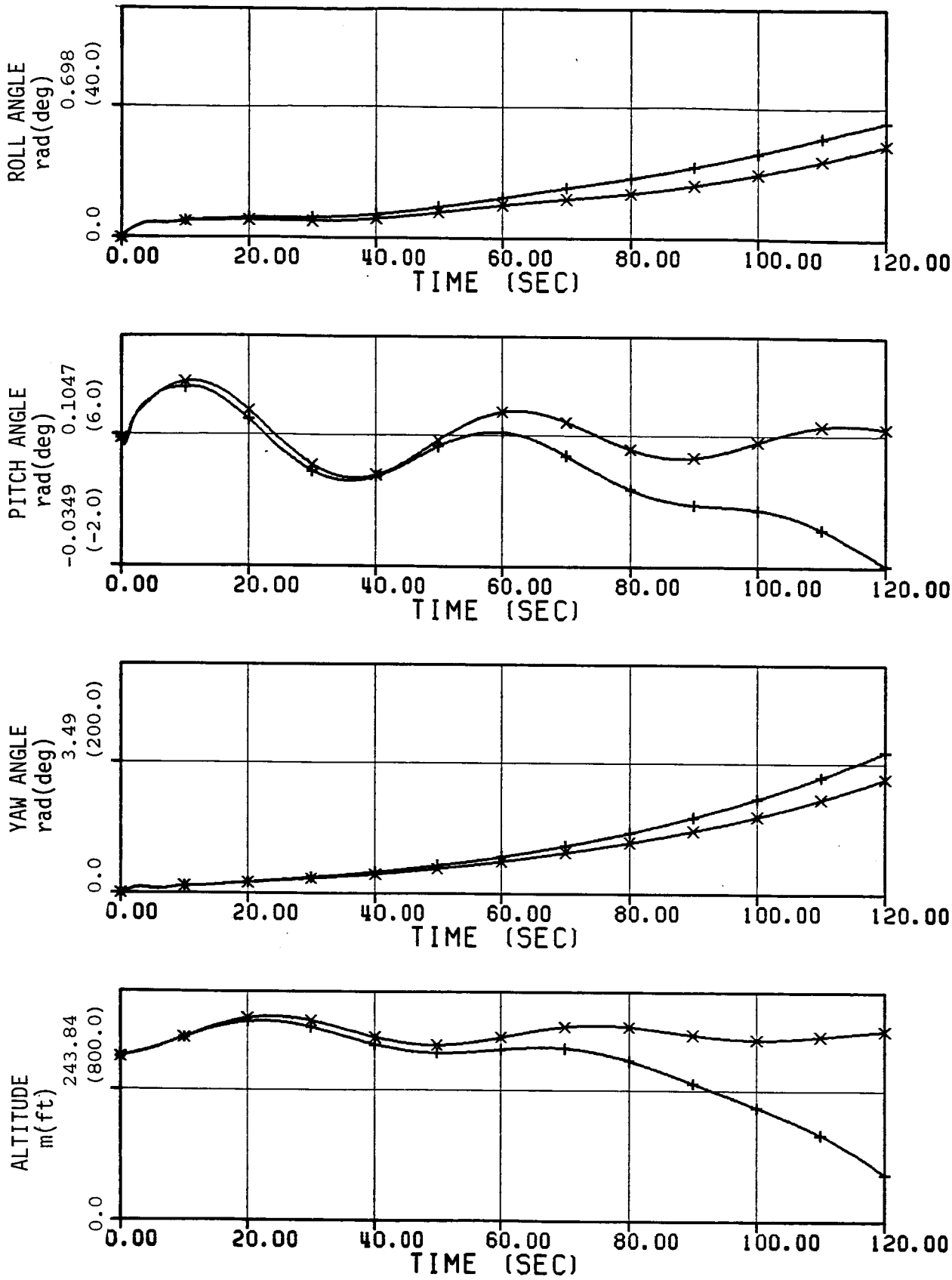

Figure A.1. Linear and nonlinear response for perturbations in airspeed, angle of attack, sideslip angle, and the angular velocities (Cont.)

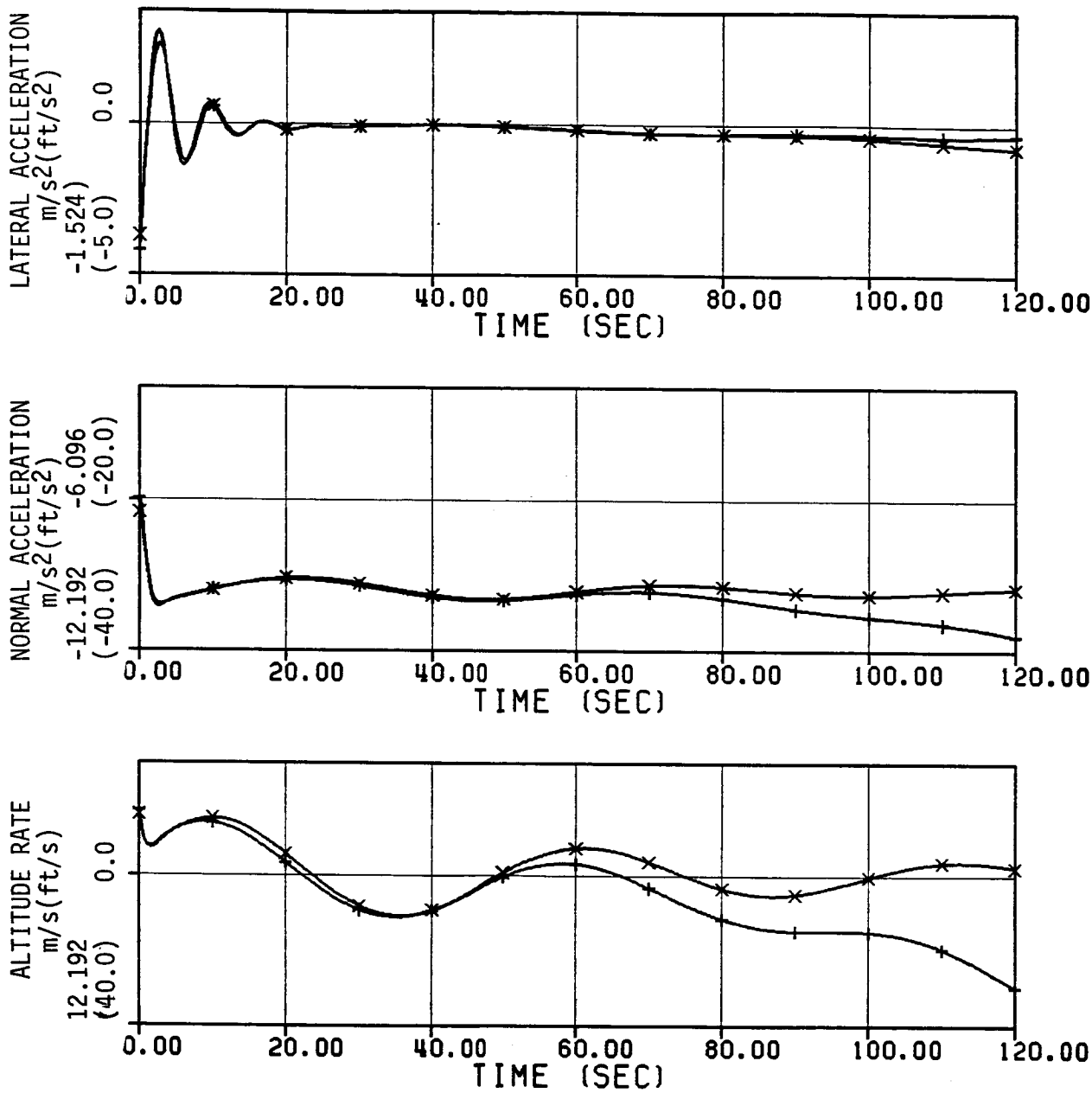

Figure A.1. Linear and nonlinear response response for perturbations in airspeed, angle of attack, sideslip angle, and the angular velocities (Cont.)

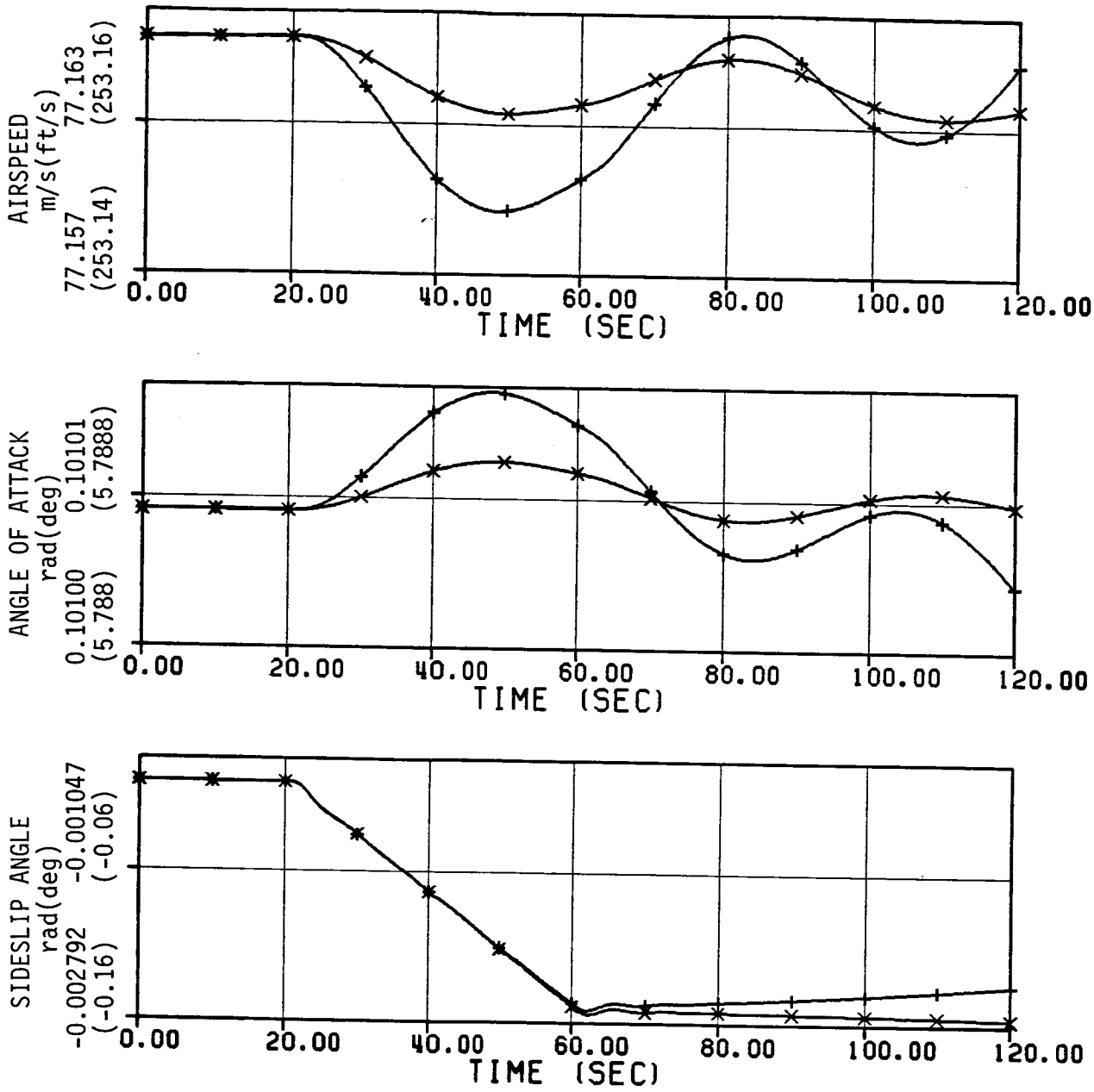

Figure A.2. Linear and nonlinear responses for a perturbation in rudder

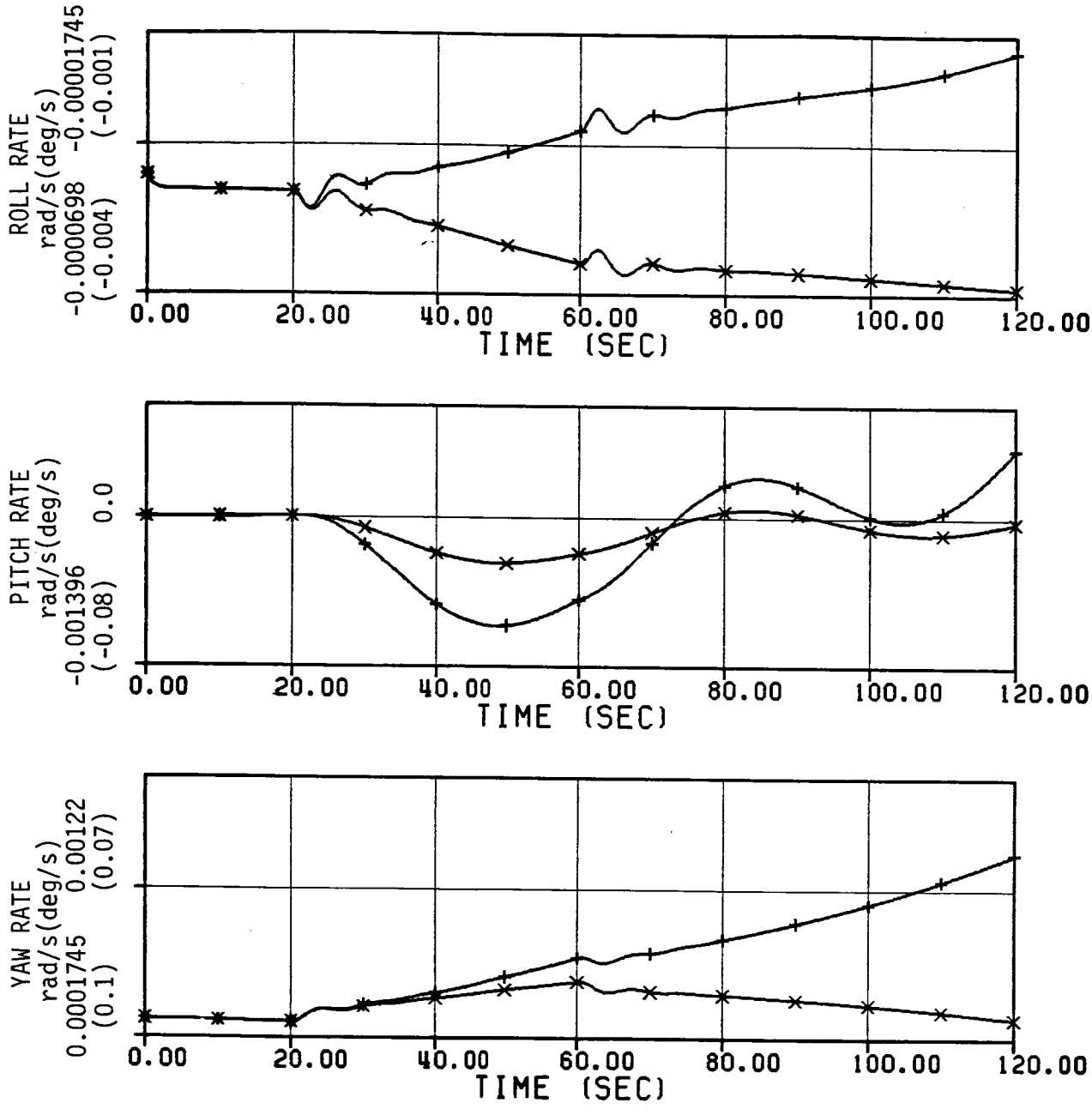

Figure A.2. Linear and nonlinear responses for a perturbation in rudder (cont.)

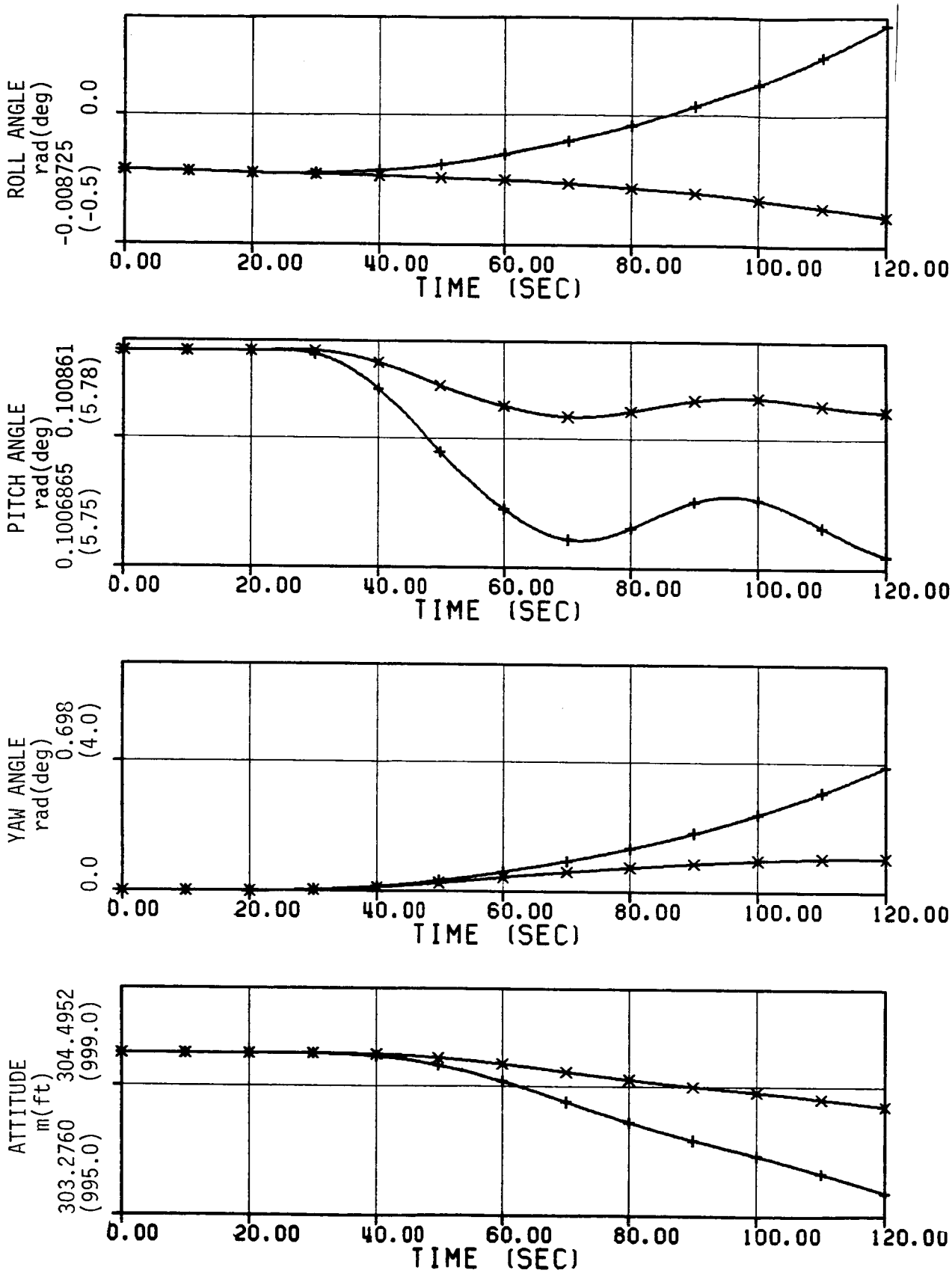

Figure A.2. Linear and nonlinear responses for a perturbation in rudder (Cont.)

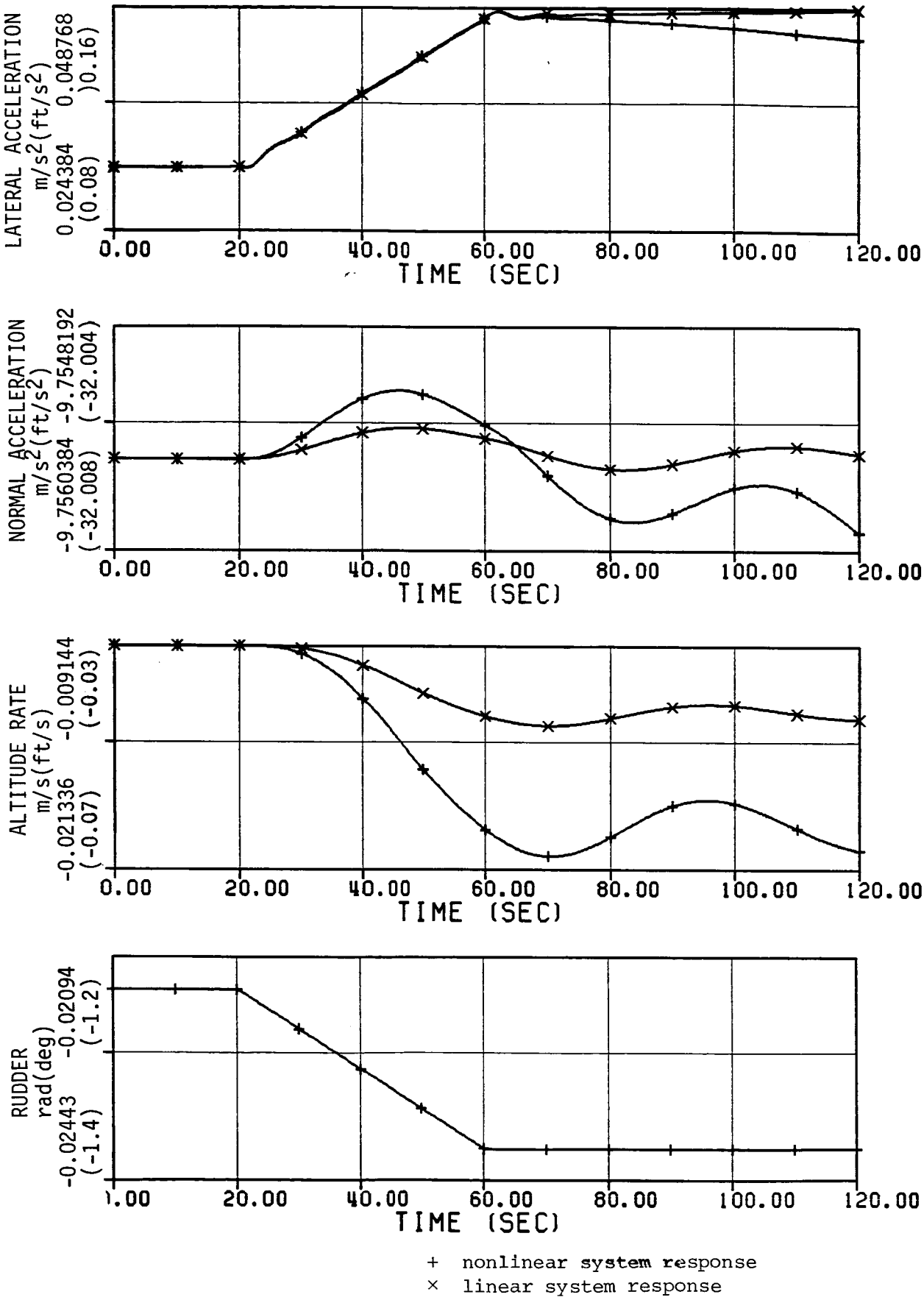

Figure A.2. Linear and nonlinear responses for a perturbation in rudder (Cont.)

APPENDIX B

THE DISCRETE-TIME DETECTION FILTER

As the detection filter was implemented on a digital computer, the detection filter was designed as a discrete-time system. While detection filter theory is not strictly valid for discrete-time systems, a satisfactory design is possible if the sampling rate is sufficiently rapid. This appendix will simply state the extension to discrete time. For more detail and explanation, see Reference 8.

The first step in designing a discrete-time detection filter is to describe the continuous linear model

$$\dot{\underline{x}} = A\underline{x} + B\underline{u} \tag{B.1}$$

$$\underline{y} = C\underline{x} + D\underline{y} \tag{B.2}$$

as a discrete-time system. This is commonly done by converting the state differential equation into a difference equation. This conversion results in a discrete-time model of the form

$$\underline{x}(k+1) = \Phi\underline{x}(k) + \Gamma\underline{u}(k) \tag{B.3}$$

$$\underline{y}(k) = C\underline{x}(k) + D\underline{u}(k) \tag{B.4}$$

where $\underline{x}(k)$, $\underline{u}(k)$, and $\underline{y}(k)$ are the state, input, and measurement vectors at sampling time t_k. For constant sampling interval, Δt, the sampling time may be expressed as $t_k = k \cdot \Delta t$ where $k = 0,1,2,3,\ldots$. The matrix Φ is referred to as the state transition matrix as it describes how the state propagates independent the effect of the control inputs over the sampling interval Δt. The input matrix, Γ, describes the effect of the control vector on the state over the sampling interval. If $\underline{u}(t)$ only changes at the sampling times t_k, then the state difference equation, Eq. (B.3), exactly represents the state differential equation, Eq. (B.1). However, if $\underline{u}(t)$ is changing over the sampling interval, Eq. (B.3) only approximates Eq. (B.1). In this case, the sampling interval Δt must be sufficiently small so that the assumption of $\underline{u}(t)$ being constant over the sampling interval is valid. The sampling interval chosen for design and implementation of the detection filter in this memo was 20 milliseconds. With this sampling interval, the control input vector $\underline{u}(t)$ should be approximately constant over the interval.

Given the discrete-time linear model, the detection filter properties and design are analogous to the continuous-time case presented in Section 3. Only actuator failures for the case where there is input-output coupling will be considered here. Consider a failure in the ith actuator. Before, the actual control surface deflections, $\underline{u}(t)$, were expressed as the sum of the expected control surface deflections input to the detection filter, $\underline{u}(t)$, and the unexpected ith control surface deflection $n(t)$. Now, $\underline{u}(t)$, $\underline{u}'(t)$, and $n(t)$ will be assumed to be piecewise constant functions, only changing at sampling times t_k. Therefore, the actual control surface deflection at t_k is

$$\underline{u}(k) = \underline{u}'(k) + \underline{e}_i n(k) \qquad \text{(B.5)}$$

where $\underline{u}'(k)$ and $n(k)$ are the expected control surface deflection to the detection filter and the difference between the actual and expected ith control surface deflection at sampling time t_k, respectively. Again, $\underline{e}_i$ is a column vector with zeros in every row except for a one in the ith row. The discrete-time error dynamics produced by this failure are

$$\underline{q}(k+1) = (\Phi - KC)\underline{q}(k) + (\underline{\gamma}_i - K\underline{d}_i)n(k) \qquad (B.6)$$

$$\underline{r}(k) = C\underline{q}(k) + \underline{d}_i n(k) \qquad (B.7)$$

where $\underline{q}(k)$ and $\underline{r}(k)$ are the discrete filter state error and residual respectively. $\underline{\gamma}_i$ is the ith column of the Γ matrix.

If a detection filter can be designed for this system and if $\underline{u}(t)$, $\underline{u}'(t)$, and $n(t)$ only change at sampling times t_k such that Eq. (B.5) is satisfied, the $(\underline{\gamma}_i - K\underline{d}_i)$ term in Eq. (B.6) will produce a unidirectional residual. The direction of the residual will be $C(\underline{\gamma}_i - K\underline{d}_i)$. Therefore, the signature produced by a failure in the ith control surface can be constrained to a plane spanned by $C(\underline{\gamma}_i - \underline{K}\,\underline{d}_i)$ and $\underline{d}_i$. This is identical to the continuous-time results presented in Section 3.2 except that the ith column of the continuous input matrix, $\underline{b}_i$, has been replaced by the ith column of the discrete input matrix, $\underline{\gamma}_i$. However, $\underline{u}(t)$, $\underline{u}'(t)$, and $n(t)$ have been assumed to be piecewise constant functions changing at the sampling times t_k. As before, the sampling interval must be sufficiently small so this assmption is valid.

For a fully measured system, there are only two minor differences in designing a discrete detection filter as compared to designing a continuous detection filter (presented in Section 3.3).

(1) The filter eigenvalue must be chosen in discrete-time domain.

(2) The gain matrix K must be calculated to satisfy the relationship

$$\Phi - KC = \lambda I$$

TECHNICAL REPORT STANDARD TITLE PAGE

1. Report No.	2. Government Accession No.	3. Recipient's Catalog No.

4. Title and Subtitle

The Evaluation of Failure Detection and Isolation Algorithms for Restructurable Controls

5. Report Date
November 1985

6. Performing Organization Code

7. Author(s)
P. Motyka, W. Bonnice, S. Hall, E. Wagner

8. Performing Organization Report No.
CSDL-R-1799

9. Performing Organization Name and Address
The Charles Stark Draper Laboratory Inc.
555 Technology Square
Cambridge, Massachusetts 02139

10. Work Unit No.

11. Contract or Grant No.
NAS1-17556

12. Sponsoring Agency Name and Address
Natural Aeronautics and Space Administration
Washington, D.C. 20546

13. Type of Report and Period Covered
Interim Report
Dec. 1983 - May 1984

14. Sponsoring Agency Code

15. Supplementary Notes
Langley Technical Monitor: W. Thomas Bundick

16. Abstract

Three failure detection and identification techniques were compared to determine their usefulness in detecting and isolating failures in an aircraft flight control system; excluding sensor and flight control computer failures. The algorithms considered were the detection filter, the Generalized Likelihood Ratio test and the Orthogonal Series Generalized Likelihood Ratio test. A modification to the basic detection filter is also considered which uses secondary filtering of the residuals to produce unidirectional failure signals. The algorithms were evaluated by testing their ability to detect and isolate control surface failures in a nonlinear simulation of a C-130 aircraft. It was found that failures of some aircraft controls are difficult to distinguish because they have a similar effect on the dynamics of the vehicle. Quantitative measures for evaluating the distinguishability of failures are considered. A system monitoring strategy for implementing the failure detection and identification techniques was considered. This strategy identified the mix of direct measurement of failures versus the computation of failure necessary for implementation of the technology in an aircraft system.

17. Key Words Suggested by Author	18. Distribution Statement
Failure Detection and Isolation Restructurable Controls Generalized Likelihood Ratio Failure Detection Filter	Unclassified - Unlimited Subject Category - 04

19. Security Classif. (of this report)	20. Security Classif. (of this page)	21. No. of Pages	22. Price
Unclassified	Unclassified	191	